ON LOCALIZATION AND TRACKING USING RECEIVED SIGNAL STRENGTH MEASUREMENTS

A THESIS SUBMITTED TO
THE GRADUATE SCHOOL OF NATURAL AND APPLIED SCIENCES
OF
MIDDLE EAST TECHNICAL UNIVERSITY

BY

ALPTEKIN YILMAZ

IN PARTIAL FULFILLMENT OF THE REQUIREMENTS
FOR
THE DEGREE OF MASTER OF SCIENCE
IN
ELECTRICAL AND ELECTRONICS ENGINEERING

FEBRUARY 2015

Approval of the thesis:

ON LOCALIZATION AND TRACKING USING RECEIVED SIGNAL STRENGTH MEASUREMENTS

submitted by **ALPTEKIN YILMAZ** in partial fulfillment of the requirements for the degree of **Master of Science in Electrical and Electronics Engineering Department, Middle East Technical University** by,

Prof. Dr. Gülbin Dural Ünver
Dean, Graduate School of **Natural and Applied Sciences** _____

Prof. Dr. Gönül Turhan Sayan
Head of Department, **Electrical and Electronics Engineering** _____

Prof. Dr. Ali Özgür Yılmaz
Supervisor, **Electrical and Electronics Eng. Dept,METU** _____

Assoc. Prof. Dr. Umut Orguner
Co-supervisor, **Electrical and Electronics Eng. Dept,METU** _____

Examining Committee Members:

Prof. Dr. Yalçın Tanık
Electrical and Electronics Engineering Dept., METU _____

Prof. Dr. Ali Özgür Yılmaz
Electrical and Electronics Engineering Dept., METU _____

Prof. Dr. Mübeccel Demirekler
Electrical and Electronics Engineering Dept., METU _____

Prof. Dr. Sencer Koç
Electrical and Electronics Engineering Dept., METU _____

Assoc. Prof. Dr. Sinan Gezici
Electrical and Electronics Engineering Dept., Bilkent Univ. _____

Date: 20.02.2015

I hereby declare that all information in this document has been obtained and presented in accordance with academic rules and ethical conduct. I also declare that, as required by these rules and conduct, I have fully cited and referenced all material and results that are not original to this work.

Name, Last Name: ALPTEKIN YILMAZ

Signature :

ABSTRACT

ON LOCALIZATION AND TRACKING USING RECEIVED SIGNAL STRENGTH MEASUREMENTS

Yılmaz, Alptekin
M.S., Department of Electrical and Electronics Engineering
Supervisor : Prof. Dr. Ali Özgür Yılmaz
Co-Supervisor : Assoc. Prof. Dr. Umut Orguner

February 2015, 129 pages

In this study, first, some received signal strength (RSS) based localization techniques, including maximum likelihood estimation (MLE), multidimensional scaling (MDS) and weighted least squares (WLS), are investigated and compared to each other via a simulation study within the perspective of a collaborative localization scenario. MLE using RSS measurement model, called RSS-MLE is known in the literature to be significantly biased. An important observation of this work is that the aforementioned bias can be clearly reduced in some collaborative localization scenarios when the non-connectivity information is incorporated into maximum likelihood (ML) cost function. We refer to the ML algorithm including the non-connectivity information as hybrid RSS-MLE (h-RSS-MLE).

In order to support the reduced bias observation and determine the conditions in which h-RSS-MLE can mitigate the bias, we derive an analytical expression for the bias of the ML estimator based on a second order Taylor series expansion of MLE cost function by incorporating connectivity constraints into the problem. Since this analysis

gives results which do not match the simulation results in a 2-D scenario, we also derive another expression based on a Taylor series expansion of the RSS measurements. The latter analysis is validated under some 2-D non-collaborative localization scenarios through a simulation study for MLE optimized by a grid-search.

Finally, we make simulations as well as an experimental study to compare the localization algorithms with some conventional tracking methods including Kalman filters and a particle filter. It is observed in the experiments that the tracking methods can increase the accuracy about one meter compared to the localization algorithms for a non-collaborative case.

Keywords: Localization, tracking, received signal strength, maximum likelihood estimation, non-connectivity information, bias analysis, Taylor series expansion, Cramér-Rao lower bound, Kalman filter, particle filter, grid-search.

ÖZ

ALINAN SİNYAL GÜCÜ ÖLÇÜMLERİNİ KULLANAN KONUMLANDIRMA VE TAKİP ÜZERİNE

Yılmaz, Alptekin
Yüksek Lisans, Elektrik ve Elektronik Mühendisliği Bölümü
Tez Yöneticisi : Prof. Dr. Ali Özgür Yılmaz
Ortak Tez Yöneticisi : Assoc. Prof. Dr. Umut Orguner

Şubat 2015, 129 sayfa

Bu çalışmada ilk olarak, en yüksek benzerlik kestirimini (MLE), çok boyutsal seviyelendirmeyi (MDS) ve ağırlıklandırılmış en küçük kareleri (WLS) içeren, alınan sinyal gücüne (RSS) dayanan bazı konumlandırma teknikleri araştırılmakta ve işbirlikçi bir konumlandırma senaryosu bakış açısı içerisinde yapılan bir benzetim çalışması yoluyla birbirleriyle karşılaştırılmaktadır. RSS-MLE olarak adlandırılan RSS ölçüm modelini kullanan MLE, literatürde ciddi derecede yönelimli olarak bilinir. Bu çalışmanın önemli bir gözlemi, bazı işbirlikçi konumlandırma senaryolarında, bağlantısızlık bilgisinin en yüksek benzerlik (ML) maliyet fonksiyonuna dahil edildiği durumda, bahsedilen yönelimin açıkça azaltılabildiğidir. Bağlantısızlık bilgisini içeren ML algoritmasını, melez RSS-MLE (h-RSS-MLE) olarak anıyoruz.

Azaltılan yönelim gözlemini desteklemek ve h-RSS-MLE'nin yönelimi düşürebileceği durumları belirlemek için, probleme bağlantı kısıtını dahil ederek, ML kestiriminin yönelimi için, MLE maliyet fonksiyonunun ikinci derece Taylor seri açılımına dayanan bir analitik ifade türetiyoruz. Bu analiz, bir 2-D senaryosundaki benzetim

sonuçlarıyla uyuşmadığı için, biz ayrıca RSS ölçümlerinin Taylor seri açılımına dayanan başka bir ifade türetiyoruz. Son analiz, işbirlikçi olmayan bazı 2-D konumlandırma senaryoları altında, ızgara arama ile çözülen MLE için yapılan bir benzetim çalışmasıyla doğrulanmaktadır.

Son olarak, konumlandırma algoritmalarını, Kalman süzgeçlerini ve bir parçacık süzgecini içeren bazı geleneksel takip yöntemleriyle karşılaştırmak için, deneysel bir çalışmayla birlikte benzetimler yapmaktayız. Konumlandırma algoritmalarıyla karşılaştırıldığında, takip yöntemlerinin işbirlikçi olmayan bir durum için, bir metre civarında doğruluğu artırabildiği deneylerde gözlenmektedir.

Anahtar Kelimeler: Konumlandırma, takip, alınan sinyal gücü, en yüksek benzerlik kestirimi, bağlantısızlık bilgisi, yönelim analizi, Taylor seri açılımı, Cramér-Rao alt sınırı, Kalman süzgeci, parçacık süzgeci, ızgara arama.

To my beloved family,
and my friends

ACKNOWLEDGMENTS

I would like to express my sincere gratitude to my advisor, Prof. Dr. Ali Özgür Yılmaz for his guidance, patience and encouragement during thesis work. I'm also indebted to him for giving me the opportunity to participate in two research projects supported by Türk Telekom Argela and ASELSAN. I have gained lots of experiences and perspectives in these projects.

I would like to thank my co-advisor, Assoc. Prof. Dr. Umut Orguner for his good advice, patience, inspiring comments and motivations during this thesis. The door of Dr. Orguner is always open to me for technical discussions and he always helped me patiently understand the basic concepts in the estimation theory which is actually main part of this study. It was an unforgettable experience to work with him during my thesis study. This study would not have been possible without his assistance and guidance.

I am grateful to the companies, Türk Telekom Argela and ASELSAN Inc. for their financial support during my thesis. Additionally, the experiences gained in the projects which were financially supported by these companies must be also acknowledged.

I am also thankful to my colleague, Melih Doğan who provided me programmed Arduino Boards and ZigBee modules having been utilized for the experimental work.

I would like to express my special thanks to my elder colleagues Dr. Gökhan Muzaffer Güvensen and Dr. Tuğcan Aktaş for their motivation and suggestions. Especially, i would like to appreciate our informative and joyful conversations and their invaluable mentorships about the area and life. I am also thankful to my dear friends Ali Bulut Üçüncü, Pınar Şen, Seçil Özdemir, Samet Gelincik, Ömer Melih Gül and Yunus Can Gültekin for their endless support and our pleasant talks.

Finally, i would like to express my deepest gratitudes to my family for their priceless support to me in my entire life.

TABLE OF CONTENTS

LIST OF TABLES

TABLES

LIST OF FIGURES

FIGURES

LIST OF ABBREVIATIONS

AN	Anchor Node
AOA	Angle of Arrival
BN	Blindfolded Node
CDF	Cumulative Distribution Function
CRLB	Cramér-Rao Lower Bound
EFI	Equivalent Fisher Information
EKF	Extended Kalman Filter
FIM	Fisher Information Matrix
FSS-MLE	Maximum Likelihood Estimation Using Finite Search Space
GPS	Global Positioning System
h-FSS-MLE	Hybrid FSS-MLE
h-RSS-MLE	Hybrid RSS-MLE
IID	Independent Identically Distributed
IM	Iterative Multilateration
KF	Kalman Filter
LS	Least Squares
MAP	Maximum A Posteriori
MC	Monte Carlo
MDS	Multidimensional Scaling
ML	Maximum Likelihood
MLE	Maximum Likelihood Estimation
MSE	Mean Squared Error
MVU	Minimum Variance Unbiased
NLOS	Non-Line of Sight
PDF	Probability Density Function
PF	Particle Filter
RMSE	Root Mean Squared Error
RSS	Received Signal Strength
RSS-MLE	MLE based on RSS Measurements
SIR	Sequential Importance Resampling
SMACOF	Scaling by Majorizing a Convex Function
SNR	Signal-to-Noise Ratio

STD	Standard Deviation
TDOA	Time Difference of Arrival
TOA	Time of Arrival
UKF	Unscented Kalman Filter
WLS	Weighted Least Squares
WSN	Wireless Sensor Network

CHAPTER 1

INTRODUCTION

Wireless sensor networks (WSN) have emerged in many applications for monitoring, controlling and tracking in daily life. WSN is a network which consists of units which are capable of sensing the physical quantities, e.g., temperature, motion, humidity and also have ability to communicate with each other in a centralized or peer-to-peer manner [3]. In WSN, sensing the data without location information of the sensor is meaningless and the location information of the units we call nodes or sensors can also be beneficial to improve the performance of wireless networks for network planning, network adaptation, load balancing and cognitive radio applications [16, 29, 51]. Therefore localization and tracking attracts much attention in industry and academia.

Localization is the process which extracts the position knowledge of an object from noisy observations, i.e., measurements, observed by sensors in the network. This process is exactly an estimation problem. In tracking concept, the only difference is that the dynamics of the environment, e.g., predicted motion parameters of the object or change of measurement parameters related to environment so called channel, is involved in the estimation problem as done in Kalman filter [24]. Global Positioning System (GPS) is the most widely used system for positioning and localization especially in outdoor environments, however GPS is not applicable in indoor case due to non-line-of-sight (NLOS) propagation. Since there are various obstacles in indoor environments such as walls, some equipments influencing the electromagnetic wave propagation which result in less trustable observations in estimation problem. To get more comprehensive understanding about indoor radio propagation channel, [21] can

be a good reference. Due to the unavailability of GPS, the ubiquitous use of the wireless systems particularly in the last decade has made the use of RF signals in indoor environment a viable approach in determining real-time location and tracking. Since RF signals are already present in almost all media of interest, researchers both in industry and academia have developed many different techniques based on RF signals in order to get the position of the objects.

RF signals can include position-related information of a source or destination node in miscellaneous ways. The ones which we call as measurement techniques, so called metrics, are time of arrival (TOA), time difference of arrival (TDOA), angle of arrival (AOA) and received signal strength (RSS). Each of these metrics has its own advantages and disadvantages [16, 19, 30, 50]. For instance, TOA is more complex than the other techniques in the sense of hardware, because it requires perfect time synchronization, but more accurate results can be observed with TOA. AOA can offer less accuracy than TOA, actually moderate in most applications, but negative aspect of AOA is that precise angle measurements need array antennas [19, 30, 50]. Among a multitude of measurement metrics, the use of RSS is a very popular choice with low complexity, no extra hardware and cost of devices, since almost all wireless devices have the capability to measure and report it outside directly [16]. Despite the low complexity of RSS techniques, it is not so reliable, since it suffers from deeply varying fading characteristics of the multipath radio channels that cause significant errors in location estimation. Detailed information for some positioning systems utilizing the aforementioned measurement techniques can be found in [19, 30, 31, 50]. Sometimes different measurement schemes are fused in order to obtain better localization or tracking performance. For example, [28] proposes a procedure where RSS measurements are utilized to correct TDOA estimation when multipath effect of the channel is dominant, otherwise they are not considered in tracking algorithm.

As expressed before, the localization methods based on RSS metric are so prominent due to its low complexity. Localization errors are relatively higher than in TOA or AOA, since there exists higher nonlinear relation between RSS metric and the position of the target to be estimated and RSS metric is highly affected by time and spatial variation of a radio channel which is called fading [15,45]. Some methods can be followed as mentioned in [7, 11, 35, 49] to reduce high variation of radio environment

which decrease the precision of the position information of the node in RSS readings. The methods generally consider diversity concept in wireless communications by using the fact that RSS readings are independent in different time, frequency, antenna orientations, wave polarization and number of the antennas in the wireless systems. Different techniques exist to combine RSS readings with the purpose of increasing total signal-to-noise ratio (SNR) which can be found in [15, 45]. The most intuitive way of stabilising RSS readings is to take average over RSS readings from statistically independent resources, e.g., frequency, time or space, as expressed in [35, 49].

Localization approaches are generally divided into two parts: non-collaborative and collaborative localization. In non-collaborative localization, measurements considered in the algorithm are between only anchors (i.e., reference node whose positions are priorly known) and blindfolded nodes (i.e., agents whose positions unknown namely to be estimated). In other words, the measurements between blindfolded ones are not utilized in the estimation problem, while these inter-blindfolded nodes measurements are considered in the collaborative approach in addition to anchor related information. It is stated in [34] that more position unknown nodes, i.e., blindfolded nodes, can improve accuracy or performance of the localization techniques, even though the number of the unknown parameters to be estimated increases. Patwari et. al. proves this statement by comparing Cramér-Rao lower bound (CRLB) values in [34]. It is also reported in [50] that the number of anchors and anchor placement also affect the performance of the localization systems. More detailed information related to the comparison of collaborative and non-collaborative schemes can be obtained from [30, 33, 34, 47, 50].

As all other positioning systems, RSS based ones require two phases: Calibration and localization phases. In the calibration phase, the signal strength values are measured at some locations and then some channel parameters, which are necessary in the localization phase, are estimated according to them [10, 30, 50]. The measurements are taken to estimate the location of the target node by utilizing channel parameters which are found in the calibration phase. Finally, it should be noted that the localization methods having high immunity to calibration errors are desired.

Based on the RSS metric, localization methods can also be classified according to

how the RSS metric is utilized in algorithm. These are fingerprinting, range-based and range-free techniques. In fingerprinting approach, the measurements are taken during the calibration phase at different points of the observation area, which are called fingerprints or landmarks in fingerprinting literature [16], stored and used in the localization phase. The unknown position of the target node is estimated by finding the closest fingerprint which is collected in calibration, to measured one in localization phase. It requires obviously good calibration, i.e., large number of measurement campaigns in the calibration phase, to estimate the unknown position accurately [10]. Range-based techniques consider the fact that RSS values decay with increase of inter-node distances. An analytical propagation model is assumed in solving the estimation problem. Finally, range-free localization utilizes connectivity information with respect to RSS threshold power or deployment distribution of the nodes, which is stated in [10]. Three aforementioned methods are also compared in terms of performance of calibration and localization phases in [10]. It is said in [10] that range-based method is the best among the three approaches. Additionally, the fingerprinting methods give good results relatively, although it needs better calibration for localization. There exists studies [13,14] which compare connectivity and range-based methods in terms of CRLB in the literature. Giorgetti et. al. show that there is a critical number of connected nodes depending on RSS threshold value in which range-based localization is better than connectivity based one. He also gives an optimal number of connections which results in maximum connectivity based information with regard to Fisher Information in [14].

Maximum likelihood estimation (MLE) [29,34,36], multidimensional scaling (MDS) [6, 9, 29], weighted least squares algorithm (WLS), multilateration [30, 50] and iterative multilateration (IM) [42] are some of localization methods in the literature. Localization problems, algorithms, strategies and factors affecting the localization performance are surveyed in various articles [18, 19, 30, 31, 33, 50]. MLE and MDS are two commonly used methods in range-based RSS localization, especially in collaborative localization as in [27, 29, 48]. Being asymtotically unbiased and efficient makes MLE special and the conventional estimation technique [46]. Two types of maximum likelihood (ML) cost functions were proposed in the literature. In one line of work [29, 34], the cost function is composed only of the terms in the likelihood

function corresponding to the connected nodes (i.e., nodes with which a communication link is established). We call the resulting MLE algorithm with this type of ML cost function as RSS-MLE. On the other hand, the complete likelihood function for the problem contains also the terms corresponding to the unconnected nodes. These additional terms serve to incorporate into estimation problem the information that the blindfolded sensor is so far from the corresponding nodes that no connection is established. This type of ML cost function was proposed and used in [36]. We call the resulting MLE algorithm for this case the hybrid RSS-MLE (h-RSS-MLE) algorithm meaning that both connected and unconnected nodes are present in ML cost function. It can be also said that h-RSS-MLE fuses the measurements coming from range and connectivity based information. It is also mentioned in [27, 29, 48] that RSS-MLE cost function has multiple extremum points which requires good initialization. Therefore, a grid-search method to optimize the cost function can be utilized instead of gradient based algorithms, e.g., steepest descent, Quasi-Newton methods etc., The main drawback is that it has much higher algorithmic complexity than gradient based ones, though it guarantees the global optimum, especially when the number of unknown parameters increases in the estimation problem. In this study, we call the ML cost functions corresponding to RSS-MLE and h-RSS-MLE optimized by grid-search method within predefined constraints as maximum likelihood estimation using finite search space (FSS-MLE) and h-FSS-MLE respectively. A method to reduce complexity of grid-search method for RSS-MLE case is proposed in [38].

The overall performance of RSS based localization methods can be enhanced by applying some tracking algorithms. This is because an adaptive filter approach, e.g., Kalman filter, which is mostly preferred in real-time or off-line tracking scenarios, has an accumulative nature because of its measurement update and prediction update phase using some dynamic process (motion) model and measurement model together. The performance can also be enhanced by using some inertial measurement unit (IMU), e.g., accelerometer, gyroscope, beside the inter-node measurements in tracking approach. The aforementioned situations for getting higher accuracy in positioning are analyzed in a theoretical information based approach, so called Equivalent Fisher information (EFI) in [43].

Another important issue in RSS based estimation is that bias of the estimation causes

undesired errors which cannot be easily compensated. Although it is possible that mean squared error (MSE) of a biased estimator is lower than the minimum variance unbiased (MVU) estimator as emphasized in [25], the bias of an estimator is not usually desirable. RSS-MLE is known to be significantly biased in most of localization scenarios in the literature as stated in [9,29,34]. For this reason, an analytical bias expression can be a beneficial tool to predict system performance or mitigate unwanted bias terms in localization and tracking algorithms. There exists some attempts to find analytical bias formula for MLE based localization techniques among researchers in localization. [50] and [44] offer a method based on Taylor series approximation of the cost function which takes zero value at estimated points around true location of the target. By considering the methods in aforementioned articles, [41] provides an analytical expression for AOA, TOA and TDOA based MLE and [40] proposes a way of reducing bias in tracking algorithm by utilizing the bias expressions given in [41]. To our best knowledge, an analytical expression of bias does not exist for RSS based MLE in literature.

As mentioned before, owing to the fact that RSS techniques have low complexity and range-based localization promises more accurate results than the others, we consider RSS range based localization and tracking as the topic in this thesis. We first compare some collaborative localization methods, namely, RSS-MLE, h-RSS-MLE, WLS and MDS in a uniform grid deployment of nodes in a square area. It is seen that initialization of the MLE with WLS and MDS approaches, improves the RSS-MLE performance [29]. Additionally it is observed that adaptive neighborhood selection method proposed in [9] reduces the bias considerably for RSS-MLE. As a result, by considering the simulation results, we conclude that RSS-MLE is the best estimator among other estimators and h-RSS-MLE can be approximately unbiased without utilizing adaptive neighborhood selection (for the aforementioned sensor deployment). To our best knowledge, this bias-reducing effect of h-RSS-MLE has not been reported in the literature before.

In order to investigate the bias-reducing effect of h-RSS-MLE further, we put an effort into deriving an analytical bias formula for both RSS-MLE and h-RSS-MLE. An analytical expression for bias under connectivity constraints, which is also applicable for no connectivity constraint, i.e., no RSS threshold power, is derived by following

the same methodology as [41]. This analytical expression is validated via a simulation study conducted on a 1-D example. However it is also observed in the simulations that this analytical approach is not valid for the 2-D case, probably due to the high non-linearity of the assumed RSS propagation model. In order to overcome this difficulty, we made a Taylor series approximation of RSS distance measurements around true distance values to be able to give another analytical bias formula for RSS-MLE which is applicable for grid-search based optimization. It is seen that this new bias formula is valid in some simulation results at high SNR. Finally we compare some existing tracking algorithms with MLE in a non-collaborative case, using both simulated and real data, under different connectivity constraints. In the experimental study using real data, it is observed that the tracking algorithms, particularly the particle filter, improves the localization accuracy about one meter.

The rest of this thesis is organized as follows. In Chapter 2, the general localization problem related to RSS measurements is defined and some existing RSS range based localization methods are compared with some simulation results. Tracking algorithms are described and compared to MLE localization via both a simulation study and experiments in Chapter 3. Chapter 4 and 5 present the derivation and validation of the aforementioned analytical bias formulae along with simulation studies. We conclude the thesis with conclusion and future work in Chapter 6. Additionally some useful mathematical derivations and tools related to the study including some algorithms, RSS-MLE and h-RSS-MLE cost functions, CRLB and some useful expressions utilized in analytical bias formulas can be found in Appendices.

CHAPTER 2

LOCALIZATION

In this chapter, RSS measurement model and some localization techniques based on this model, e.g., MDS, MLE and WLS, are presented and compared via simulation studies. Simulation study includes both collaborative and non-collaborative localization scenarios. Furthermore, two variants of MLE cost functions are introduced and analyzed via the simulation study. In some scenarios, it is observed that one of them having extra information in it, has ability to mitigate bias, but not in all.

2.1 Problem Definition

Consider a network which consists of n blindfolded and m anchor nodes, namely $N = n + m$ nodes. The position of the blindfolded node (BN) is unknown and to be estimated, while anchor nodes (AN) have knowledge about their coordinates. In our study, the aim is to estimate the location of BN based on the pairwise RSS measurements among the nodes. In non-collaborative location estimation, RSS measurements are only made among BN and AN. However RSS measurements among all sensors are taken into account in collaborative location estimation, and then coordinates of all blind nodes are calculated together in the algorithm. It is known that pairwise RSS measurements are related to distance between connected nodes due to the path loss model [29], [15]. The path loss model [15] we used is given as follows:

$$P_{ij} = P_0 - 10\alpha \log_{10} \frac{d_{ij}}{d_0} + v_{ij} \tag{2.1}$$

for $1 \leq i \leq N, 1 \leq j \leq N$ and $i \neq j$, where P_0 is RSS measured at reference distance d_0 in dBm, d_{ij} is the Euclidean distance between node i and node j and α is the path

loss exponent. P_{ij} is the received power in dBm for the signal transmitted from node i to node j. Independent, identically distributed (IID) random variables $v_{ij} \sim \mathcal{N}(0, \sigma_v^2)$ are defined as log-normal shadowing effects of multipath environments. Path loss exponent α and σ_v depend on the channel characteristics. In the literature, pairwise measurements are considered as reciprocal, i.e, $P_{ij} = P_{ji}$ [29], [34]. For given P_{ij} in (2.1) and $d_0 \triangleq 1$, the MLE of distance between the node i and j is given in [34] (distance measurements corresponding to RSS measurements) as

$$\delta_{ij} = 10^{(P_0 - P_{ij})/10\alpha} \tag{2.2}$$

Derivation of this formula can be found in Appendix A. The MLE of distances can be used as measured parameters in the localization algorithm [34]. As it is seen, logarithm of measured distance has normal distribution with mean $\log d_{ij}$ and standard deviation $\sigma = (\sigma_v \log 10)/10\alpha$ namely $\log \delta_{ij} \sim \mathcal{N}(\log d_{ij}, \sigma)$. In our simulations when the received power P_{ij} at node i is larger than P_{thr} (RSS threshold of device), it can be said that connectivity between node i and j is obtained, in other words RSS measurement is obtained. By using the δ_{ij} measurements and connectivity information of the nodes, coordinates of the blindfolded sensors are estimated by an appropriate estimation rule.

2.2 Multidimensional Scaling (MDS)

MDS is a method that analyzes measurements of similarity or dissimilarity among the pairs of objects as distances between points of a low dimensional multidimensional space [6]. MDS is widely used in psychology, sociology and marketing. MDS can be used to solve localization problem [27, 29]. Configuration matrix for MDS can be written as

$$\mathbf{X} = [\mathbf{r_1},\ \mathbf{r_2},\ \cdots,\ \mathbf{r_N}] \tag{2.3}$$

where $\mathbf{r_i} = [\mathbf{x_{i1}},\ \mathbf{x_{i2}},\ \cdots,\ \mathbf{x_{iM}}]$ is the coordinates of the ith node in M dimensional space. Configuration matrix can be partitioned as $\mathbf{X} = \left[\mathbf{X}_{\text{BN}}^{\text{T}},\ \mathbf{X}_{\text{AN}}^{\text{T}}\right]^{\text{T}}$ where $\mathbf{X}_{\text{BN}}$, $\mathbf{X}_{\text{AN}}$ are configuration matrices of blindfolded nodes and anchor nodes respectively. MDS cost function (raw stress) is given in [6, 29] as

$$C_{\text{MDS}}(\mathbf{X}) = \sum_{i=1}^{N-1} \sum_{j=i+1}^{N} w_{ij} \left(d_{ij}(\mathbf{X}) - \delta_{ij}\right)^2 \tag{2.4}$$

where $d_{ij}(\mathbf{X}) = \|\mathbf{r}_i - \mathbf{r}_j\|$ and δ_{ij} is dissimilarity, and weights w_{ij}:

$$w_{ij} = \begin{cases} 1, & \text{if } \delta_{ij} \text{ is observed } (\delta_{ij} \leqslant d_{thr}) \\ 0, & \text{otherwise} \end{cases} \tag{2.5}$$

where d_{thr} is the threshold distance (d_{thr} is related to RSS threshold value P_{thr} in our problem). MDS solution can be obtained by minimizing the MDS cost function in (2.4). This minimization can be done by using Scaling by Majorizing a Convex Function (SMACOF) [6, 29] or gradient based methods such as Quasi-Newton or trust-region methods. These gradient based minimization methods can be found in MATLAB Optimization Toolbox. Minimization by SMACOF algorithm is easier than gradient based methods [6]. SMACOF algorithm can be seen in Appendix B. In MDS anchor nodes are also considered as unknown parameters. These are estimated together with blindfolded nodes by minimizing the cost function in (2.4). Procrustes similarity transformation is used to get same coordinate system as anchor nodes [6, 29]. Procrustes transformation can be made by minimizing the cost function:

$$L(s, \mathbf{t}, \mathbf{T}) = \mathrm{Tr}\left\{ \left[\mathbf{X}_{\text{AN}} - \left(s\hat{\mathbf{X}}_{\text{AN}}\mathbf{T} + \mathbf{1}\mathbf{t}^{\mathrm{T}} \right) \right]^{\mathrm{T}} \left[\mathbf{X}_{\text{AN}} - \left(s\hat{\mathbf{X}}_{\text{AN}}\mathbf{T} + \mathbf{1}\mathbf{t}^{\mathrm{T}} \right) \right] \right\} \tag{2.6}$$

where $\mathbf{T}$ is the reflection matrix such that $\mathbf{T}^{\mathrm{T}}\mathbf{T} = \mathbf{I}$ ($\mathbf{I}$: identity matrix), $\mathbf{1}$ is a vector of all ones, $\mathbf{t}$ is a translation vector, s is scaling factor, $\mathbf{X}_{\text{AN}}$ is the known configuration of anchor nodes and $\hat{\mathbf{X}}_{\text{AN}}$ is the configuration of MDS solution of anchor nodes. Then by using $\mathbf{T}$, s and $\mathbf{t}$ obtained by minimizing (2.6). Final configuration matrix of MDS solution of blindfolded nodes $\hat{\mathbf{X}}_{\text{BN}}$ is transformed into the same coordinate system as $\mathbf{X}_{\text{AN}}$. This transformation can be made by using the information of $\mathbf{T}$, s and $\mathbf{t}$. This can be seen in the following expression

$$\mathbf{X}_{\text{BN-trans}} = s\hat{\mathbf{X}}_{\text{BN}}\mathbf{T} + \mathbf{1}\mathbf{t}^{\mathrm{T}} \tag{2.7}$$

$\mathbf{X}_{\text{BN-trans}}$ is the desired configuration matrix of blindfolded nodes in our localization problem. An implementation of Procrustes transformation can be found in MATLAB Statistics Toolbox.

2.3 Maximum Likelihood Estimation (MLE)

Maximum likelihood estimation is an estimation method that maximizes the a priori likelihood function. MLE has an advantage of being asymptotically efficient and

unbiased [46]. MLE cost function using RSS measurements is given in [29, 34, 36] and the derivation of the MLE cost function can be found in Appendix A. MLE of configuration matrix of blindfolded nodes in 2-D can be obtained by minimizing MLE cost function as follows

$$C_{\text{RSS-MLE}}(\mathbf{X}) = \sum_{i=1}^{n} \sum_{j=i+1}^{N} w_{ij} \left(\log d_{ij} - \log \delta_{ij}\right)^2 \tag{2.8}$$

where n is the number of blindfolded nodes, $N = n + m$ is total number of nodes in the network. Configuration matrix $\mathbf{X} = [\mathbf{r}_1, \mathbf{r}_2, \cdots, \mathbf{r}_N]^{\mathrm{T}}$, $\mathbf{r}_i = [x_i, y_i]^{\mathrm{T}}$ in 2-D space, w_{ij} is connectivity parameter which is indicated in (2.5). δ_{ij} is the pairwise distance measurement parameter between node i and j. As we mentioned in the introduction, we call the MLE cost function which is composed only of terms in the likelihood function corresponding to the connected nodes (i.e., $w_{ij} = 1$) as RSS-MLE in (2.8). Another MLE cost function which we call as h-RSS-MLE, utilizes the information of non-connectivity of the nodes in the cost function. Actually this information is that nodes are so far from the corresponding nodes that no connection is established. h-RSS-MLE cost function can be written as follows [36]

$$\begin{aligned} C_{\text{h-RSS-MLE}}(\mathbf{X}) = & \sum_{i=1}^{n} \sum_{j=i+1}^{N} \frac{1}{2} \left(\frac{10\alpha}{\sigma_v \log 10}\right)^2 w_{ij} \left(\log d_{ij} - \log \delta_{ij}\right)^2 \\ & - (1 - w_{ij}) \log Q(t_{ij}) \end{aligned} \tag{2.9}$$

where $Q(.)$ is the Q-function; $t_{ij} = \left(P_0 - P_{thr} - 10\alpha \log_{10} d_{ij}\right)/\sigma_v$ and P_{thr} is (connectivity) threshold power for the nodes. Note that the second term on the right hand side of (2.9) represents the information that there is no connection between ith and jth nodes. By means of this additional term, even though no RSS measurement is collected from corresponding node, its existence is represented in the h-RSS-MLE cost function to provide the information that ith node is probably far from the corresponding jth node. Another important point to notice is that when one replace $Q(t_{ij})$ by unity (or equivalently $\log Q(t_{ij})$ by zero), h-RSS-MLE cost function reduces into RSS-MLE cost function in (2.8). ML estimation rule for localization of the blindfolded nodes is defined as an optimization problem given as

$$\hat{\mathbf{X}}_{\text{MLE}} = \arg\min_{\mathbf{X}} C_{\text{RSS-MLE,h-RSS-MLE}} \tag{2.10}$$

where $\mathbf{X}$ is the unknown configuration matrix (position matrix) for the blindfolded nodes and $\hat{\mathbf{X}}$ is its estimate. Minimization of MLE cost functions in (2.8) and (2.9) can be made generally through gradient based algorithms. However as it can be seen, MLE cost functions are neither quasi-convex nor convex [48], i.e., it has many local optima beside the global optima. Therefore it is possible to obtain a solution at any local optima by selecting an initial value for optimization. Solution at any local optima except at global one causes some extra error. Especially when the number of nodes increases, possibility of this problem increases. Hence, in general, another estimation rule can be utilized for finding an initial value for the ML optimization problem, such as MDS or multilateration. It is said that MLE cost function is more suitable to our statistical problem than MDS cost function in [29]. It is also stated in [29] that when the variance of pairwise distance measurements are constant, MDS solution is asymptotically efficient as the MLE solution. However statistical parameters of δ_{ij}s are not constant with respect to positions. Mean and variance of pairwise measured distances δ_{ij}s are

$$E(\delta_{ij}) = d_{ij} \exp\left(\frac{\sigma^2}{2}\right) \tag{2.11}$$

$$var(\delta_{ij}) = d_{ij}^2 \left[\exp(\sigma^2) - 1\right] \exp(\sigma^2) \tag{2.12}$$

Suitable weight assignments are proposed in [29] as follows, according to the statistics given above

$$w_{ij} = \begin{cases} \frac{1}{d_{ij}^2}, & \text{if } \delta_{ij} \text{ is observed } (\delta_{ij} \leqslant d_{thr}) \\ 0, & \text{otherwise} \end{cases} \tag{2.13}$$

or

$$w_{ij} = \begin{cases} \frac{1}{d_{ij}}, & \text{if } \delta_{ij} \text{ is observed } (\delta_{ij} \leqslant d_{thr}) \\ 0, & \text{otherwise} \end{cases} \tag{2.14}$$

Actually MDS solution with weights inversely proportional to d_{ij}^2 is asymptotically efficient. But d_{ij}^2s are not available to us. Instead of these, δ_{ij}^2s are used in the algorithms. Other weight assignments in (2.14) can be used to compensate undesired bias resulting from the weight assignments in (2.13). Additionally, an approximation can be made to see which weight assignment of MDS solution can reduce to MLE

solution. The approximation is given by [6].

$$\begin{aligned} C_{\text{RSS-MLE}} &= \sum_{i=1}^{n} \sum_{j=i+1}^{N} \log^2 \left(d_{ij}/\delta_{ij} \right) \\ &\approx \sum_{i=1}^{n} \sum_{j=i+1}^{N} \left(1 - d_{ij}/\delta_{ij} \right)^2 \\ &= C_{\text{MDS}}(\mathbf{X}) \end{aligned} \tag{2.15}$$

In addition to gradient optimization of both ML cost functions (RSS-MLE or h-RSS-MLE), a grid-search method can be utilized in the optimization problem. The most important property of grid-search optimization is that it does not require an initialization. Therefore it can guarantee the global solution of an optimization problem. However it can be ultimately complex compared to the gradient methods. Additionally, gradient methods and grid-search can give different results although they use the same ML cost function. Therefore we call RSS-MLE cost function optimized by grid-search as FSS-MLE in this thesis (or h-FSS-MLE where the non-connectivity information is used like in h-RSS-MLE).

2.4 Weighted Least Squares (WLS)

In this section, we present weighted least squares method for the localization problem. The WLS cost function is given in (2.16).

$$C_{\text{WLS}} = \sum_{i=1}^{n} \sum_{j=i+1}^{N} w_{ij} \left(d_{ij} - \delta_{ij} \right)^2 \tag{2.16}$$

The WLS method has actually the same cost function as MDS method, except the fact that the position of the anchors is also estimated in MDS together with the unknown ones. The WLS method does not require a Procrustes transformation, since the position of the anchors is assumed to be known in the WLS cost function.

2.5 Simulation Results

In this section, first, we compare RSS-MLE and other some existing localization algorithms introduced in previous sections for uniform-grid deployment of the nodes

and four anchors on the corners in 80 m $\times$ 80 m observation area via simulation. Actually the simulation environment does totally fit the scenario created in [29]. Second, another simulation is made to emphasize the reduced bias of h-RSS-MLE in the same simulation environment.

2.5.1 Comparison of the Performance of RSS-MLE and the Other Methods

We have the same scenario as in [29] for simulation, which can be seen in Figure 2.1. The anchors are given on the corners and the others are blindfolded nodes. The simulation parameters are in Table 2.1. 200 Monte Carlo (MC) simulations are per-

Table2.1: Simulation Parameters for Collaborative Localization

Simulation Parameters	Value
Area of node field	80 m $\times$ 80 m
Number of grids	8
Path loss exponent α	3
Standard deviation σ_v	6 dB
RSS threshold power P_{thr}	-80 dBm
First meter RSS power P_0	-30 dBm

formed to obtain the location estimation bias, standard deviation (STD) and root-mean square error (RMSE) values for MLE, weighted MDS, weighted LS, hybrid WLS-MLE (WLS-MLE) and hybrid MDS-MLE (MDS-MLE) methods with performance criteria in Appendix D. MDS-MLE means that output of MDS estimation is given to MLE algorithms as initial values in the optimization problem. In simulations, MDS cost functions with different weights were solved through different optimization methods such as BFGS Quasi-Newton and SMACOF algorithm with random initialization. Note that we have 128 unknowns ($2 \times$ number of all nodes) in this scenario in MDS algorithm with optimization methods SMACOF and BFGS Quasi-Newton algorithm. For WLS-MLE method, three different weighted LS solution ($2 \times n$ unknowns) by BFGS Quasi-Newton (120 unknowns in this scenario) are utilized as initial values for BFGS Quasi-Newton optimization method solving the MLE cost function in (2.8) while three weighted MDS solutions by SMACOF

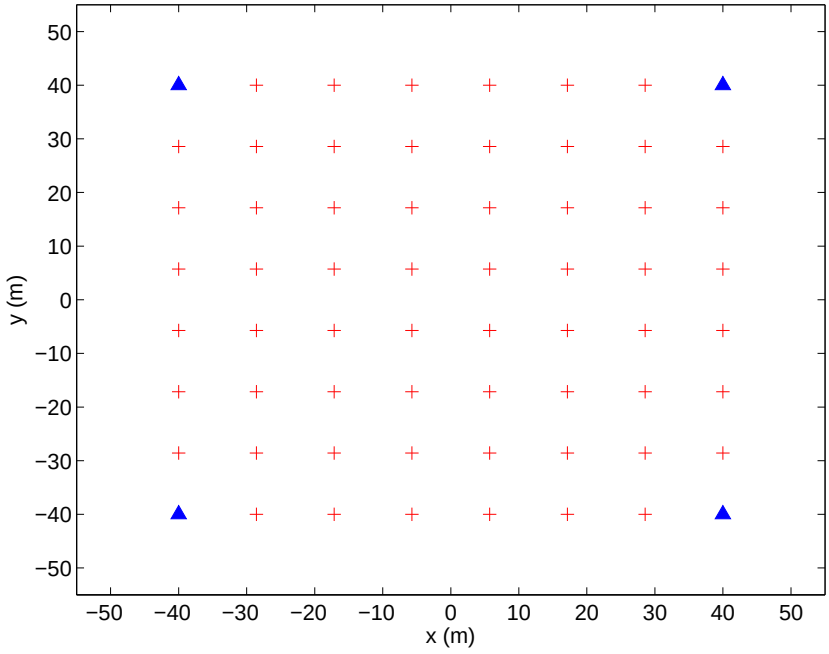

Figure 2.1: Location of the nodes in 80 m $\times$ 80 m: Position of each blindfolded sensor (+), position of the anchors (▲)

algorithm (128 unknowns) and BFGS Quasi-Newton (128 unknowns) are utilized as initial values for MLE. It is observed that MLE with MDS and WLS perform better than MLE with random initialization. It has been also seen that they converge to the solution faster [29]. Finally after obtaining the results, the adaptive neighborhood selection method proposed in [9] is used to compensate the bias. The weights W1, W2 and W3 for MDS and WLS are in (2.5), (2.13) and (2.14) respectively. CRLB is calculated according to the formula given in Appendix C. The performance results related to bias, RMSE, STD and time complexity for MDS with different weight assignments by SMACOF algorithm and RSS-MLE are given in Table 2.2, while the results can be seen in Table 2.3 when MDS cost function is solved by Quasi-Newton method instead of SMACOF algorithm. Table 2.3 compares the performance of WLS and MLE. Additionally the performance results of these localization techniques with adaptive neighborhood selection method are presented in Table 2.5, 2.6 and 2.7. It should also be noted that a computer equipped with a Intel Core i5 1.7 GHz central processing unit and 6 GB RAM is utilized in the simulations. Furthermore, we don't focus on maximizing the performance of the codes in MATLAB for simulations.

Table2.2: 2-D Collaborative Localization Results for MDSs by SMACOF Algorithm and MLE by BFGS Quasi-Newton

Method	Bias (m)	STD (m)	RMSE (m)	Time on Average (s)
MDS(W1)	21.7663	23.9773	32.3834	1.0586
MDS(W2)	17.6229	16.8188	24.3606	0.7163
MDS(W3)	16.73	17.8697	24.4789	0.7122
MLE	19.0465	19.4004	27.1872	24.3456
MDS(W1)-MLE	16.6652	18.8002	25.1233	6.5557
MDS(W2)-MLE	11.3479	13.5890	17.7042	4.7416
MDS(W3)-MLE	12.0078	14.4785	18.81	3.7957
CRLB-MLE	-	5.15	-	-

Table2.3: 2-D Collaborative Localization Results for WLSs by BFGS Quasi-Newton and MLE by BFGS Quasi-Newton

Method	Bias (m)	STD (m)	RMSE (m)	Time on Average (s)
WLS(W1)	11.7366	8.0843	14.2515	2.1485
WLS(W2)	11.9283	6.5738	13.6198	1.7025
WLS(W3)	11.3405	5.9033	12.7850	1.5697
MLE	19.9465	19.4004	27.1872	24.3456
WLS(W1)-MLE	8.3849	8.276	11.7813	4.2297
WLS(W2)-MLE	7.4662	6.4234	9.849	3.0712
WLS(W3)-MLE	7.5093	6.4534	9.9025	2.6938
CRLB-MLE	-	5.15	-	-

Table2.4: 2-D Collaborative Localization Results for MDSs by BFGS Quasi-Newton and MLE by BFGS Quasi-Newton

Method	Bias (m)	STD (m)	RMSE (m)	Time on Average (s)
MDS(W1)	22.129	24.9344	33.3379	3.2352
MDS(W2)	19.306	18.3796	26.6538	3.0345
MDS(W3)	17.6232	19.0976	25.9865	2.8116
MLE	19.0465	19.4004	27.1872	24.3456
MDS(W1)-MLE	16.441	18.3894	24.6673	7.1516
MDS(W2)-MLE	13.15789	15.6514	20.4473	5.5433
MDS(W3)-MLE	13.0356	15.4419	20.2084	4.2263
CRLB-MLE	-	5.15	-	-

Table2.5: 2-D Collaborative Localization Results for MDSs by SMACOF Algorithm and MLE by BFGS Quasi-Newton with Adaptive Neighborhood Selection Method

Method	Bias (m)	STD (m)	RMSE (m)	Time on Average (s)
MDS(W1)	1.8714	24.3344	24.4062	1.3164
MDS(W2)	10.2272	12.6829	16.2916	0.9263
MDS(W3)	4.9499	13.4284	14.3116	0.8558
MLE	8.1616	24.6939	26.0077	39.5641
MDS(W1)-MLE	8.2168	26.3152	27.5682	18.9578
MDS(W2)-MLE	2.4415	14.6201	14.8226	12.8603
MDS(W3)-MLE	2.9773	16.42	16.6878	11.7802
CRLB-MLE	-	5.15	-	-

Table2.6: 2-D Collaborative Localization Results for WLSs by BFGS Quasi-Newton and MLE by BFGS Quasi-Newton with Adaptive Neighborhood Selection Method

Method	Bias (m)	STD (m)	RMSE (m)	Time on Average (s)
WLS(W1)	3.0538	9.8341	10.2973	2.9919
WLS(W2)	8.0826	6.5599	10.4096	2.7522
WLS(W3)	3.4405	5.6101	6.5811	2.3142
MLE	8.1616	24.6939	26.0077	39.5641
WLS(W1)-MLE	0.655	6.1358	6.1706	10.309
WLS(W2)-MLE	0.5633	5.7112	5.7389	7.4268
WLS(W3)-MLE	0.6323	5.7095	5.7444	6.9280
CRLB-MLE	-	5.15	-	-

Table2.7: 2-D Collaborative Localization Results for MDSs by BFGS Quasi-Newton and MLE by BFGS Quasi-Newton with Adaptive Neighborhood Selection Method

Method	Bias (m)	STD (m)	RMSE (m)	Time on Average (s)
MDS(W1)	2.1859	26.1138	26.2052	4.5996
MDS(W2)	11.0131	15.4119	18.9424	4.6819
MDS(W3)	4.9662	14.579	15.4016	3.8832
MLE	8.1616	24.6939	26.0077	39.5641
MDS(W1)-MLE	6.3971	23.0444	23.9159	22.1396
MDS(W2)-MLE	4.3325	19.355	19.834	17.6155
MDS(W3)-MLE	3.1946	16.8319	17.1324	16.228
CRLB-MLE	-	5.15	-	-

Cumulative distribution functions (CDF) of position estimation errors of MDS by SMACOF, MLE and MDS-MLEs are given in Figure 2.2, while cumulative distribution functions of estimation errors of MDS by Quasi-Newton, MLE and MDS-MLEs can be seen in Figure 2.4. Figure 2.3 compares distribution functions of position estimation errors of WLS, MLE and WLS-MLEs. Furthermore the distribution functions of estimation errors of aforesaid localization techniques with adaptive neighborhood selection method can be found in Figures 2.5, 2.6 and 2.7.

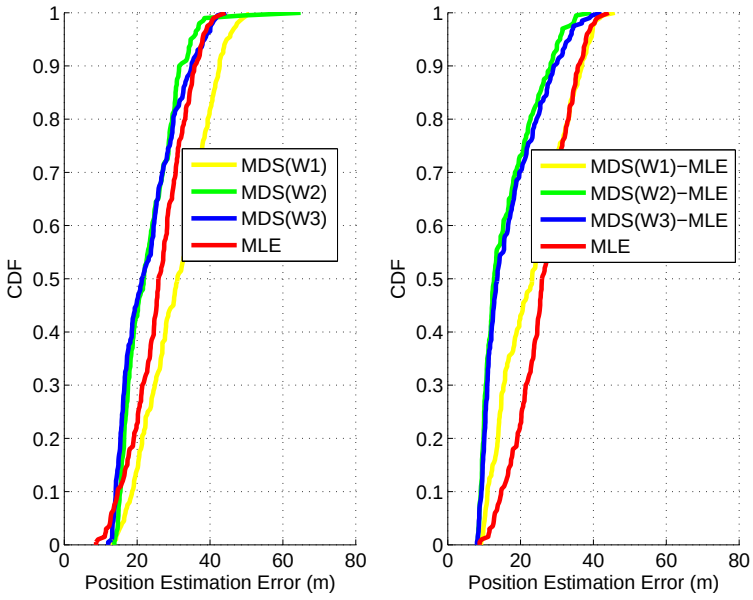

Figure 2.2: CDF of position estimation errors of MDSs by SMACOF algorithm (left) and MDS-MLE (right) without adaptive neighborhood selection method

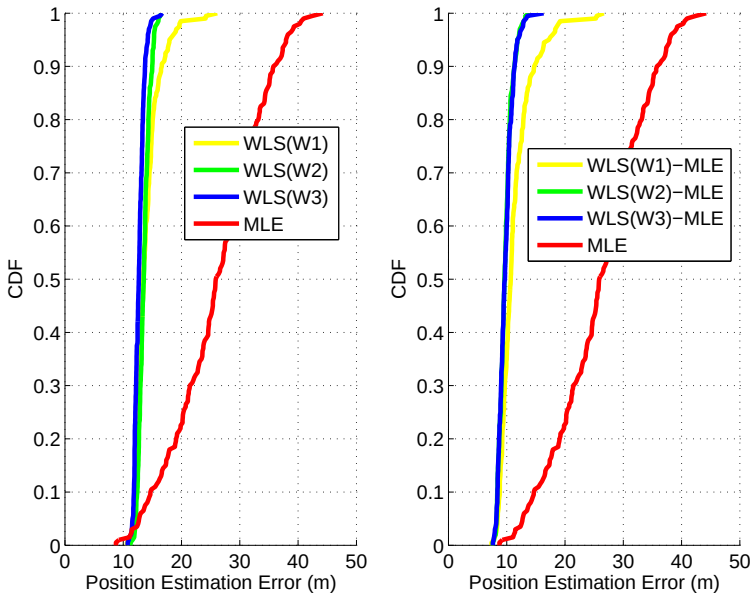

Figure 2.3: CDF of position estimation errors of WLSs by BFGS Quasi-Newton (left) and WLS-MLE (right) without adaptive neighborhood selection method

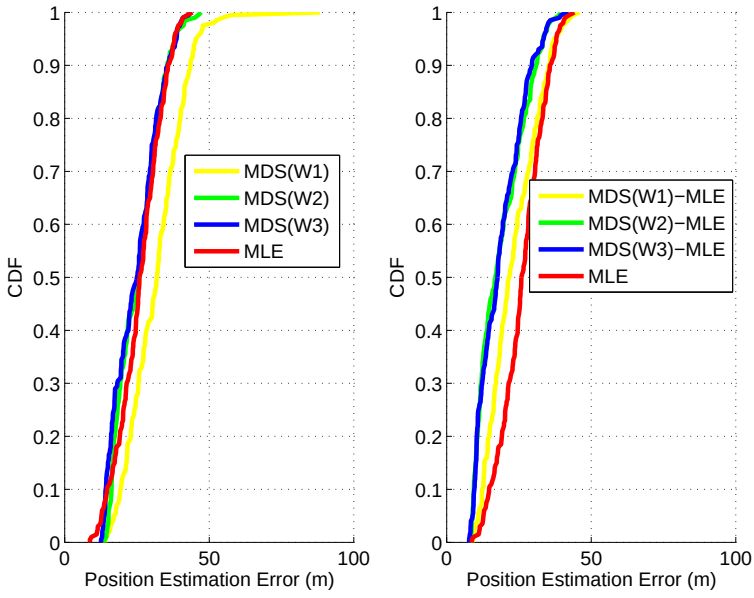

Figure 2.4: CDF of position estimation errors of MDSs by BFGS Quasi-Newton (left) and MDS-MLE (right) without adaptive neighborhood selection method

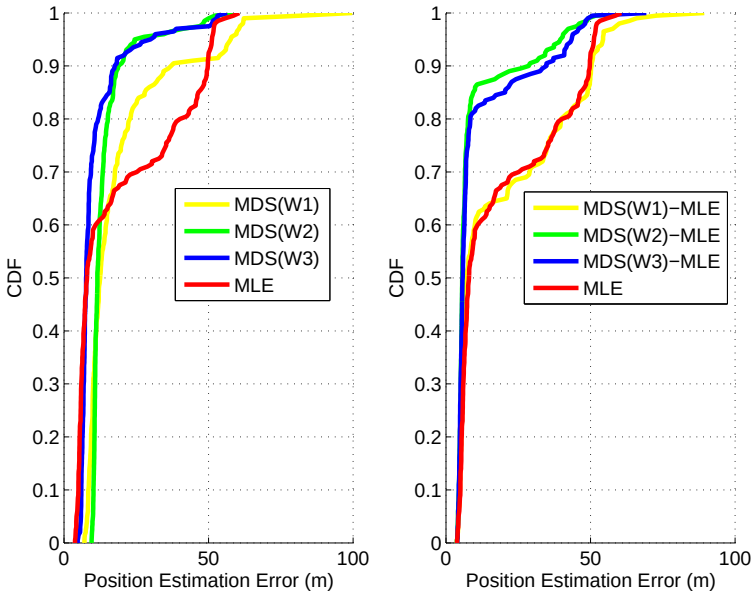

Figure 2.5: CDF of position estimation errors of MDSs by SMACOF algorithm (left) and MDS-MLE (right) with adaptive neighborhood selection method

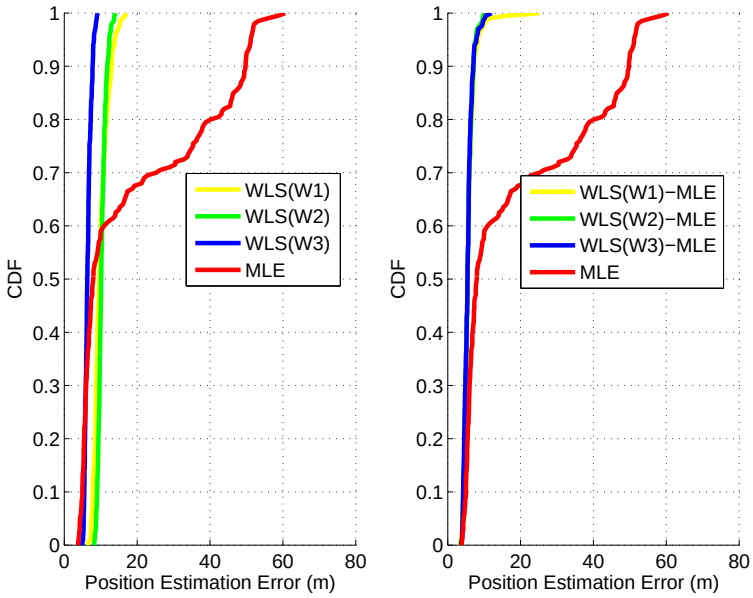

Figure 2.6: CDF of position estimation errors of WLSs by BFGS Quasi-Newton (left) and WLS-MLE (right) with adaptive neighborhood selection method

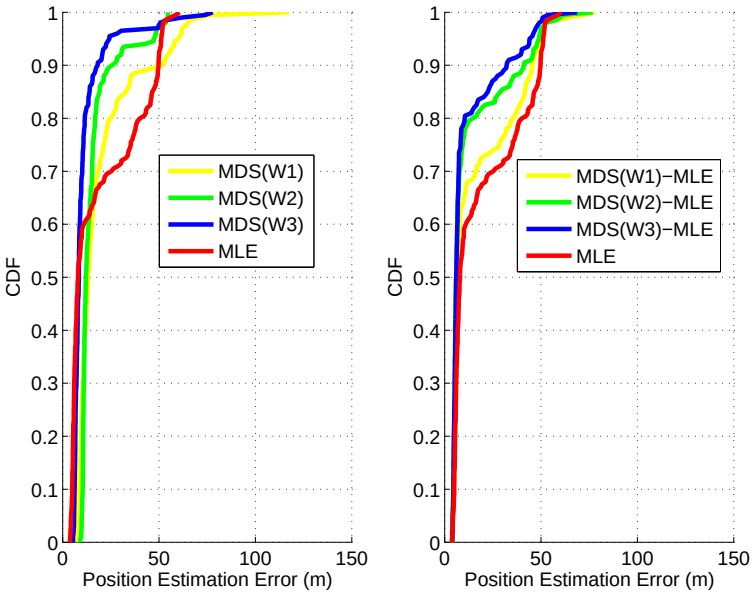

Figure 2.7: CDF of position estimation errors of MDSs by BFGS Quasi-Newton (left) and MDS-MLE (right) with adaptive neighborhood selection method

Based on simulation results, WLS(W3) and WLS(W3)-MLE with adaptive neighborhood selection method have the best results. To obtain better understanding for the performance of the localization methods, a pictorial representation of the error performance, namely 1-σ error ellipses, bias and CRLB ellipses can be provided for each blindfolded node. For that, error ellipses, CRLB and bias of each blindfolded node, whose position is found by WLS(W3) without adaptive neighborhood selection method and with it, can be seen in Figures 2.8 and 2.9 respectively. Moreover a picture related to the error performance of WLS(W3)-MLE without adaptive neighborhood selection method is given in Figure 2.10. Figure 2.11 gives the error ellipses and bias of each node by WLS(W3)-MLE with adaptive neighborhood selection method.

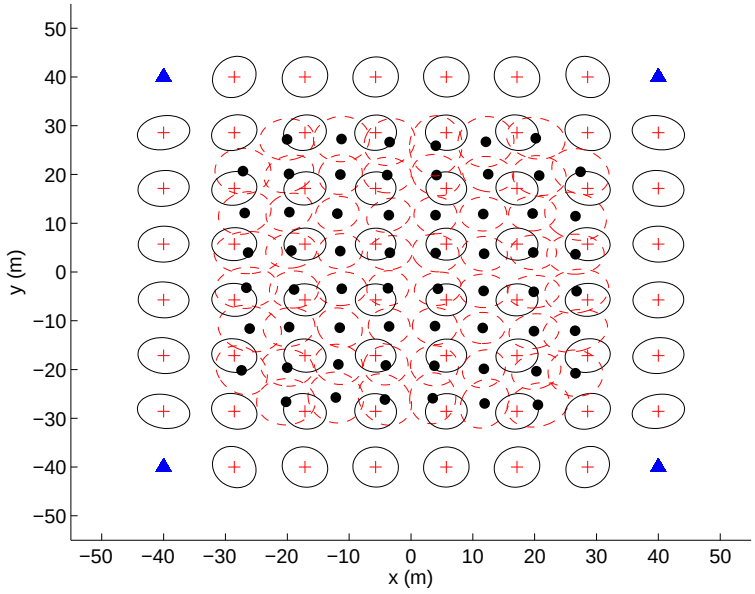

Figure 2.8: 2-D collaborative WLS(W3) localization without adaptive neighborhood selection met.: True position of each blindfolded sensor (+), mean of estimate of each blindfolded node (•), the CRB on the 1-sigma error ellipse (—), 1-sigma error ellipse (− − −) and (▲) points the anchor location

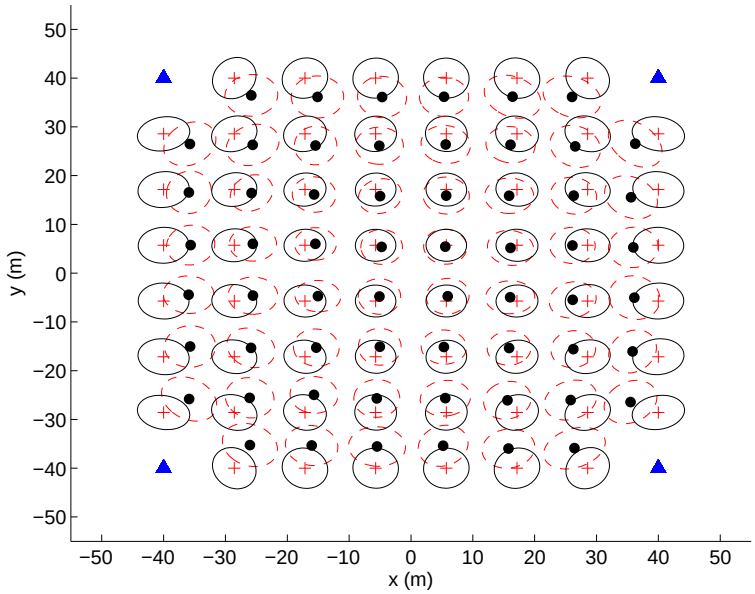

Figure 2.9: 2-D collaborative WLS(W3) localization with adaptive neighborhood selection met.: True position of each blindfolded sensor (+), mean of estimate of each blindfolded node (•), the CRB on the 1-sigma error ellipse (—), 1-sigma error ellipse (− − −) and (▲) points the anchor location

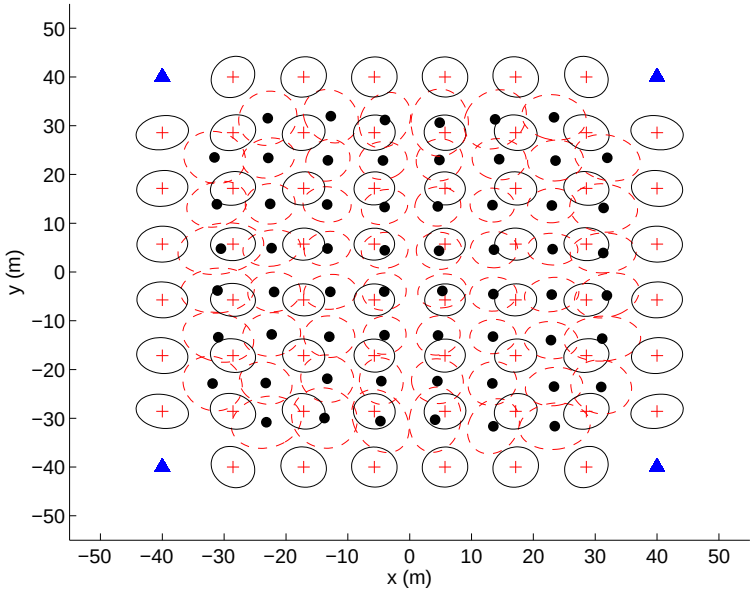

Figure 2.10: 2-D collaborative WLS(W3)-MLE localization without adaptive neighborhood selection met.: True position of each blindfolded sensor (+), mean of estimate of each blindfolded node (•), the CRB on the 1-sigma error ellipse (—), 1-sigma error ellipse (− − −) and (▲) points the anchor location

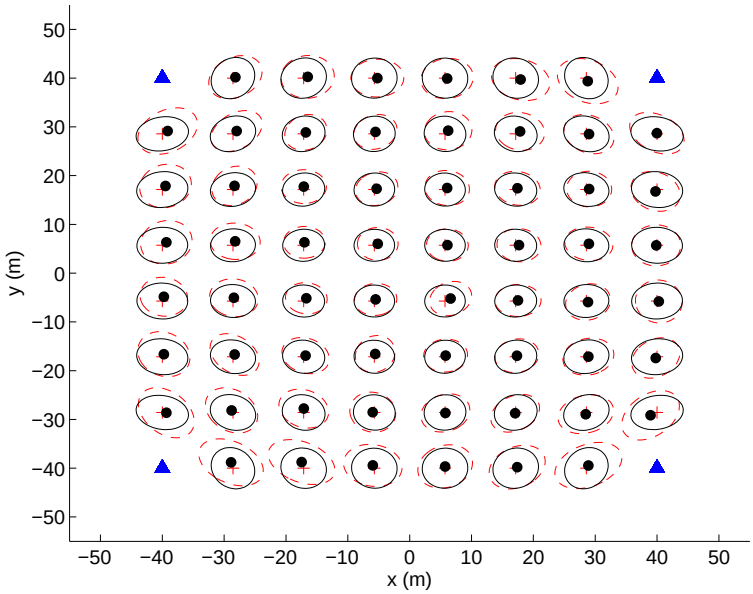

Figure 2.11: 2-D collaborative WLS(W3)-MLE localization with adaptive neighborhood selection met.: True position of each blindfolded sensor (+), mean of estimate of each blindfolded node (•), the CRB on the 1-sigma error ellipse (—), 1-sigma error ellipse (− − −) and (▲) points the anchor location

It can be observed in Figures 2.9 and 2.11 that the bias is reduced by the utilization of the adaptive neighborhood selection method. Furthermore it can also be seen that nodes at the center of the field have 1-σ error ellipse being very close to the CRLB. Error ellipses of the nodes in the corner of the field have a correlation between x and y positions.

2.5.2 Comparison of the Performance of RSS-MLE and h-RSS-MLE

A collaborative localization scenario is considered with four anchors placed at corners of a 80 m $\times$ 80 m area and sixty blindfolded nodes which are placed on a uniform grid as in [29], which is same as in Figure 2.1. A total of 200 MC simulation runs are made. Channel parameters are given in Table 2.1 and the same as in the Section 2.5.1. However the optimization is initialized with true position values of blindfolded nodes in order to get rid of the local optima problem. The results are illustrated in Figures 2.12 and 2.13 where we provide a pictorial presentation of the bias, the RMSE performance and in Table 2.8 where numerical results are presented. The bias statistics provided in Table 2.8 makes it evident that the average bias of RSS-MLE is more than 15 times larger than that of h-RSS-MLE. Moreover, the variance of h-RSS-MLE is a little smaller than that of RSS-MLE which leads to the fact that RMSE of h-RSS-MLE is significantly lower than RSS-MLE.

Table2.8: 2-D Collaborative Localization Results for RSS-MLE and h-RSS-MLE

Estimation Method	**Overall Bias (m)**	**STD (m)**	**RMSE (m)**
RSS-MLE	7.09	5.59	9.02
h-RSS-MLE	0.38	5.31	5.32
CRB for RSS-MLE	-	5.15	-
CRB for h-RSS-MLE	-	4.77	-

The incorporation of the non-connectivity information into the ML cost is, on the average, expected to let the ML estimator know the fact that a blindfolded sensor is far from the anchors with which connectivity could not be achieved. Therefore, the addition of these terms would have the effect of pushing the estimate away from the

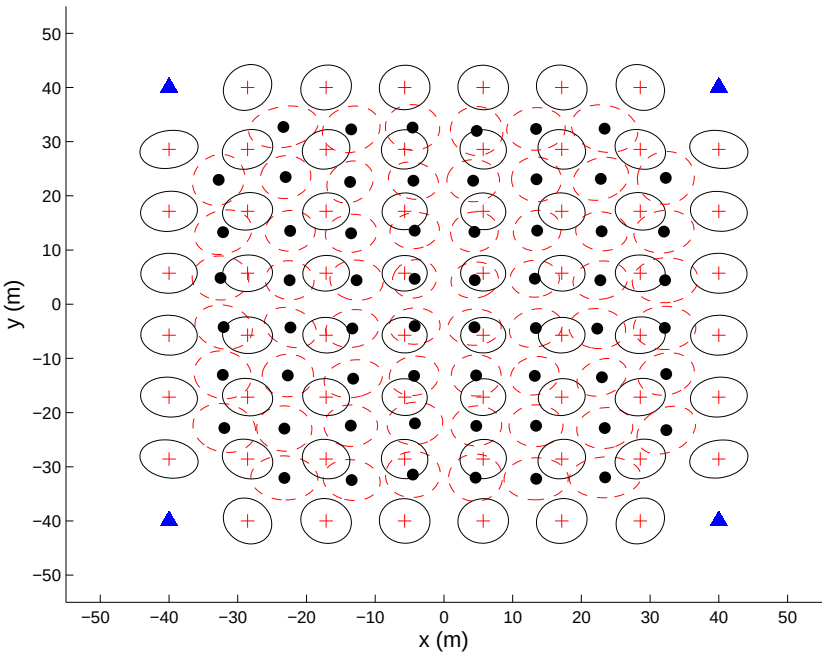

Figure 2.12: 2-D collaborative RSS-MLE localization: True position of each blindfolded sensor (+), mean of estimate of each blindfolded node (•), the CRB on the 1-sigma error ellipse (—), 1-sigma error ellipse (− − −) and (▲) points the anchor location

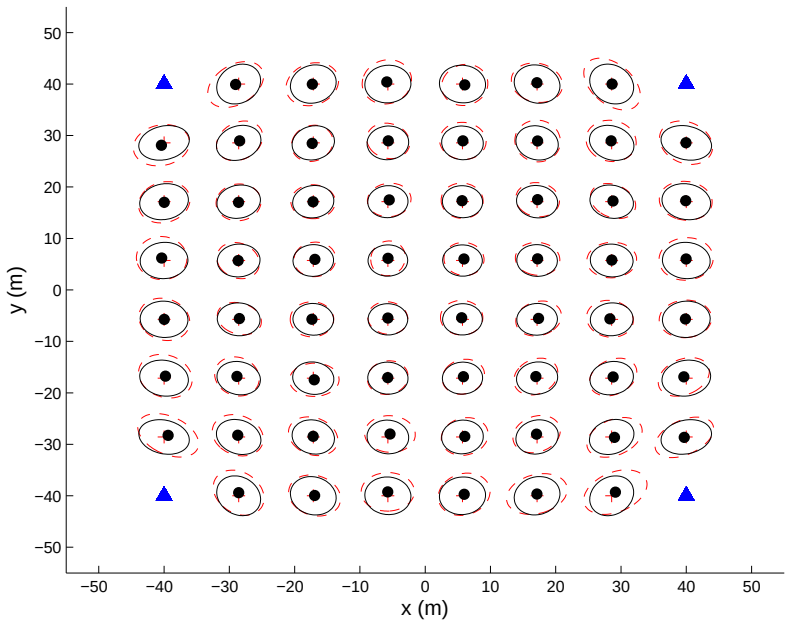

Figure 2.13: 2-D collaborative h-RSS-MLE localization: True position of each blindfolded sensor (+), mean of estimate of each blindfolded node (•), the CRB on the 1-sigma error ellipse (—), 1-sigma error ellipse (− − −) and (▲) points the anchor location

unconnected anchors. Our simulation results show on the average that the estimates of RSS-MLE, which does not use the non-connectivity terms in its cost function, are biased towards the possibly unconnected anchors. As the number of unconnected anchors increase, so does the bias as clearly shown in Figures 2.12 and 2.13 with bias increasing towards the edges of the region of interest. Hence, the addition of the non-connectivity terms into the cost function of h-RSS-MLE compensates for these undesirable effects. To our best knowledge, this compensation effect has not been reported in the literature before.

The reduction of bias has critical importance especially for tracking applications. Kalman filtering methods used in target tracking could, in theory, reduce the high variance in the measurements by using "averaging in time". However a significant bias in the measurements would always appear in Kalman filter estimates if not compensated. Hence reducing the bias has utmost importance for accurate dynamic estimation.

It should be noted that we have observed that h-RSS-MLE definitely reduces the bias in collaborative localization only for a uniform-grid deployment scenario of the nodes as in Figure 2.1. Therefore one non-collaborative simulation environment must be created to confirm the advantage of h-RSS-MLE over RSS-MLE. The related parameters are enlisted in Table 2.9. Besides RSS-MLE and h-RSS-MLE, we evaluated

Table2.9: Simulation Parameters for Non-Collaborative Localization

Simulation Parameters	Value
Area of node field	10 m $\times$ 10 m
Number of anchors	4
Path loss exponent α	3
Standard deviation σ_v	6 dB
RSS threshold power P_{thr}	-65 dBm
First meter RSS power P_0	-30 dBm
Number of MC Run	2000

FSS-MLE and h-FSS-MLE in the simulation study to reach the global solution of the ML cost functions. For that, we searched the solution for ML cost functions in two

different search spaces which are 10 m $\times$ 10 m and 100 m $\times$ 100 m respectively. We suppose that FSS-MLE or h-FSS-MLE will be the same as RSS-MLE or h-RSS-MLE when the area of search space is large enough. That is the reason why we chose 100 m $\times$ 100 m as the area of search space for simulations addition to 10 m $\times$ 10 m. We also would like to see the difference between localization techniques, FSS-MLE and RSS-MLE (or h-FSS-MLE and h-RSS-MLE), by choosing these search spaces. Anchors are located on the corners of 10 m $\times$ 10 m area and their coordinates are (0,0), (0,10), (10,0) and (10,10). Blindfolded nodes are placed inside the area of 10 m $\times$ 10 m. The placement of nodes are given in Figure 2.14 as follows

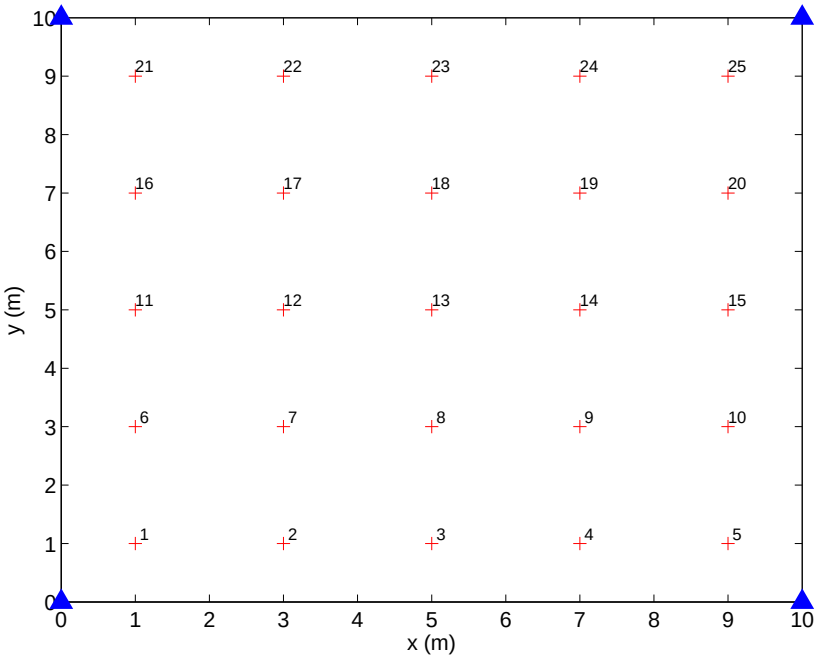

Figure 2.14: Location of the nodes in 10 m $\times$ 10 m: Position of each blindfolded sensor (+), position of the anchors (▲)

For each numbered node (blindfolded node), a MC simulation is made to obtain bias and RMSE values of FSS-MLE and h-FSS-MLE techniques having different areas of search space. Figures 2.15, 2.16 and 2.17 present the bias of FSS-MLE and h-FSS-MLE. Furthermore RMSE performance of FSS-MLE and h-FSS-MLE is given in Figure 2.18.

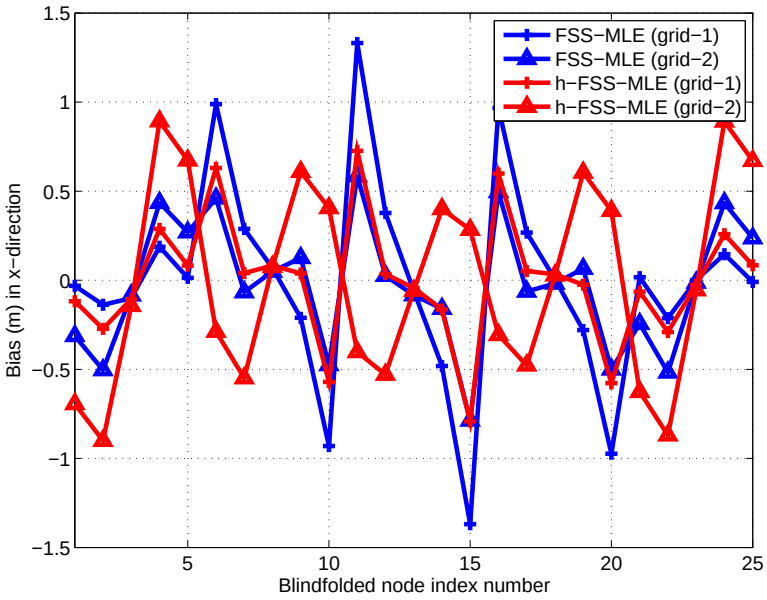

Figure 2.15: Bias performance of non-collaborative FSS-MLE and h-FSS-MLE localization of blindfolded nodes given in Figure 2.14 in x-axis: FSS-MLE (grid-1) (-+), FSS-MLE (grid-2) (-▲), h-FSS-MLE (grid-1) (-+), h-FSS-MLE (grid-2) (-▲) where grid-1: 10 m $\times$ 10 m and grid-2: 100 m $\times$ 100 m

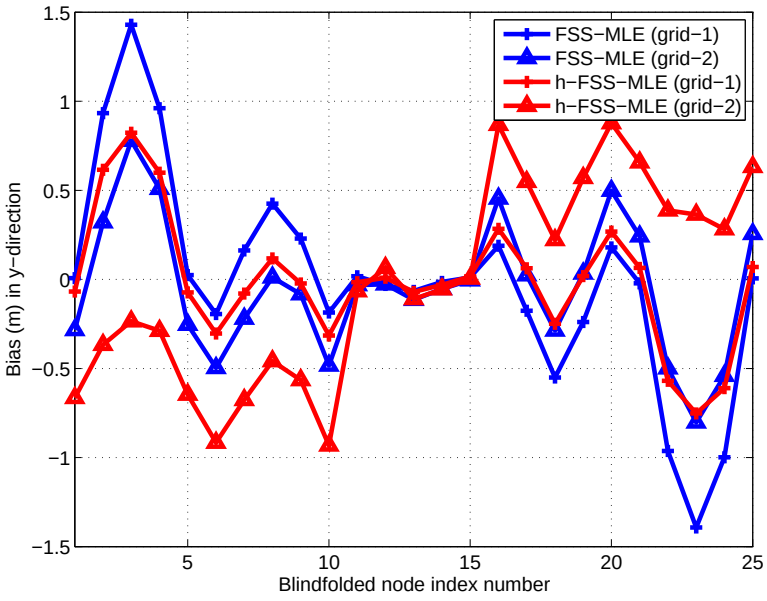

Figure 2.16: Bias performance of non-collaborative FSS-MLE and h-FSS-MLE localization of blindfolded nodes given in Figure 2.14 in y-axis: FSS-MLE (grid-1) (-+), FSS-MLE (grid-2) (-▲), h-FSS-MLE (grid-1)(-+), h-FSS-MLE (grid-2) (-▲) where grid-1: 10 m $\times$ 10 m and grid-2: 100 m $\times$ 100 m

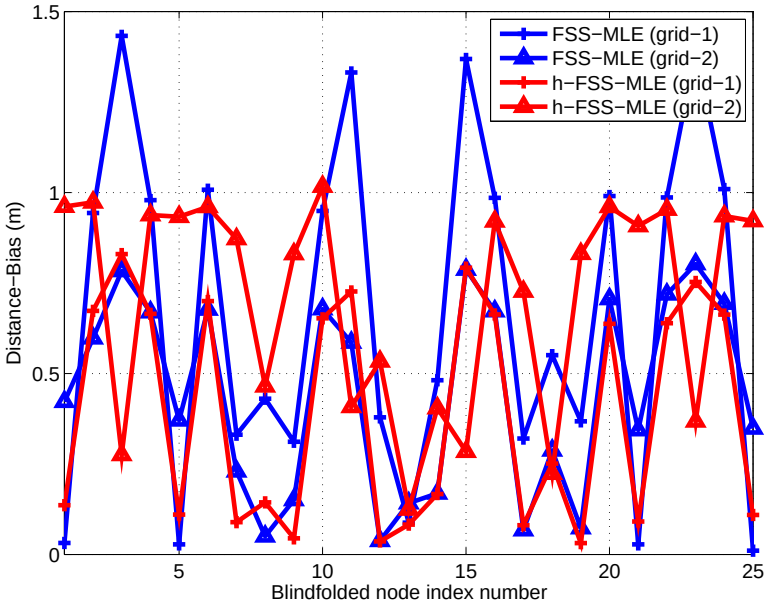

Figure 2.17: Bias performance of non-collaborative FSS-MLE and h-FSS-MLE localization of blindfolded nodes given in Figure 2.14 in distance: FSS-MLE (grid-1) (-+), FSS-MLE (grid-2) (-▲), h-FSS-MLE (grid-1) (-+), h-FSS-MLE (grid-2) (-▲) where grid-1: 10 m $\times$ 10 m and grid-2: 100 m $\times$ 100 m

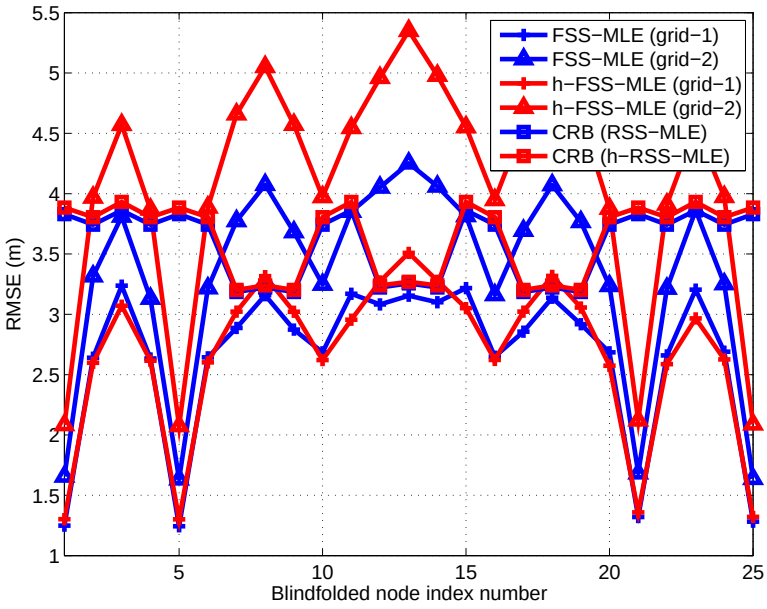

Figure 2.18: RMSE performance of non-collaborative FSS-MLE and h-FSS-MLE localization of blindfolded nodes given in Figure 2.14: FSS-MLE (grid-1) (-+), FSS-MLE (grid-2) (-▲), h-FSS-MLE (grid-1) (-+), h-FSS-MLE (grid-2) (-▲), CRB (RSS-MLE) (-■), CRB (h-RSS-MLE) (-■) where grid-1: 10 m $\times$ 10 m and grid-2: 100 m $\times$ 100 m

As it is seen in the bias curves (Figures 2.15, 2.16 and 2.17), bias reduction property of h-RSS-MLE in 2-D collaborative localization with uniform grid placement scenario of nodes given in previous section cannot be observed in non-collaborative scenarios. Namely the non-connectivity information between related blindfolded node and anchors does not always help maximum likelihood estimator reduce the bias and RMSE, although h-RSS-MLE gives an information about the unconnected anchor, e.g., a peak value in cost function around the related anchor. A picture that characterizes this relation is given in Figure 2.19.

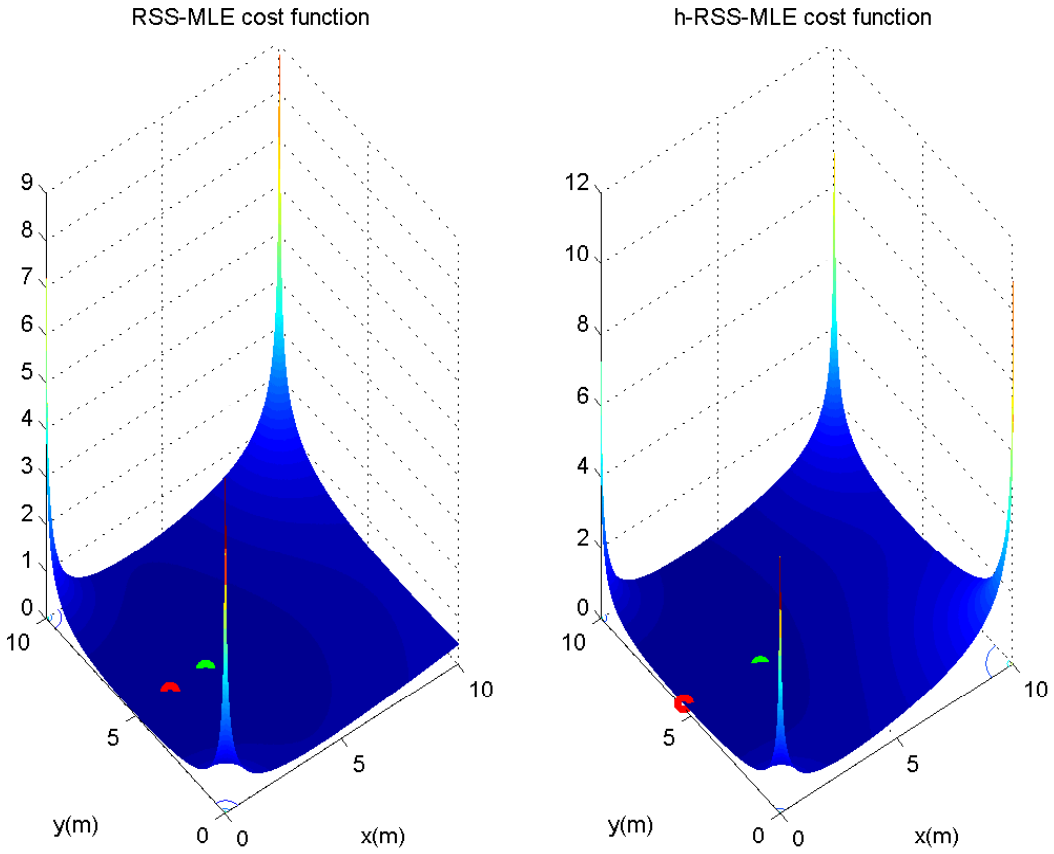

Figure 2.19: Comparison of RSS-MLE (left) and h-RSS-MLE (right) cost functions obtained in one realization: Blindfolded node at (3,5) (●) and estimated position of blindfolded node (●)

It is important to state that the anchors on (0,0), (0,10) and (10,10) are connected to the blindfolded node. Due to the fact that the cost function has a maximum point

around the position of the anchors as reported in [38], we can state that an unconnected anchor with the information of probability of non-connectivity is treated like a pseudo-anchor by looking at Figure 2.19. Our expectation would be that h-RSS-MLE is always better than RSS-MLE in this situation, since more anchor-related information is fused in its cost function. However additional information coming from unconnected anchors does sometimes worsen the estimator as given in Figure 2.19 in non-collaborative localization. Additionally it can be said that FSS-MLE (or h-FSS-MLE) can give different results depending on search space, when we compare the results in Figures 2.15-2.18. Due to that, it can be also said that FSS-MLE can be considered as a maximum a posteriori (MAP) estimator including a prior knowledge about the position to be estimated, i.e., finite search space.

CHAPTER 3

TRACKING

In this chapter, some tracking methods based on RSS measurements are introduced and their performances are compared to each other in simulation and experimental study.

In tracking, the purpose is to estimate the dynamic state (e.g., position, velocity) of an observed object by considering some dynamic and sensor models. The state model including the kinematic model and the measurement model is given in (3.1). Some conventional tracking methods exist in the literature [4, 18] (e.g., Kalman filter (KF), the extended Kalman filter (EKF) and particle filter (PF)). All of these approaches try to find the estimate of state $x_{k|k}$ as indicated in (3.2). Consider the model below

$$\begin{aligned} x_{k+1} =& f(x_k) + w_k \\ y_k =& h(x_k) + v_k \end{aligned} \tag{3.1}$$

where

- $x_k \in \mathbb{R}^{n_x}$ is the state with the initial state $x_0 \sim p(x_0)$;
- $y_k \in \mathbb{R}^{n_y}$ is the measurement;
- $w_k \in \mathbb{R}^{n_x}$ is the white process noise with a known distribution $p(w)$ independent from x_k;
- $v_k \in \mathbb{R}^{n_y}$ is the white measurement noise with a known distribution $p(v)$ independent from x_k.

The aim is to find the posterior density of the state $p(x_k|y_{1:k})$ where

$$y_{1:k} \triangleq \{y_1, y_1, \ldots, y_k\}.$$

Then state estimate $\hat{x}_{k|k}$ can be found as

$$\hat{x}_{k|k}^{\text{MMSE}} = E\left[x_k|y_{1:k}\right] \tag{3.2}$$

3.1 Kalman Filter (KF)

Consider the linear model below:

$$\begin{aligned} x_{k+1} &= Ax_k + w_k \\ y_k &= Cx_k + v_k \end{aligned} \tag{3.3}$$

with $w_k \sim \mathcal{N}(w_k; 0, Q)$, $v_k \sim \mathcal{N}(v_k; 0, R)$ and $x_0 \sim \mathcal{N}(x_0; \hat{x}_{0|0}, P_{0|0})$. By considering the linearity of measurement and process models above and Gaussian measurement and process noises, it can be shown that all posterior densities and likelihood functions are Gaussian.

- $p(x_k|y_{1:k-1}) = \mathcal{N}(x_k; \hat{x}_{k|k-1}, P_{k|k-1})$
- $p(y_k|y_{1:k-1}) = \mathcal{N}(y_k; \hat{y}_{k|k-1}, S_{k|k-1})$
- $p(x_k|y_{1:k}) = \mathcal{N}(x_k; \hat{x}_{k|k}, P_{k|k})$
- $p(y_k|x_k) = \mathcal{N}(y_k; Cx_k, R)$
- $p(x_k|x_{k-1}) = \mathcal{N}(x_k; Ax_{k-1}, Q)$

It is known that the sufficient statistics is the mean and covariance in Gaussian densities. Therefore infinite dimensional estimation problem turns into a finite dimensional estimation problem. Kalman filter (KF) is optimum under the assumption of independent Gaussian noise and the linearity of the model [18]. Kalman filter algorithm can be seen in Table 3.1 which is directly taken from [32].

Table3.1: Kalman Filter [32]

- Start with $\hat{x}_{0|0}$, $P_{0|0}$, set $k = 1$.
- For each k:
  - Prediction Update

$$\begin{aligned}\hat{x}_{k|k-1} =& A\hat{x}_{k-1|k-1}\\ P_{k|k-1} =& AP_{k-1|k-1}A^{\mathrm{T}} + Q\end{aligned}$$

  - Measurement Update

$$\begin{aligned}\hat{x}_{k|k} =& \hat{x}_{k|k-1} + K_k(y_k - \hat{y}_{k|k-1})\\ P_{k|k} =& P_{k|k-1} - K_k S_{k|k-1} K_k^{\mathrm{T}}\end{aligned}$$

    where

$$\begin{aligned}\hat{y}_{k|k-1} =& C\hat{x}_{k|k-1}\\ S_{k|k-1} =& CP_{k|k-1}C^{\mathrm{T}} + R\\ K_k =& P_{k|k-1}C^{\mathrm{T}}S_{k|k-1}^{-1}\end{aligned}$$

3.2 Extended Kalman Filter (EKF)

Many important real world applications involve models which are nonlinear and non-Gaussian, so Kalman filter cannot be applied directly. A very common approach is the linearization of the state space model (Taylor series expansion) to apply Kalman filter. This filter is called extended Kalman filter (EKF) [4, 18]. If the nonlinearity of the model is mild, EKF can give good results. The algorithm can be found in Table 3.2 which has been totally taken from [32]. Additionally, two versions of extended Kalman filter [5], i.e., serial and parallel EKF, can be formed according to EKF algorithm in Table 3.2. These variants of EKF are provided in Table 3.3 and Table 3.4 respectively. In parallel EKF, all measurements are processed together simultaneously by augmenting them in a measurement vector. On the other hand, the measurements are sorted according to their strength and iteratively processed in serial EKF. In addition to extended Kalman filtering, another tracking method using the Gaussian assumption for posterior density is unscented Kalman filter (UKF) in non-

Table3.2: Extended Kalman Filter [32]

- Start with $\hat{x}_{0|0}$, $P_{0|0}$, set $k = 1$.
- For each k
  - Prediction Update

$$\begin{aligned}\hat{x}_{k|k-1} =& f(\hat{x}_{k-1|k-1})\\ P_{k|k-1} =& F P_{k-1|k-1} F^{\mathrm{T}} + Q\end{aligned}$$

    where $F = \frac{\partial f}{\partial x_{k-1}}|_{x_{k-1}=\hat{x}_{k-1|k-1}}$.
  - Measurement Update

$$\begin{aligned}\hat{x}_{k|k} =& \hat{x}_{k|k-1} + K_k(y_k - \hat{y}_{k|k-1})\\ P_{k|k} =& P_{k|k-1} - K_k S_{k|k-1} K_k^{\mathrm{T}}\end{aligned}$$

    where

$$\begin{aligned}\hat{y}_{k|k-1} =& h(\hat{x}_{k|k-1}) \qquad S_{k|k-1} = H P_{k|k-1} H^{\mathrm{T}} + R\\ K_k =& P_{k|k-1} H^{\mathrm{T}} S_{k|k-1}^{-1}\end{aligned}$$

    with $H = \frac{\partial h}{\partial x_k}|_{x_k=\hat{x}_{k|k-1}}$.

---

linear estimation problems [23]. This filter approximates the posterior density as in EKF as Gaussian, but this approximation is made through deterministically chosen sigma points with corresponding weights from the posterior density. The main idea is to calculate the first and second order statistics from a nonlinear function of deterministically chosen sigma points (samples). It can be more suitable than EKF due to some limitations stated in [23]. Finally these two filters, EKF and UKF, do generally work well in the case of mild nonlinearities and relatively low uncertainties.

Table3.3: Serial Extended Kalman Filter

- Start with $\hat{x}_{0|0}$, $P_{0|0}$, set $k = 1$.
- For each k
  - Prediction Update

$$\begin{aligned}\hat{x}_{k|k-1} =& f(\hat{x}_{k-1|k-1}) \\ P_{k|k-1} =& F P_{k-1|k-1} F^{\mathrm{T}} + Q\end{aligned}$$

    where $F = \frac{\partial f}{\partial x_{k-1}}|_{x_{k-1}=\hat{x}_{k-1|k-1}}$.
  - Sort the measurements such that $y_k = [\ y_{max} \quad \cdots \quad y_{min}\ ]$
  - set $i = 1$, **while** $i \leqslant N$ **do**
    - Measurement Update

$$\begin{aligned}\hat{x}_{k|k-1} =& \hat{x}_{k|k-1} + K_k(y_{k,i} - \hat{y}_{k|k-1}) \\ P_{k|k-1} =& P_{k|k-1} - K_k S_{k|k-1} K_k^{\mathrm{T}}\end{aligned}$$

      where

$$\begin{aligned}\hat{y}_{k|k-1} =& h_i(\hat{x}_{k|k-1}) \\ S_{k|k-1} =& H_i P_{k|k-1} H_i^{\mathrm{T}} + R \\ K_k =& P_{k|k-1} H_i^{\mathrm{T}} S_{k|k-1}^{-1}\end{aligned}$$

      with $H_i = \frac{\partial h_i}{\partial x_k}|_{x_k=\hat{x}_{k|k-1}}$
      which is linearized matrix for ith anchor corresponding to the measurement $y_{k,i}$
      end while

$$\begin{aligned}\hat{x}_{k|k} &= \hat{x}_{k|k-1} \\ P_{k|k} &= P_{k|k-1}\end{aligned}$$

Table3.4: Parallel Extended Kalman Filter

- Start with $\hat{x}_{0|0}$, $P_{0|0}$, set $k = 1$.
- For each k
  - Prediction Update

$$\begin{aligned}\hat{x}_{k|k-1} =& f(\hat{x}_{k-1|k-1}) \\ P_{k|k-1} =& F P_{k-1|k-1} F^{\mathrm{T}} + Q\end{aligned}$$

    where $F = \frac{\partial f}{\partial x_{k-1}}|_{x_{k-1}=\hat{x}_{k-1|k-1}}$
  - $h = \begin{bmatrix} h_1 & h_2 & \cdots & h_N \end{bmatrix}^{\mathrm{T}}$ for N number of measurements
  - $y_k = \begin{bmatrix} y_1 & y_2 & \cdots & y_N \end{bmatrix}^{\mathrm{T}}$: measurement vector
  - Measurement Update

$$\begin{aligned}\hat{x}_{k|k} =& \hat{x}_{k|k-1} + K_k(y_k - \hat{y}_{k|k-1}) \\ P_{k|k} =& P_{k|k-1} - K_k S_{k|k-1} K_k^{\mathrm{T}}\end{aligned}$$

    where

$$\begin{aligned}\hat{y}_{k|k-1} =& h(\hat{x}_{k|k-1}) \qquad S_{k|k-1} = H P_{k|k-1} H^{\mathrm{T}} + R \\ K_k =& P_{k|k-1} H^{\mathrm{T}} S_{k|k-1}^{-1}\end{aligned}$$

    with $H = \frac{\partial h}{\partial x_k}|_{x_k=\hat{x}_{k|k-1}}$.

3.3 Particle Filter (PF)

The particle filter method tries to approximate the original posterior density of state x_k given measurements $y_{1:k} \triangleq \{y_1, y_1, \ldots, y_k\}$. As in unscented Kalman filtering, it utilizes the samples of the posterior density, but these samples are chosen randomly. These samples are called particles in the literature. Although many variants of particle filters exist, we use the SIR (Sequential Importance Resampling) particle filter. It is stated that particle filter has more immunity to nonlinearities of models than EKF and UKF. More information about particle filters can be obtained in [17, 20]. The algorithm can be found in Table 3.5. Note that it has been taken from [32].

- Resampling: The weights in a particle filter converges to all zero except for a single nonzero weight without resampling [17]. The resampling process deletes the particles with relatively small weights and generate new particle from the particles having high weights. The process is repeated in each iteration of SIR particle filter. At the end of resampling, all particle weights become identical. Note that we applied multinomial resampling algorithm which is presented in [17] for our tracking problem in the simulation and experimental study.

Table3.5: SIR Particle Filter [32]

- Start with $x_{0|0}^{(i)} \sim p(x_0)$, $\pi_{0|0}^{(i)} = 1/N$ for $i = 1, \ldots, N$, set $k = 1$.
- For each k
  - Prediction Update
    - Sample process noise $w_{k-1}^{(i)} \sim p(w_{k-1})$.
    - Set the predicted particles and weights as

$$x_{k|k-1}^{(i)} = f\left(x_{k-1|k-1}^{(i)}\right) + w_{k-1}^{(i)} \qquad \pi_{k|k-1}^{(i)} = \pi_{k-1|k-1}^{(i)}$$

      for $i = 1, \ldots, N$.
    - Obtain the predicted state estimate $\hat{x}_{k|k-1}$ and its covariance $P_{k|k-1}$ as

$$\hat{x}_{k|k-1} = \sum_{i=1}^{N} \pi_{k|k-1}^{(i)} x_{k|k-1}^{(i)}$$

$$P_{k|k-1} = \sum_{i=1}^{N} \pi_{k|k-1}^{(i)} \left(x_{k|k-1}^{(i)} - \hat{x}_{k|k-1}\right)\left(x_{k|k-1}^{(i)} - \hat{x}_{k|k-1}\right)^{\mathrm{T}}$$

  - Measurement Update
    - Set the estimated particles and weights as

$$x_{k|k}^{(i)} = x_{k|k-1}^{(i)}$$

$$\pi_{k|k}^{(i)} = \frac{\tilde{\pi}_{k|k}^{(i)}}{\sum_{i=1}^{N} \tilde{\pi}_{k|k}^{(i)}}$$

      for $i = 1, \ldots, N$ where

$$\tilde{\pi}_{k|k}^{(i)} = \pi_{k|k-1}^{(i)} p\left(y_k \left| x_{k|k}^{(i)} \right.\right)$$

    - Obtain the state estimate $\hat{x}_{k|k}$ and its covariance $P_{k|k}$ as

$$\hat{x}_{k|k} = \sum_{i=1}^{N} \pi_{k|k}^{(i)} x_{k|k}^{(i)}$$

$$P_{k|k} = \sum_{i=1}^{N} \pi_{k|k}^{(i)} \left(x_{k|k}^{(i)} - \hat{x}_{k|k}\right)\left(x_{k|k}^{(i)} - \hat{x}_{k|k}\right)^{\mathrm{T}}$$

3.4 Simulation Results

The anchors and blindfolded node trajectory can be seen in Figure 3.1. The blindfolded node trajectory is generated by a random-walk model. 1000 MC simulation runs are made to find bias and RMSE values of static localization and filters. The filters are KF, serial and parallel EKFs and SIR particle filter. For static localization, non-collaborative MLE cost function is solved through grid-search as the optimization method, since it is important for MLE not to be affected by the local optima problem, which plays a critical role in performance. In KF, the output values of static localization are used as measurement. CRLBs at the estimate position are utilized as measurement covariance. RSS values are our measurements in EKF and SIR PF. Additionally, connectivity according to P_{thr} is considered in all filters. The simulation parameters are given in Table 3.6. The measurement model is in (2.1) which is $h(.)$

Table3.6: Simulation Parameters for Non-Collaborative Tracking

Simulation Parameters	Value
Path loss exponent α	3
Standard deviation σ	6 dB
RSS threshold power P_{thr}	-63,-80 dBm
First meter RSS power P_0	-30 dBm

in (3.1). We have a linear process model given in .

$$\mathbf{x}_k = \begin{bmatrix} \mathbf{I}_2 & T\mathbf{I}_2 \\ \mathbf{0}_2 & \mathbf{I}_2 \end{bmatrix} \mathbf{x}_{k-1} + \begin{bmatrix} \frac{T^2}{2}\mathbf{I}_2 \\ T\mathbf{I}_2 \end{bmatrix} \mathbf{w}_k \tag{3.4}$$

where $\mathbf{I}_2$ and $\mathbf{0}_2$ are identity and zero matrices with 2 x 2 respectively, T is sampling period and $\mathbf{w}_k$ is process noise which is assumed to be $\mathcal{N}(\mathbf{w}_k; 0, \mathbf{Q})$. Filters are initialized as follows

$$\hat{\mathbf{x}}_{0|0} = \begin{bmatrix} \hat{\mathbf{x}}_{\text{RSS-MLE,h-RSS-MLE}} & 0 & 0 \end{bmatrix} \tag{3.5}$$

$$\mathbf{P}_{0|0} = \begin{bmatrix} \mathbf{CRLB}|_{\hat{x}_{\text{RSS-MLE,h-RSS-MLE}}} & \mathbf{0}_2 \\ \mathbf{0}_2 & 0.25^2\mathbf{I}_2 \end{bmatrix} \tag{3.6}$$

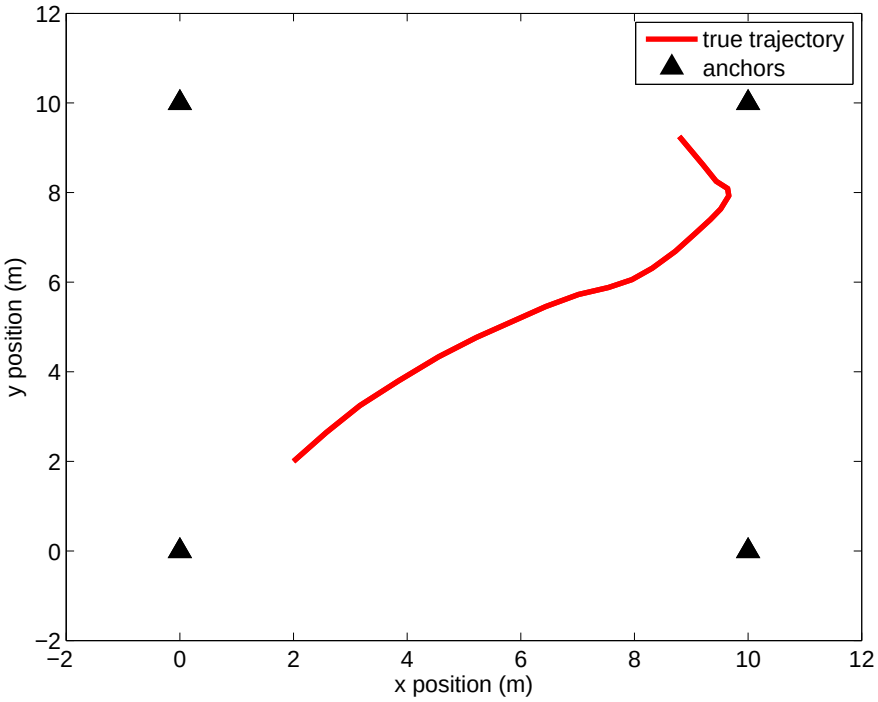

Figure 3.1: True trajectory and positions of the anchors

For Kalman filter, measurement noise covariance :

$$\mathbf{R} = \mathbf{CRLB}|_{\hat{\mathbf{x}}_{\text{RSS-MLE,h-RSS-MLE}}} \tag{3.7}$$

For other filters, measurement noise covariance :

$$\mathbf{R} = \sigma^2 \mathbf{I}_m \tag{3.8}$$

where m is the number of anchors. The process noise covariance is

$$\mathbf{Q} = 0.3^2 \mathbf{I}_2 \tag{3.9}$$

Figures 3.2 and 3.3 give the bias results for different P_{thr} (-63, -80 dBm). Furthermore, Figures 3.4 and 3.5 present the RMSE performance of the filters for P_{thr} (-63, -80 dBm). The cumulative distribution functions of RMSE values of the filters averaged over time can be seen in Figures 3.6 and 3.7 for different threshold power values. It is seen in the performance figures of the algorithms that bias performance of the filters is not so good as static localization. But filters surpass the static localization methods in RMSE sense, PF is especially the best as expected. We observed

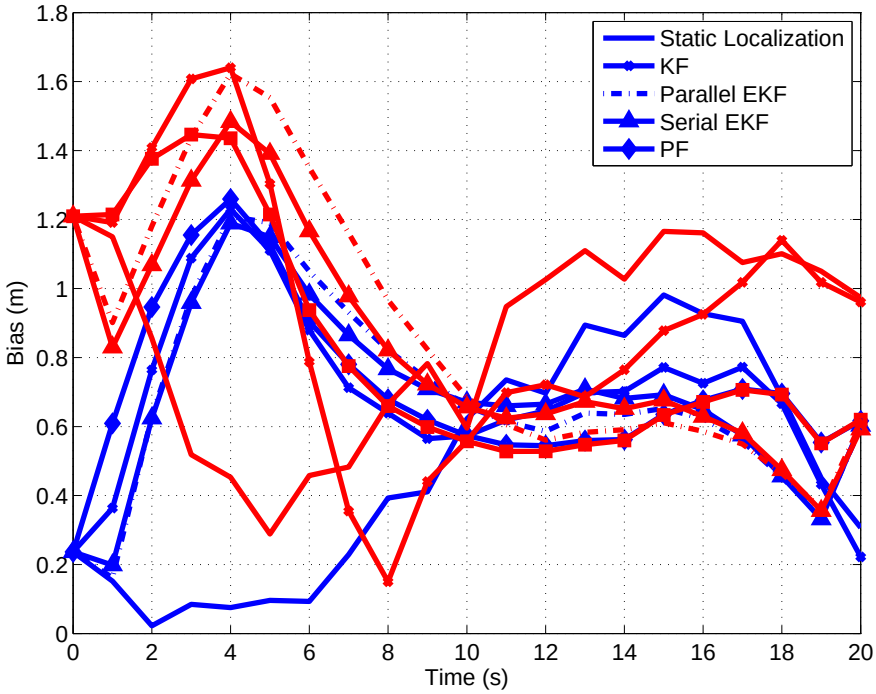

Figure 3.2: Bias comparison of non-collaborative tracking methods: $P_{thr} = -63$ dBm, 4 anchors (RSS-MLE: blue, h-RSS-MLE: red)

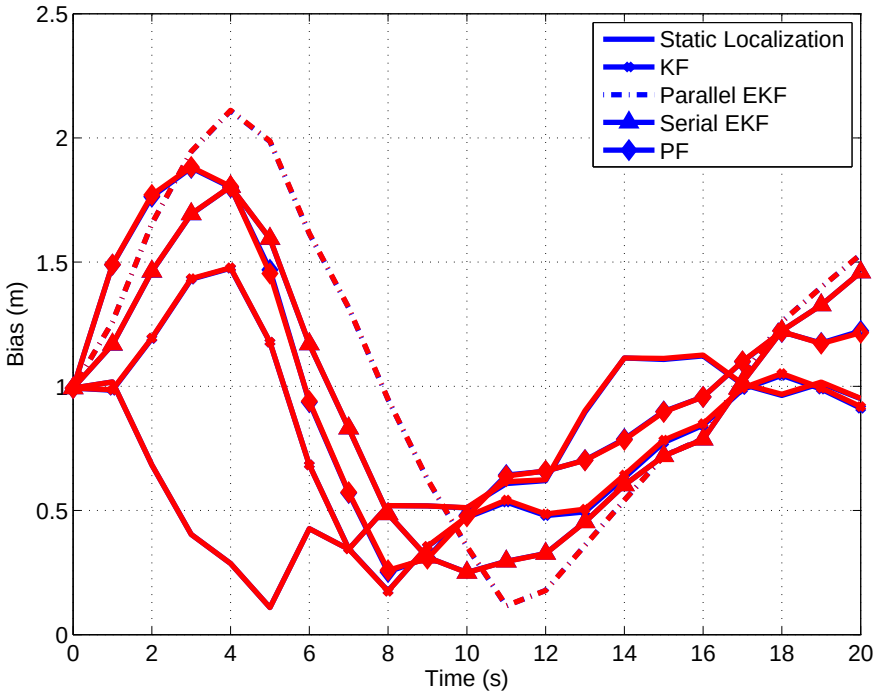

Figure 3.3: Bias comparison of non-collaborative tracking methods: $P_{thr} = -80$ dBm, 4 anchors (RSS-MLE: blue, h-RSS-MLE: red)

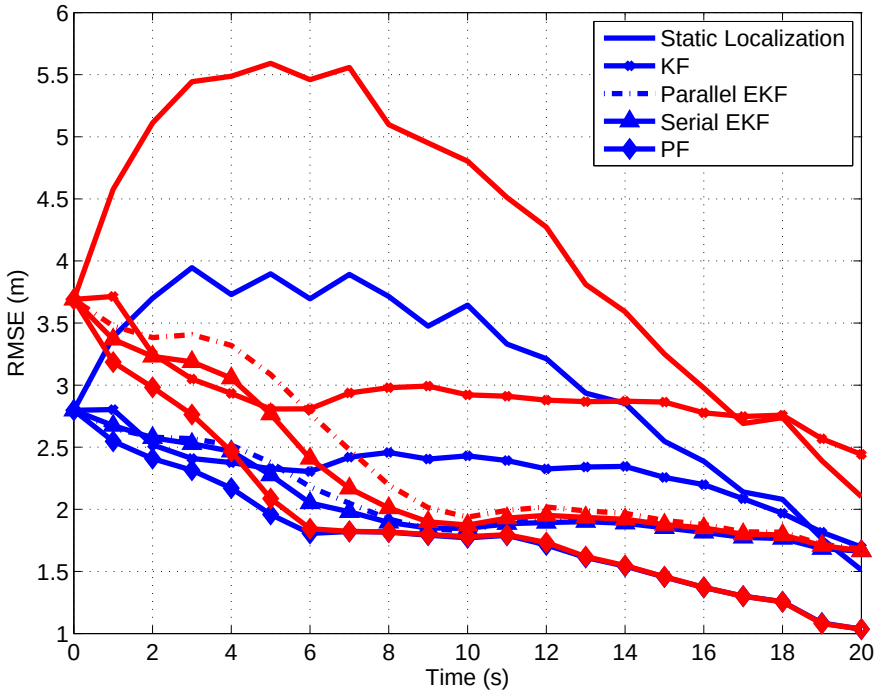

Figure 3.4: RMSE comparison of non-collaborative tracking methods: $P_{thr} = -63$ dBm, 4 anchors (RSS-MLE: blue, h-RSS-MLE: red)

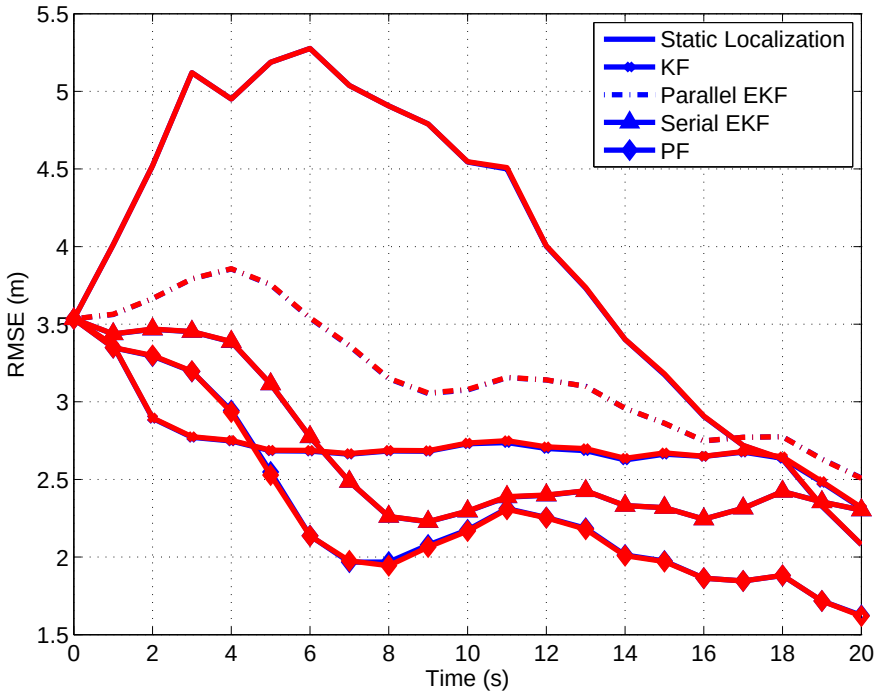

Figure 3.5: RMSE comparison of non-collaborative tracking methods: $P_{thr} = -80$ dBm, 4 anchors (RSS-MLE: blue, h-RSS-MLE: red)

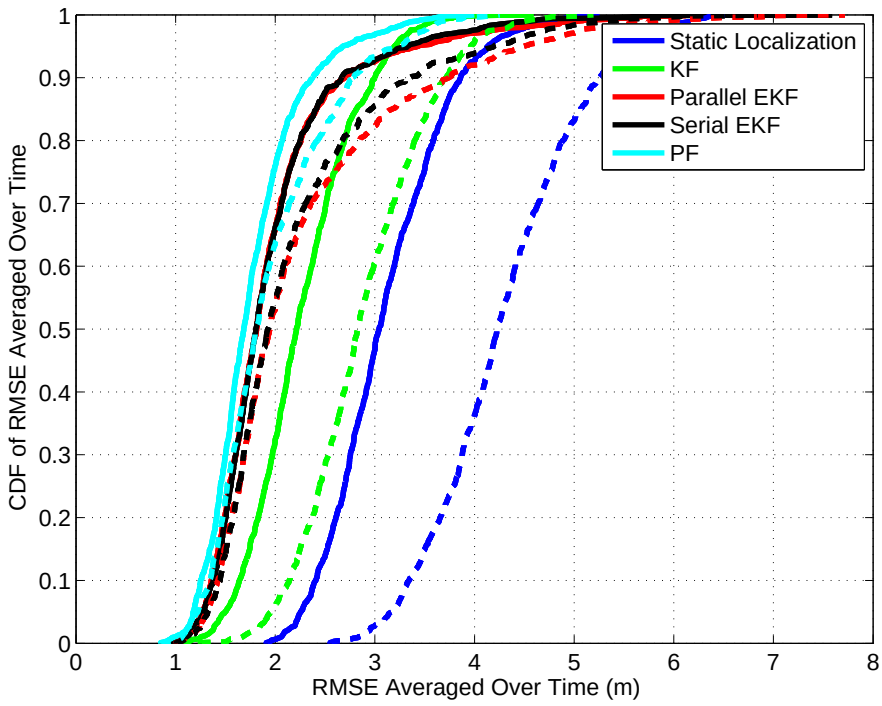

Figure 3.6: CDFs of RMSE averaged over time of non-collaborative localization and tracking methods: $P_{thr} = -63$ dBm, 4 anchors, (RSS-MLE: solid line, h-RSS-MLE: dashed line)

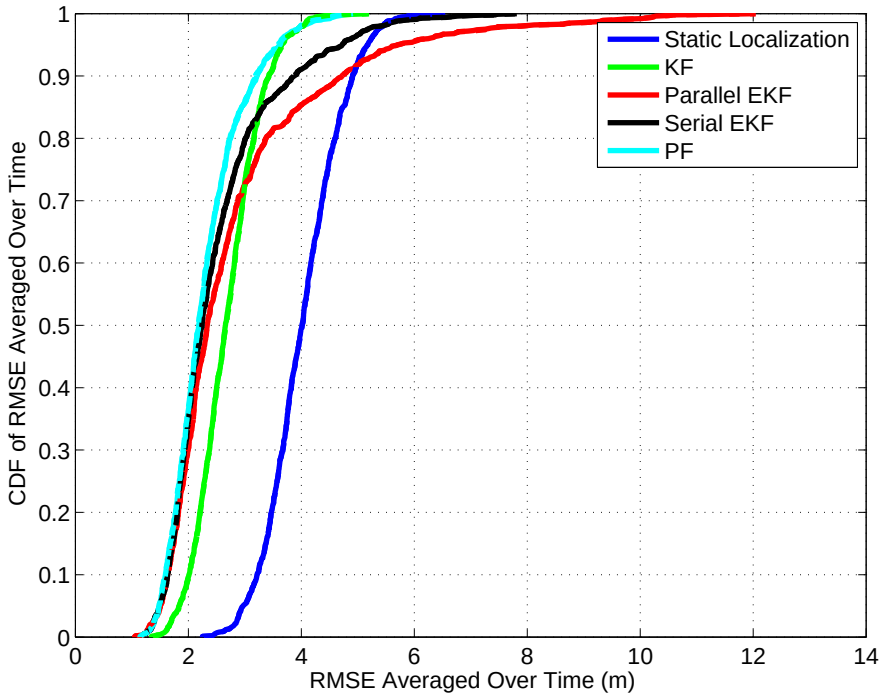

Figure 3.7: CDFs of RMSE averaged over time of non-collaborative localization and tracking methods: $P_{thr} = -80$ dBm, 4 anchors, (RSS-MLE: solid line, h-RSS-MLE: dashed line)

h-RSS-MLE does not reduce the bias for this non-collaborative scenario. Furthermore, RMSE of h-RSS-MLE is not less than RSS-MLE, although h-RSS-MLE has additional extra non-connectivity information in its cost function.

3.5 Experimental Study

Very often, the models considered in design and calculations does not fit the real world. Therefore some experimental studies are performed to see the real performance of the localization and tracking algorithms. We performed an experiment for tracking and localization by using Xbee Series 2 based devices. Our experiment consists of two phases: Calibration phase and measurement phase. In calibration phase, RSS measurements are processed under the assumption that the position of the nodes is known, to estimate channel parameters. RSS values are obtained to perform localization and tracking algorithms by using estimated channel parameters in measurement phase. Details about specification of the devices which we used in the experiment, are given in Section 3.5.1. Calibration phase and experimental results are presented in Sections 3.5.2 and 3.5.3 respectively.

3.5.1 Experimental Setup

Arduino Uno R3 boards are used as wireless sensor nodes in testbed implementations. Arduino Uno R3 board specifications are provided in Table 3.7 [1, 2]. ATmega328 microcontrollers are the control units of the sensor nodes. To enable wireless communication between sensor nodes, each board is extended using Arduino Wireless Shield equipped with an Xbee Series 2 RF module and 2GB SD card. The transmit power and the receiver sensitivity of a module are, respectively, 3 dBm and -100 dBm. Xbee modules with PCB antenna are used in experiments. For the power supplies, AC/DC adapter DC 12V, 1.5A are used.

Digi's Xbee Series 2 radio modules use the Zigbee Protocol. The modules operate within one of the sixteen channels in the ISM 2.4 GHz frequency band. There are two types of modes of the Xbee, AT mode and API mode. API supports communication with the Xbee modules in a frame-based way. In fact, a control unit sends data frames

Table3.7: Arduino Uno R3 Board Specifications

Microcontroller	ATmega328
Operating Voltage	5 V
Input Voltage (recommended)	7-12 V
Input Voltage (limits)	6-20 V
Digital I/O Pins	14 (of which 6 provide PWM output)
Analog Input Pins	6
DC Current per I/0 Pin	40 mA
DC Current per 3.3 V pin	50 mA
Flash Memory	32 KB (ATmega328) of which 0.5 KB used by bootloader
SRAM	2 KB (ATmega328)
EEPROM	1 KB (ATmega328)
Clock Speed	16 MHz

containing destination address and transmission data to the transmitter Xbee module together with transmission options. In experiments, we used broadcast messages for the communication between blindfolded node and anchors. The RSS measurements are logged in SD cards which are on the anchors.

3.5.2 Calibration Phase

Calibration is made to find the channel parameters, i.e., path loss exponent α, σ and P_0 which are used in the aforementioned localization and tracking algorithms. In the calibration phase, the nodes are placed as indicated in Figure 3.8, and the position coordinates of the nodes are assumed to be known. Our environment is a typical class environment which consists of tables, and there is no obstruction between the receiver and transmitters. It is located in in Middle East Technical University (METU), Department of Electrical and Electronics Engineering, Block A. The name of the class is EA-201. By considering the path loss model in (2.1), the estimate of path loss exponent α and first-meter reference power P_0 is found as follows.

$$\begin{bmatrix} \hat{P}_0 \\ \hat{\alpha} \end{bmatrix} = \left(\mathbf{H}^T\mathbf{H}\right)^{-1}\mathbf{H}^T\mathbf{P} \tag{3.10}$$

where

- $\mathbf{P} = \begin{bmatrix} P_1 & P_2 & \cdots & P_m \end{bmatrix}^T$: measurement vector.
- $\mathbf{H} = \begin{bmatrix} \mathbf{1} & -10\log_{10}\mathbf{d} \end{bmatrix}$
- $\mathbf{1}$: vector of ones.

Note that positions of the nodes are assumed to be known in (3.10), and least squares (LS) estimation in (3.10) is optimum (unbiased and minimum variance which achieves CRLB) under linearity of model and Gaussianity assumption [22]. For more information about the estimation procedure of the path loss exponent and first-meter power, the reference [8] offers some methods. Estimated path loss model, which is found

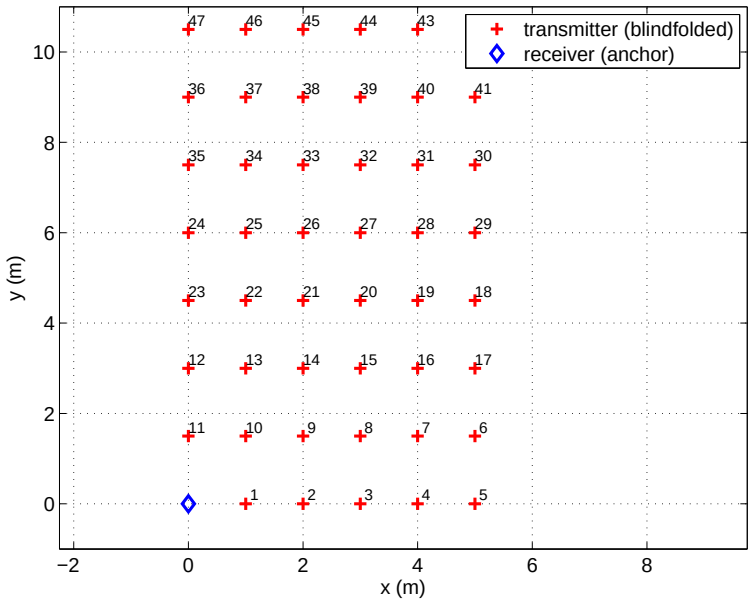

Figure 3.8: Node deployment for calibration measurement campaign

by using (3.10), is given in Figure 3.9 according to measurement campaign in Figure 3.8. Path loss exponent estimate $\hat{\alpha} = 1.75$, first-meter power $\hat{P}_0 = -46$ dBm and $\hat{\sigma}_v = 5.47$ dB. Actually $\hat{\alpha}$ is within the range of path loss exponent values for unobstructed indoor environment, which is expressed in the literature [50].

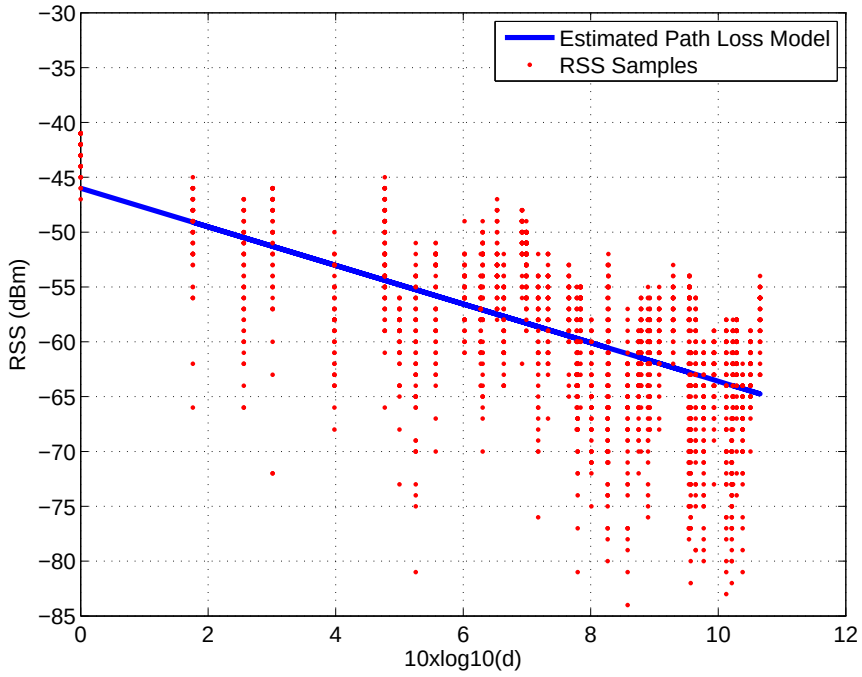

Figure 3.9: Estimated path loss model and RSS samples

3.5.3 Experimental Results

The anchors are deployed on the corners of a 5 m $\times$ 11 m area, such that the first, the second, the third and the fourth anchors are at (0,0), (0,11), (5,11) and (5,0) coordinates respectively. The blindfolded node is moved on the specific trajectory and RSS values are sent by transmitter (blindfolded node) in each 2 seconds. To enhance the experimental performance of the localization and tracking techniques, 5 samples or measurements are taken in each step of walk (i.e., waiting 10 s in each point). Additionally, α is set to 2.5, since we observed that tracking results with $\alpha = 2.5$ are much better than one with $\alpha = 1.75$. The parameters σ_v and P_0 are taken as 6 dB and -46 dBm respectively in our implementations. Obtaining better results with a channel parameter which is different from the calibrated one is possible, since the path loss model in (2.1) may not sometimes match the RSS measurements in real world [39]. Filter initializations, measurement noise covariances are taken into account as described in Section 3.4. Process noise covariance is set to the value $\mathbf{Q} = 0.005^2\mathbf{I}_2$ in our implementations. The RSS values in anchors are given in Figure 3.10.

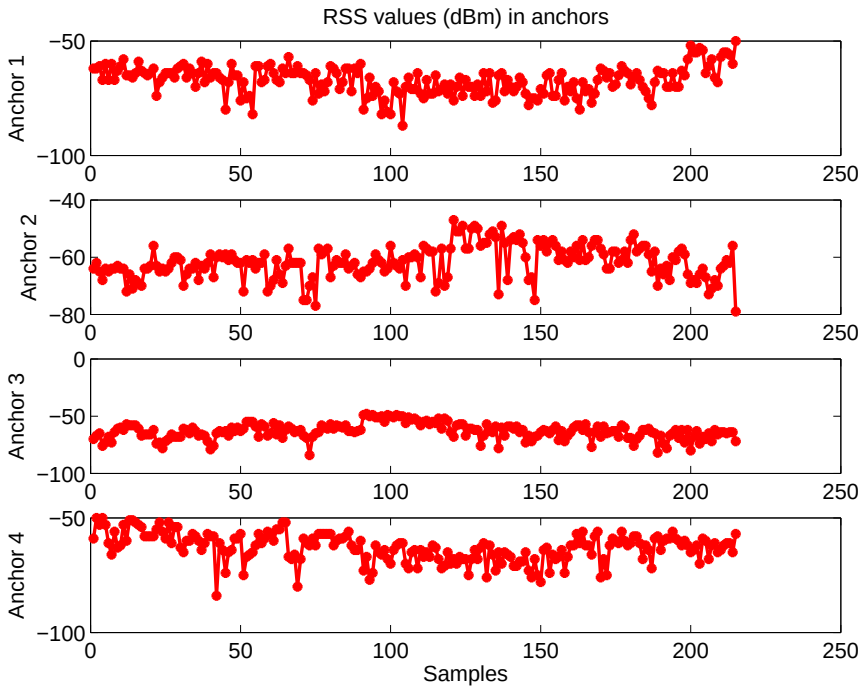

Figure 3.10: RSS values read by anchors when blindfolded node is on specific trajectory in the experiment

By processing these RSS values, various tracking, static localization estimates and their error performances are presented in Figures 3.11-3.16. The static localization method used in the experiment is selected to be non-collaborative RSS-MLE solved by grid-search as in Section 3.4. The RMSE values of the methods are 3.68, 2.13, 2.02, 2.02 and 2.00 meters for RSS-MLE, KF, serial EKF, parallel EKF and PF respectively. According to estimated trajectory of tracking algorithms and localization, it can be concluded that tracking algorithms can improve the localization accuracy about one meter for related trajectory.

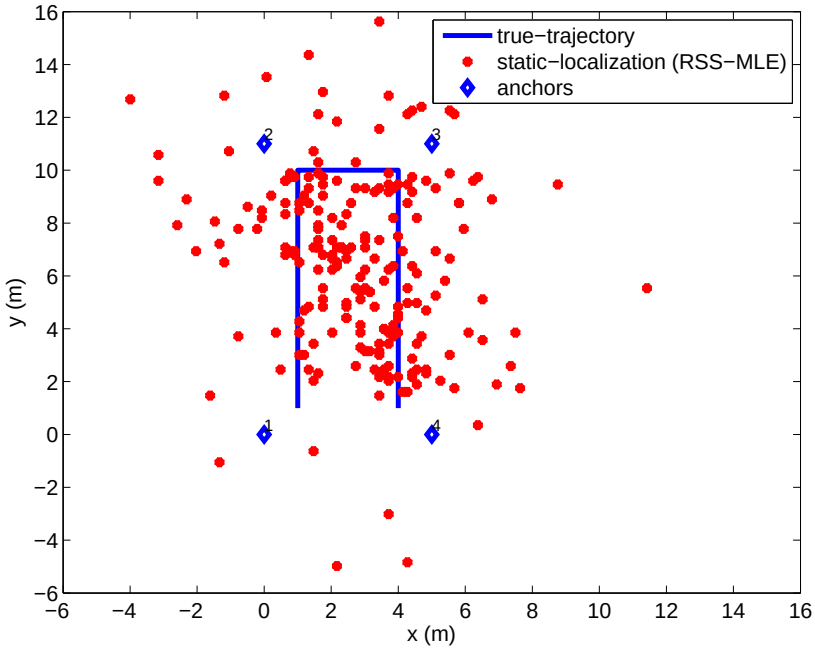

Figure 3.11: Performance of static localization (RSS-MLE) with experimental data: 215 RSS observations, $P_0 = -46$ dBm, $\sigma_v = 6$ dB, $\alpha = 2.5$

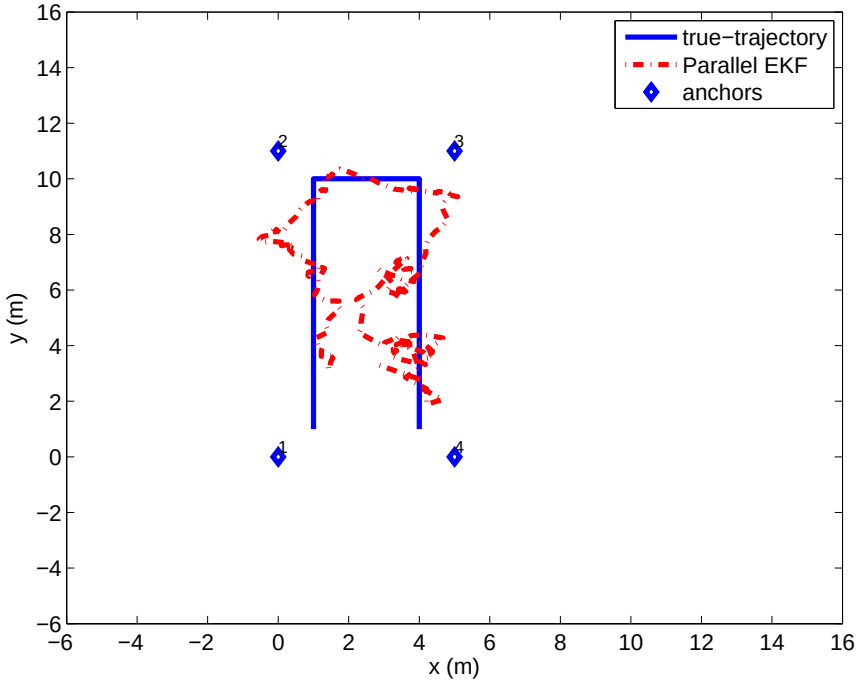

Figure 3.12: Performance of parallel extended Kalman filter with experimental data: 215 RSS observations, $P_0 = -46$ dBm, $\sigma_v = 6$ dB, $\alpha = 2.5$

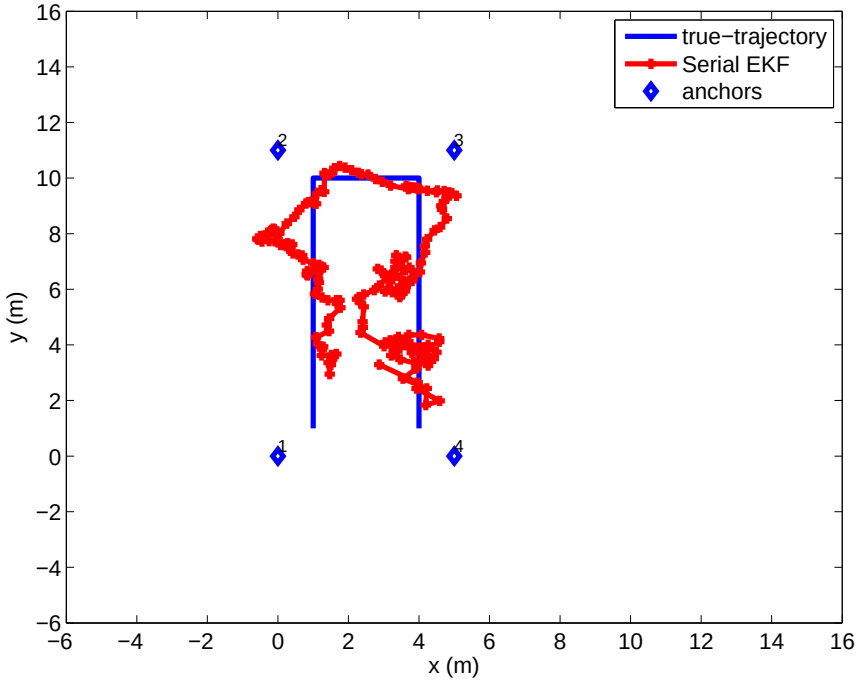

Figure 3.13: Performance of serial extended Kalman filter with experimental data: 215 RSS observations, $P_0 = -46$ dBm, $\sigma_v = 6$ dB, $\alpha = 2.5$

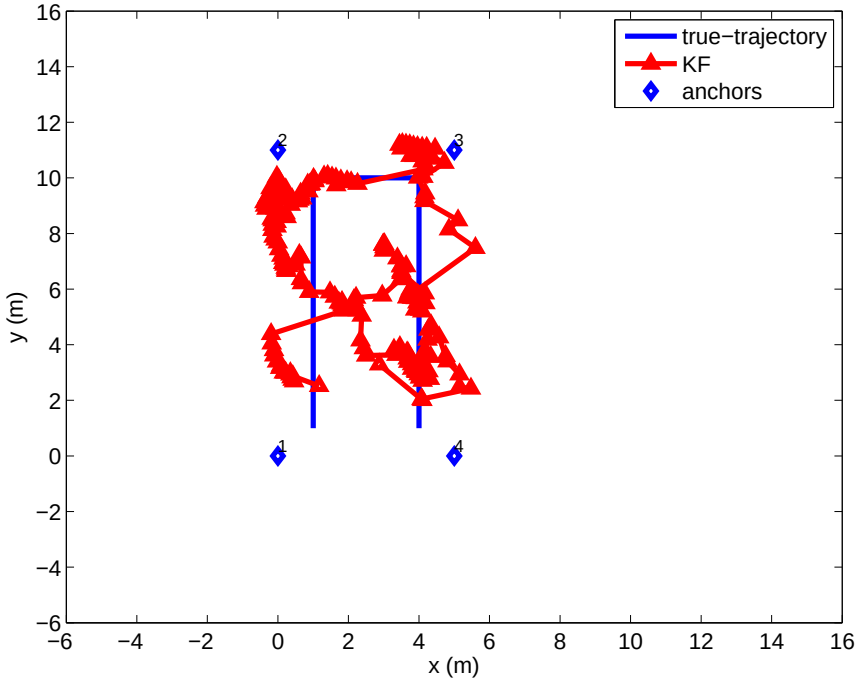

Figure 3.14: Performance of Kalman filter with experimental data: 215 RSS observations, $P_0 = -46$ dBm, $\sigma_v = 6$ dB, $\alpha = 2.5$

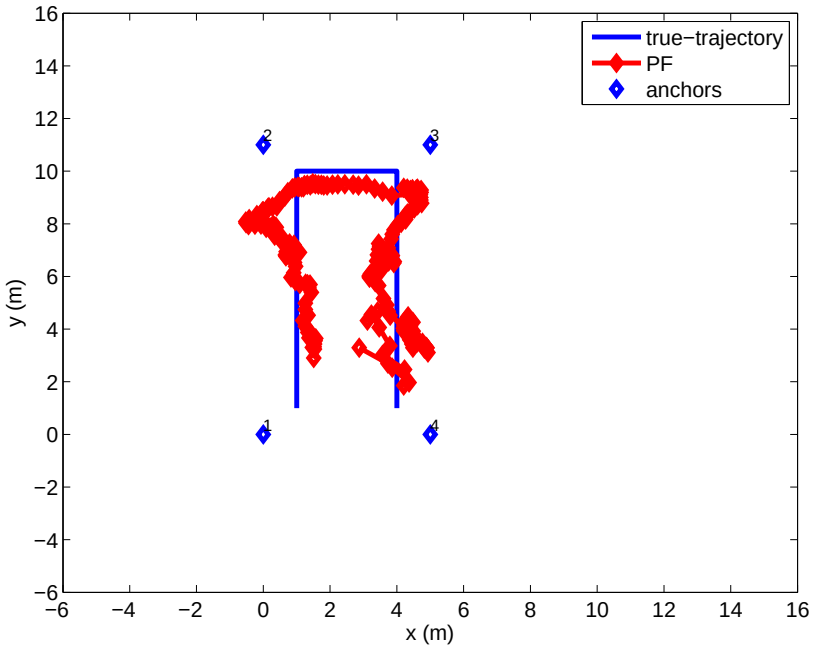

Figure 3.15: Performance of SIR particle filter (10000 particles) with experimental data: 215 RSS observations, $P_0 = -46$ dBm, $\sigma_v = 6$ dB, $\alpha = 2.5$

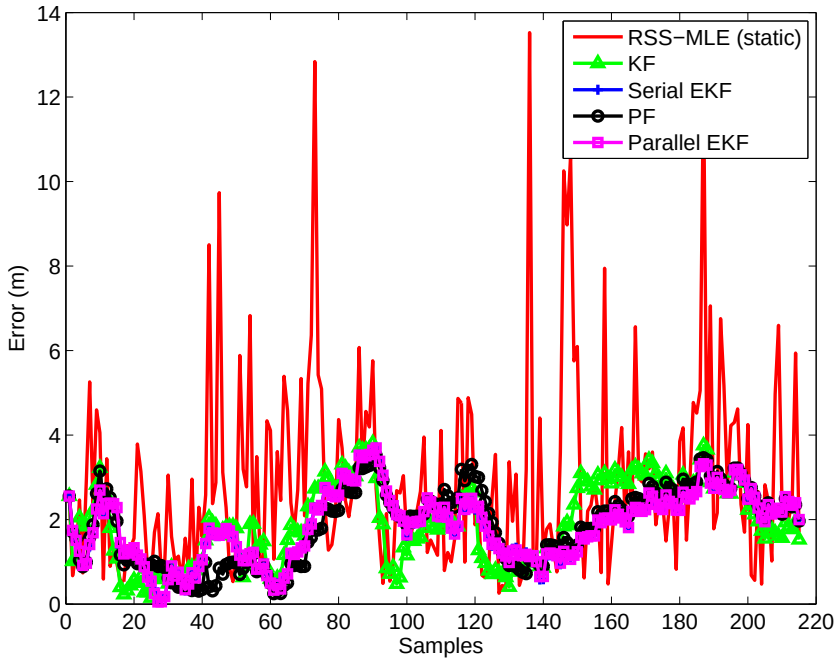

Figure 3.16: Error performance of the methods compared to ground-truth

CHAPTER 4

AN ANALYTICAL BIAS ANALYSIS OF MLE BASED ON TAYLOR SERIES EXPANSION OF MLE COST FUNCTION

In Chapter 2, it has been seen that h-RSS-MLE has a reduced bias compared to RSS-MLE. In order to understand the reason, in this chapter, following a similar methodology to that of [41] and assuming random connectivity events as in [14], we derive an analytical bias formula for h-RSS-MLE which covers RSS-MLE as a special case. An investigation of the bias can also be useful to see analytically in which deployment of nodes the reduction in bias is observed. Additionally an analytical bias expression which can also be considered as bias prediction can help mitigate the bias of an estimator and can be seen as a benchmark for performance of MLE localization. At the end of this chapter, we present a simulation study in 1-D and 2-D non-collaborative localization examples to compare bias values via both simulations and theoretical expressions.

4.1 Derivation of the Analytical Bias Formula for MLE based on RSS Range Measurements

Consider the measurement model below.

$$y_i = f_i(\mathbf{x}) + v_i \tag{4.1}$$

for $i = 1, \ldots, m$ where

- $\mathbf{x} \in \mathbb{R}^n$ is the unknown parameter vector to be estimated;

- $y_i \in \mathbb{R}$ is the measurement vector;
- $f_i(\cdot)$ is a twice differentiable, in general, nonlinear function;
- $v_i \sim \mathcal{N}(v_i; 0, \sigma^2)$ is the Gaussian measurement noise. We assume that v_i and v_j are independent when $i \neq j$.

In general, the measurements might not be obtained if there are connectivity constraints. We model the connectivity event related to the ith measurement as a Bernoulli random variable w_i, with $w_i = 1$ meaning that y_i is collected and $w_i = 0$ otherwise. The distribution of w_i is specified by $\log P(w_i = 0) = g_i(\mathbf{x})$ where $g_i(\cdot)$, $i = 1, \ldots, m$ is assumed to be a twice differentiable nonlinear function. It should be noted that in general w_i is correlated with y_i. The ML estimation of $\mathbf{x}$ then involves the following optimization problem.

$$\hat{\mathbf{x}} = \arg\min_{\mathbf{x}} J(\mathbf{x}) \tag{4.2}$$

where

$$J(\mathbf{x}) \triangleq \sum_{i=1}^{m} \frac{w_i}{2\sigma^2}(y_i - f_i(\mathbf{x}))^2 - (1 - w_i)g_i(\mathbf{x}) \tag{4.3}$$

Notice that the cost function in (4.3) is in the same form as the cost function which is derived according to the likelihood function in Appendix A. The gradient of $J(\cdot)$ denoted by $\mathbf{h}(\mathbf{x}) \triangleq \nabla_{\mathbf{x}} J(\mathbf{x})$ is given as

$$\mathbf{h}(\mathbf{x}) = \sum_{i=1}^{m} -\frac{w_i}{\sigma^2}(y_i - f_i(\mathbf{x}))\nabla_{\mathbf{x}} f_i(\mathbf{x}) - (1 - w_i)\nabla_{\mathbf{x}} g_i(\mathbf{x}) \tag{4.4}$$

$$= \sum_{i=1}^{m} -\frac{w_i}{\sigma^2} v_i \nabla_{\mathbf{x}} f_i(\mathbf{x}) - (1 - w_i)\nabla_{\mathbf{x}} g_i(\mathbf{x}). \tag{4.5}$$

The solution of the ML problem lies at a point $\hat{\mathbf{x}}$ when the condition $\mathbf{h}(\hat{\mathbf{x}}) = 0$ is satisfied. We now write a second order Taylor series approximation for the vector valued function $\mathbf{h}(\cdot)$ around $\mathbf{x}$:

$$\begin{aligned} 0 = \mathbf{h}(\hat{\mathbf{x}}) \approx \mathbf{h}(\mathbf{x}) &+ \Delta_{\mathbf{x}}^{\mathbf{x}} J(\mathbf{x})(\hat{\mathbf{x}} - \mathbf{x}) \\ &+ \frac{1}{2}\sum_{i=1}^{n} (\hat{\mathbf{x}} - \mathbf{x})^{\mathrm{T}} \Delta_{\mathbf{x}}^{\mathbf{x}} h_i(\mathbf{x})(\hat{\mathbf{x}} - \mathbf{x})\mathbf{e}_i \end{aligned} \tag{4.6}$$

where $h_i(\cdot)$ stands for the ith component of $\mathbf{h}(\cdot)$, $\Delta_{\mathbf{x}}^{\mathbf{x}}$ denotes the Hessian operator and $\mathbf{e}_i \in \mathbb{R}^n$ is a vector filled all with zeros except for its ith element which is unity. The Hessian of $J(\cdot)$ is given as

$$\begin{aligned}\Delta_{\mathbf{x}}^{\mathbf{x}} J(\mathbf{x}) =& \sum_{i=1}^{m} -\frac{w_i}{\sigma^2}(y_i - f_i(\mathbf{x}))\Delta_{\mathbf{x}}^{\mathbf{x}} f_i(\mathbf{x}) \\ &+ \frac{w_i}{\sigma^2}\nabla_x f_i(\mathbf{x})\nabla_{\mathbf{x}}^{\mathrm{T}} f_i(\mathbf{x}) - (1-w_i)\Delta_{\mathbf{x}}^{\mathbf{x}} g_i(\mathbf{x}), \\ =& \sum_{i=1}^{m} -\frac{w_i}{\sigma^2} v_i \Delta_{\mathbf{x}}^{\mathbf{x}} f_i(\mathbf{x}) \\ &+ \frac{w_i}{\sigma^2}\nabla_{\mathbf{x}} f_i(\mathbf{x})\nabla_{\mathbf{x}}^{\mathrm{T}} f_i(\mathbf{x}) - (1-w_i)\Delta_{\mathbf{x}}^{\mathbf{x}} g_i(\mathbf{x}). \end{aligned} \tag{4.7}$$

We now expand $\left(\Delta_{\mathbf{x}}^{\mathbf{x}} J(\mathbf{x})\right)^{-1}$ in a first-order Taylor series expansion [37] with respect to v_i and w_i around $v_i = 0$ and $w_i = \bar{w}_i \triangleq E[w_i]$:

$$\left(\Delta_{\mathbf{x}}^{\mathbf{x}} J(\mathbf{x})\right)^{-1} \approx \mathbf{A}^{-1} - \mathbf{A}^{-1}\mathbf{B}\mathbf{A}^{-1} - \mathbf{A}^{-1}\mathbf{C}\mathbf{A}^{-1} \tag{4.8}$$

where

$$\mathbf{A} \triangleq \sum_{i=1}^{m} \frac{\bar{w}_i}{\sigma^2}\nabla_{\mathbf{x}} f_i(\mathbf{x})\nabla_{\mathbf{x}}^{\mathrm{T}} f_i(\mathbf{x}) - (1-\bar{w}_i)\Delta_{\mathbf{x}}^{\mathbf{x}} g_i(\mathbf{x}), \tag{4.9}$$

$$\mathbf{B} \triangleq \sum_{i=1}^{m} -\frac{\bar{w}_i}{\sigma^2} v_i \Delta_{\mathbf{x}}^{\mathbf{x}} f_i(\mathbf{x}), \tag{4.10}$$

$$\mathbf{C} \triangleq \sum_{i=1}^{m} \left(\frac{1}{\sigma^2}\nabla_{\mathbf{x}} f_i(\mathbf{x})\nabla_{\mathbf{x}}^{\mathrm{T}} f_i(\mathbf{x}) + \Delta_{\mathbf{x}}^{\mathbf{x}} g_i(\mathbf{x})\right)(w_i - \bar{w}_i). \tag{4.11}$$

Now if we extract $\hat{\mathbf{x}} - \mathbf{x}$ from the equation above and take the expectation, a bias expression can be obtained from Taylor series expansion of the cost function in (4.6) as

$$E(\hat{\mathbf{x}} - \mathbf{x}) = -\left(\mathbf{E}_1 + \frac{\mathbf{E}_2}{2}\right) \tag{4.12}$$

where

$$\begin{aligned}\mathbf{E}_1 \triangleq& E\left[\left(\Delta_{\mathbf{x}}^{\mathbf{x}} J(\mathbf{x})\right)^{-1}\mathbf{h}(\mathbf{x})\right], \\ \mathbf{E}_2 \triangleq& E\left[\left(\Delta_{\mathbf{x}}^{\mathbf{x}} J(\mathbf{x})\right)^{-1}\sum_{i=1}^{n}\mathbf{e_i}\,\mathrm{tr}\left[\Delta_{\mathbf{x}}^{\mathbf{x}} h_i(\mathbf{x})(\hat{\mathbf{x}} - \mathbf{x})(\hat{\mathbf{x}} - \mathbf{x})^{\mathrm{T}}\right]\right]. \end{aligned} \tag{4.13}$$

To take the expectations in (4.13), some more approximations are necessary. By using the approximation in (4.8), $\mathbf{E}_1$ can be written as

$$\begin{aligned}
\mathbf{E}_1 \triangleq & E\left[\left(\Delta_{\mathbf{x}}^{\mathbf{x}} J(\mathbf{x})\right)^{-1} \mathbf{h}(\mathbf{x})\right] \\
\approx & E\left[\left(\mathbf{A}^{-1} - \mathbf{A}^{-1}\mathbf{B}\mathbf{A}^{-1} - \mathbf{A}^{-1}\mathbf{C}\mathbf{A}^{-1}\right)\mathbf{h}(\mathbf{x})\right], \\
= & \mathbf{A}^{-1}E[\mathbf{h}(\mathbf{x})] - E\left[\mathbf{A}^{-1}\mathbf{B}\mathbf{A}^{-1}\mathbf{h}(\mathbf{x})\right] - E\left[\mathbf{A}^{-1}\mathbf{C}\mathbf{A}^{-1}\mathbf{h}(\mathbf{x})\right] \\
= & \sum_{i=1}^{m} -\frac{E[w_i v_i]}{\sigma^2}\mathbf{A}^{-1}\nabla_{\mathbf{x}} f_i(\mathbf{x}) - (1-\bar{w}_i)\mathbf{A}^{-1}\nabla_{\mathbf{x}} g_i(\mathbf{x}) \\
& - \sum_{j=1}^{m}\sum_{i=1}^{m} \frac{\bar{w}_j}{\sigma^2}\frac{E[w_i v_i v_j]}{\sigma^2}\mathbf{A}^{-1}\Delta_{\mathbf{x}}^{\mathbf{x}} f_j(\mathbf{x})\mathbf{A}^{-1}\nabla_{\mathbf{x}} f_i(\mathbf{x}) \\
& + \frac{\bar{w}_j}{\sigma^2}E[(1-w_i)v_j]\mathbf{A}^{-1}\Delta_{\mathbf{x}}^{\mathbf{x}} f_j(\mathbf{x})\mathbf{A}^{-1}\nabla_{\mathbf{x}} g_i(\mathbf{x}) \\
& + \sum_{j=1}^{m}\sum_{i=1}^{m} \mathbf{A}^{-1}\mathbf{M}_j(\mathbf{x})\mathbf{A}^{-1}\nabla_{\mathbf{x}} f_i(\mathbf{x})\frac{E[(w_j-\bar{w}_j)w_i v_i]}{\sigma^2} \\
& + \sum_{j=1}^{m}\sum_{i=1}^{m} \mathbf{A}^{-1}\mathbf{M}_j(\mathbf{x})\mathbf{A}^{-1}\nabla_{\mathbf{x}} g_i(\mathbf{x})E[(w_j-\bar{w}_j)(1-w_i)] \qquad (4.14)
\end{aligned}$$

where

$$\mathbf{M}_j(\mathbf{x}) \triangleq \left(\frac{1}{\sigma^2}\nabla_{\mathbf{x}} f_j(\mathbf{x})\nabla_{\mathbf{x}}^{\mathrm{T}} f_j(\mathbf{x}) + \Delta_{\mathbf{x}}^{\mathbf{x}} g_j(\mathbf{x})\right). \qquad (4.15)$$

All the double summation arguments above are equal to zero when $i \neq j$ due to the expectations, which reduces them into single summations. Moreover since $w_i \in \{0,1\}$, the following equations hold.

$$\begin{aligned}
(w_i - \bar{w}_i)w_i =& (1-\bar{w}_i)w_i, \\
(w_i - \bar{w}_i)(1-w_i) =& -\bar{w}_i(1-w_i). \qquad (4.16)
\end{aligned}$$

Substituting the new expressions into (4.14), we get

$$\begin{aligned}
\mathbf{E}_1 = & \sum_{i=1}^{m} -\frac{E[w_i v_i]}{\sigma^2}\mathbf{A}^{-1}\mathbf{A}\mathbf{A}^{-1}\nabla_{\mathbf{x}} f_i(\mathbf{x}) - (1-\bar{w}_i)\mathbf{A}^{-1}\mathbf{A}\mathbf{A}^{-1}\nabla_{\mathbf{x}} g_i(\mathbf{x}) \\
& - \frac{\bar{w}_i}{\sigma^2}\frac{E[w_i v_i^2]}{\sigma^2}\mathbf{A}^{-1}\Delta_{\mathbf{x}}^{\mathbf{x}} f_i(\mathbf{x})\mathbf{A}^{-1}\nabla_{\mathbf{x}} f_i(\mathbf{x}) \\
& + \frac{\bar{w}_i}{\sigma^2}E[w_i v_i]\mathbf{A}^{-1}\Delta_{\mathbf{x}}^{\mathbf{x}} f_i(\mathbf{x})\mathbf{A}^{-1}\nabla_{\mathbf{x}} g_i(\mathbf{x}) \\
& + \mathbf{A}^{-1}\mathbf{M}_i(\mathbf{x})\mathbf{A}^{-1}\nabla_{\mathbf{x}} f_i(\mathbf{x})(1-\bar{w}_i)\frac{E[w_i v_i]}{\sigma^2} \\
& - \mathbf{A}^{-1}\mathbf{M}_i(\mathbf{x})\mathbf{A}^{-1}\nabla_{\mathbf{x}} g_i(\mathbf{x})\bar{w}_i(1-\bar{w}_i) \\
= & \sum_{i=1}^{m} \mathbf{A}^{-1}\boldsymbol{\Sigma}_i^f\mathbf{A}^{-1}\nabla_{\mathbf{x}} f_i(\mathbf{x}) + \mathbf{A}^{-1}\boldsymbol{\Sigma}_i^g\mathbf{A}^{-1}\nabla_{\mathbf{x}} g_i(\mathbf{x}) \qquad (4.17)
\end{aligned}$$

where

$$\begin{aligned}\boldsymbol{\Sigma}_i^f \triangleq & -\frac{E[w_i v_i]}{\sigma^2}\mathbf{A} - \frac{\bar{w}_i}{\sigma^2}\frac{E[w_i v_i^2]}{\sigma^2}\Delta_{\mathbf{x}}^{\mathbf{x}} f_i(\mathbf{x}) \\ & + (1-\bar{w}_i)\frac{E[w_i v_i]}{\sigma^2}\mathbf{M}_i(\mathbf{x}), \end{aligned} \tag{4.18}$$

$$\begin{aligned}\boldsymbol{\Sigma}_i^g \triangleq & -(1-\bar{w}_i)\mathbf{A} + \frac{\bar{w}_i}{\sigma^2}E[w_i v_i]\Delta_{\mathbf{x}}^{\mathbf{x}} f_i(\mathbf{x}) \\ & - \bar{w}_i(1-\bar{w}_i)\mathbf{M}_i(\mathbf{x}) \end{aligned} \tag{4.19}$$

$\mathbf{E}_2$ in (4.13) can be calculated as

$$\begin{aligned}\mathbf{E}_2 \triangleq & E\left[(\Delta_{\mathbf{x}}^{\mathbf{x}} J(\mathbf{x}))^{-1}\sum_{i=1}^{n}\mathbf{e_i}\,\mathrm{tr}\left[\Delta_{\mathbf{x}}^{\mathbf{x}} h_i(\mathbf{x})(\hat{\mathbf{x}}-\mathbf{x})(\hat{\mathbf{x}}-\mathbf{x})^{\mathrm{T}}\right]\right] \\ \approx & \mathbf{A}^{-1}\sum_{i=1}^{n}\mathbf{e_i}\,\mathrm{tr}\left[E\left(\Delta_{\mathbf{x}}^{\mathbf{x}} h_i(\mathbf{x})\right)\mathbf{CRLB}(\mathbf{x})\right] \end{aligned} \tag{4.20}$$

where we made the following approximations.

$$\begin{aligned}[\Delta_{\mathbf{x}}^{\mathbf{x}} J(\mathbf{x})]^{-1} \approx & \mathbf{A}^{-1}, \\ E\left[\Delta_{\mathbf{x}}^{\mathbf{x}} h_i(\mathbf{x}]\,(\hat{\mathbf{x}}-\mathbf{x})(\hat{\mathbf{x}}-\mathbf{x})^{\mathrm{T}}\right) \approx & E\left[\Delta_{\mathbf{x}}^{\mathbf{x}} h_i(\mathbf{x})\right] E\left[(\hat{\mathbf{x}}-\mathbf{x})(\hat{\mathbf{x}}-\mathbf{x})^{\mathrm{T}})\right], \\ E\left[(\hat{\mathbf{x}}-\mathbf{x})(\hat{\mathbf{x}}-\mathbf{x})^{\mathrm{T}})\right] \approx & \mathbf{CRLB}(\mathbf{x}). \end{aligned} \tag{4.21}$$

4.2 Bias Formulae for 1-D RSS Localization

In this section, we apply the results of the bias analysis presented in Section 4.1 to a 1-D RSS-based localization problem. For this purpose we make the following specific definitions.

- $y_i \triangleq P_i \in \mathbb{R}$ is the received signal strength measurement from the ith anchor node;
- $x \in \mathbb{R}$ is the unknown location of the blindfolded node to be estimated;
- $p_i \in \mathbb{R}$ is the known location of the ith anchor node;
- $d_i \triangleq |x - p_i|$ is the distance between the the blindfolded node and the ith anchor node;
- $f_i(x) \triangleq P_0 - 5\alpha \log_{10} d_i^2$ is the measurement function

for $i = 1, \ldots, m$. Note that we do not write the quantity $5\alpha \log_{10}\left((x-p_i)^2\right)$ in the common form $10\alpha \log_{10}|x-p_i|$ in order to avoid differentiability issues.

The connectivity event is modeled as $w_i \triangleq I(y_i \geq P_{\text{thr}})$ where P_{thr} is the lowest detectable RSS. The event $\{y_i \geq P_{\text{thr}}\}$ is equivalent to the event $\{v_i \geq P_{\text{thr}} - P_0 + 5\alpha \log_{10}\left((x-p_i)^2\right)\}$ and hence $w_i = I(v_i \geq t_i(x))$ where $t_i(x) \triangleq P_{\text{thr}} - f_i(x)$. It is also noted that $g_i(x) \triangleq \log P(w_i = 0) = \log \Phi\left(\frac{t_i(x)}{\sigma}\right)$. We now calculate the derivatives:

$$\nabla_x f_i(x) = -\frac{10\alpha}{\log 10(x-p_i)} = -\frac{1}{\beta(x-p_i)} \tag{4.22}$$

$$\Delta_x^x f_i(x) = \frac{10\alpha}{\log 10(x-p_i)^2} = \frac{1}{\beta(x-p_i)^2} \tag{4.23}$$

$$\nabla_x g_i(x) = \frac{\eta_i(x)}{\beta\sigma(x-p_i)\Phi\left(\frac{t_i(x)}{\sigma}\right)} \tag{4.24}$$

$$\Delta_x^x g_i(x) = -\frac{\eta_i(x)\left[t_i(x)\Phi\left(\frac{t_i(x)}{\sigma}\right) + \beta\sigma\Phi\left(\frac{t_i(x)}{\sigma}\right) + \eta_i(x)\right]}{\beta^2\sigma^2(x-p_i)^2\Phi^2\left(\frac{t_i(x)}{\sigma}\right)} \tag{4.25}$$

where $\beta \triangleq \frac{\log 10}{10\alpha}$ and $\eta_i(x) \triangleq \mathcal{N}\left(\frac{t_i(x)}{\sigma}; 0, 1\right)$. We have the following expected values in Appendix E.

$$\begin{aligned} \bar{w}_i &= 1 - \Phi\left(\frac{t_i(x)}{\sigma}\right), \\ E[w_i v_i] &= \sigma\eta_i(x), \\ E[w_i v_i^2] &= \sigma t_i(x)\eta_i(x) + \sigma^2\bar{w}_i. \end{aligned} \tag{4.26}$$

4.2.1 1-D Bias Expression for Hybrid RSS-MLE

The h-RSS-MLE cost function is given in Chapter 2, in (2.9). The quantities Σ_i^f and Σ_i^g can be calculated as follows.

$$\begin{aligned} \Sigma_i^f =& -\frac{\eta_i(x)}{\sigma}A - \frac{\bar{w}_i}{\sigma^2}\left(\bar{w}_i + \frac{t_i(x)\eta_i(x)}{\sigma}\right)\Delta_x^x f_i(x) \\ &+ (1-\bar{w}_i)\frac{\eta_i(x)}{\sigma}M_i(x), \end{aligned} \tag{4.27}$$

$$\Sigma_i^g = -(1-\bar{w}_i)A + \frac{\bar{w}_i}{\sigma}\eta(x)\Delta_x^x f_i(x) - \bar{w}_i(1-\bar{w}_i)M_i(x) \tag{4.28}$$

where

$$A = \sum_{i=1}^{m} \frac{\bar{w}_i}{\sigma^2}\nabla_x f_i(x)\nabla_x^{\mathrm{T}} f_i(x) - (1-\bar{w}_i)\Delta_x^x g_i(x). \tag{4.29}$$

With Σ_i^f, Σ_i^g and A given above, the expectation E_1 can be calculated using (4.17). Finally E_2 is calculated as in (4.20) using the CRLB expression given as follows

$$CRLB = \left[\sum_{i=1}^{m} \frac{\bar{w}_i \, \sigma + \eta_i(x) t_i(x) + \eta_i(x)^2 (1 - \bar{w}_i)^{-1} \sigma}{\sigma^3 \, \beta^2 \, (x - p_i)^2} \right]^{-1} \tag{4.30}$$

The final bias expression can be found as in (4.12).

4.2.2 1-D Bias Expression for RSS-MLE

RSS-MLE cost function is stated in Chapter 2, equation (2.8). Note that RSS-MLE cost function can be obtained from h-RSS-MLE cost function by setting $g_i(x) = 0, \forall x$. Hence by setting $g_i(\cdot)$ and all of its derivatives to zero in Section 4.2.1, we get

$$\begin{aligned} \Sigma_i^f = & - \frac{\eta_i(x)}{\sigma} A - \frac{\bar{w}_i}{\sigma^2} \left(\bar{w}_i + \frac{t_i(x) \eta_i(x)}{\sigma} \right) \Delta_x^x f_i(x) \\ & + (1 - \bar{w}_i) \frac{\eta_i(x)}{\sigma} \left(\frac{1}{\sigma^2} \nabla_x f_i(x) \nabla_x^{\mathrm{T}} f_i(x) \right) \end{aligned} \tag{4.31}$$

$$E_1 = \sum_{i=1}^{m} A^{-1} \Sigma_i^f A^{-1} \nabla_x f_i(x) \tag{4.32}$$

where

$$A = \sum_{i=1}^{m} \frac{\bar{w}_i}{\sigma^2} \nabla_x f_i(x) \nabla_x^{\mathrm{T}} f_i(x) \tag{4.33}$$

Finally E_2 is calculated as in (4.20) using approximate CRLB expression because of random connectivity events in Appendix C, equation (C.20) given as follows

$$CRLB = \left[\sum_{i=1}^{m} \frac{\bar{w}_i - \sigma \, \beta \, \eta(x)}{\sigma^2 \, \beta^2 \, (x - p_i)^2} \right]^{-1} \tag{4.34}$$

Then the final bias expression can be found as in (4.12).

4.3 Simulation Results

4.3.1 1-D Example

We consider three anchors which are placed at 0, 35 and 70 m and a single blindfolded node which has fixed unknown position x in the interval [0,70] m for 1-D example.

The simulation results are obtained for 24 uniformly separated x values in the interval [0,70] m and for each x value, 2000 MC simulation runs are made. The BFGS Quasi-Newton method in MATLAB is used as optimization algorithm. The optimization algorithm is initialized with the true position of the blindfolded node in order for results not to be affected by local optima. Channel parameters are given in Table 4.1. The bias and RMSE values of both algorithms (RSS-MLE and h-RSS-MLE) are presented in Figures 4.1 and 4.2 respectively. As evident from Figure 4.1, the theoretical and simulated bias values are very similar for both algorithms which validates analytical bias derivations for 1-D noncollaborative localization made in Section 4.2. The bias of RSS-MLE can reach almost twice that of h-RSS-MLE for some blindfolded node positions. Moreover, the RMSE of RSS-MLE observed in Figure 4.2 are slightly higher than those of h-RSS-MLE which makes us conclude that variance of the estimates of h-RSS-MLE are also lower than that of RSS-MLE.

Table4.1: Simulation Parameters for 1-D Localization

Simulation Parameters	Value
Path loss exponent α	3
Standard deviation σ	6 dB
RSS threshold power P_{thr}	-80 dBm
First meter RSS power P_0	-30 dBm

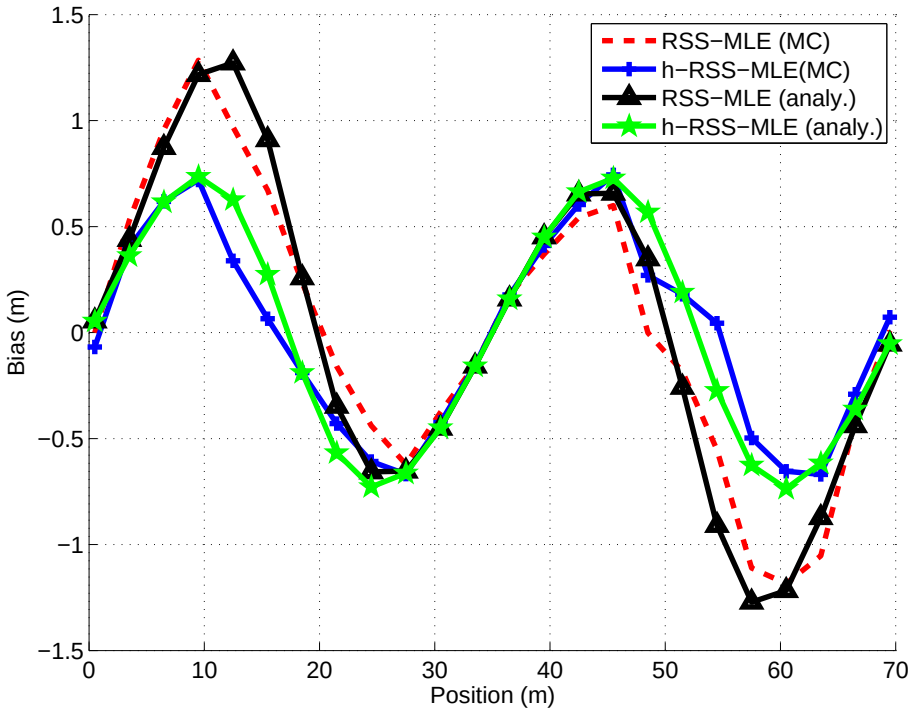

Figure 4.1: Comparison between 1-D analytical and simulation bias results of RSS-MLE and h-RSS-MLE

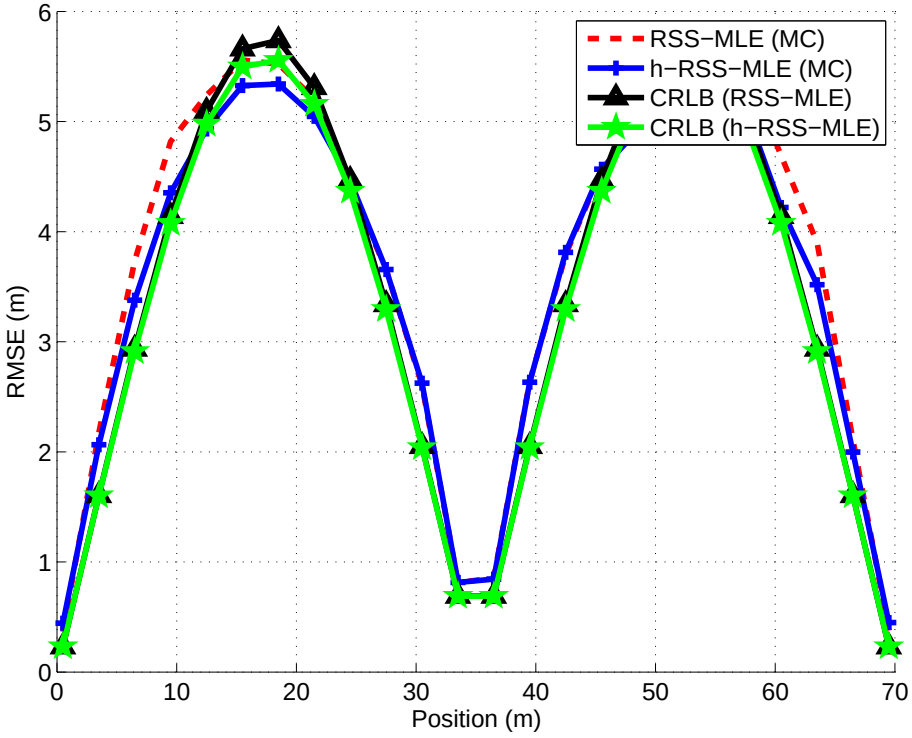

Figure 4.2: Comparison between 1-D analytical and simulation RMSE results of RSS-MLE and h-RSS-MLE

4.3.2 2-D Example

We placed four anchors on the corners of 10 m $\times$ 10 m area for 2-D simulation, namely at (0,0), (0,10), (10,0) and (10,10) respectively. The simulation parameters are given in Table 4.2. RSS-MLE and h-RSS-MLE cost functions at different thresh-

Table4.2: Simulation Parameters for 2-D Localization

Simulation Parameters	Value
Path loss exponent α	3
Standard deviation σ	logspace(1,-1,10) dB
RSS threshold power P_{thr}	-65,-80 dBm
First meter RSS power P_0	-30 dBm
Number of MC Runs	2000

old power (-65, -80 dBm) are solved by using grid-search (FSS-MLE, h-FSS-MLE) with search area of 100x100 m^2. The figures which compare 2-D bias results for threshold power -65 dBm between simulation and analytical formula according to the simulation parameters given in Table 4.2 at some position coordinates of the blindfolded node are presented in Figures 4.3-4.6. Moreover analytical and simulation results are compared at some position coordinates of the blindfolded node for threshold power -80 dBm in Figures 4.7-4.10.

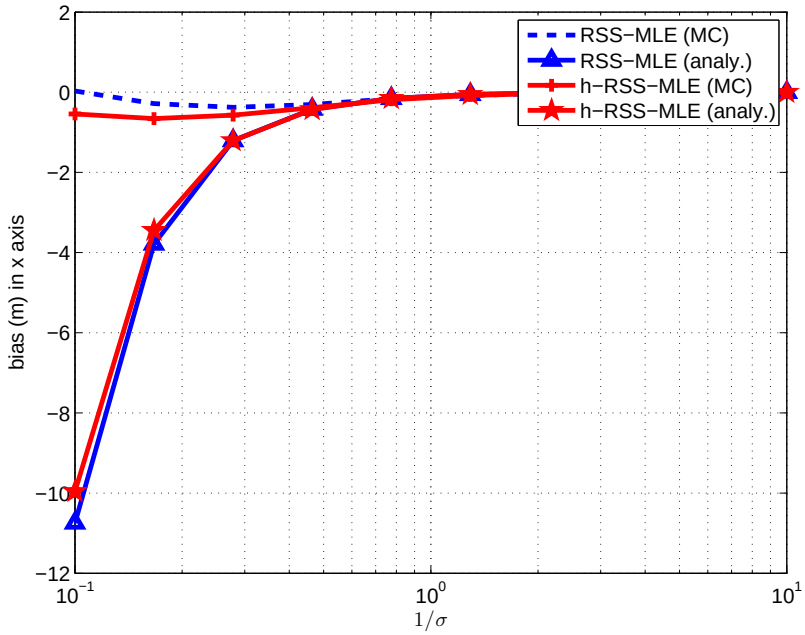

Figure 4.3: Comparison between 2-D analytical and simulation bias results of RSS-MLE and h-RSS-MLE in x-direction for blindfolded node at (1,1) and $P_{thr} = -65$ dBm

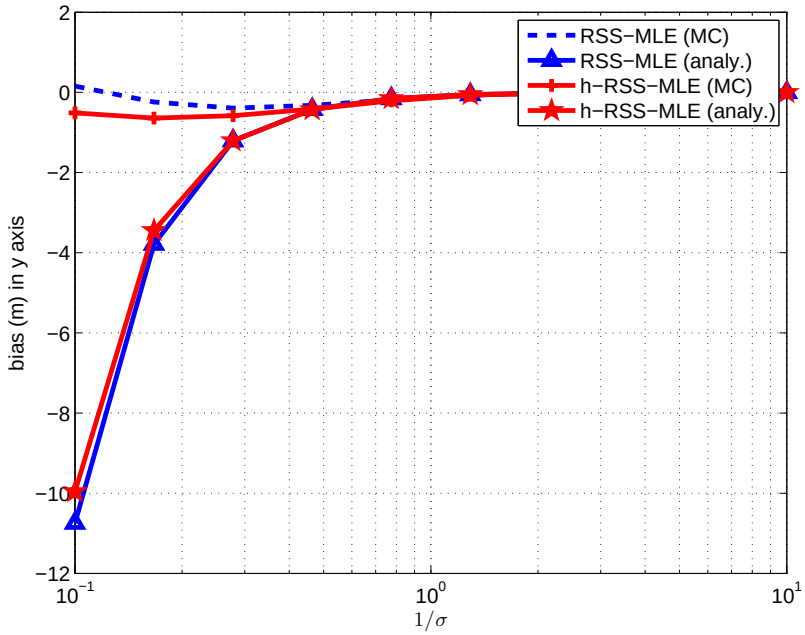

Figure 4.4: Comparison between 2-D analytical and simulation bias results of RSS-MLE and h-RSS-MLE in y-direction for blindfolded node at (1,1) and $P_{thr} = -65$ dBm

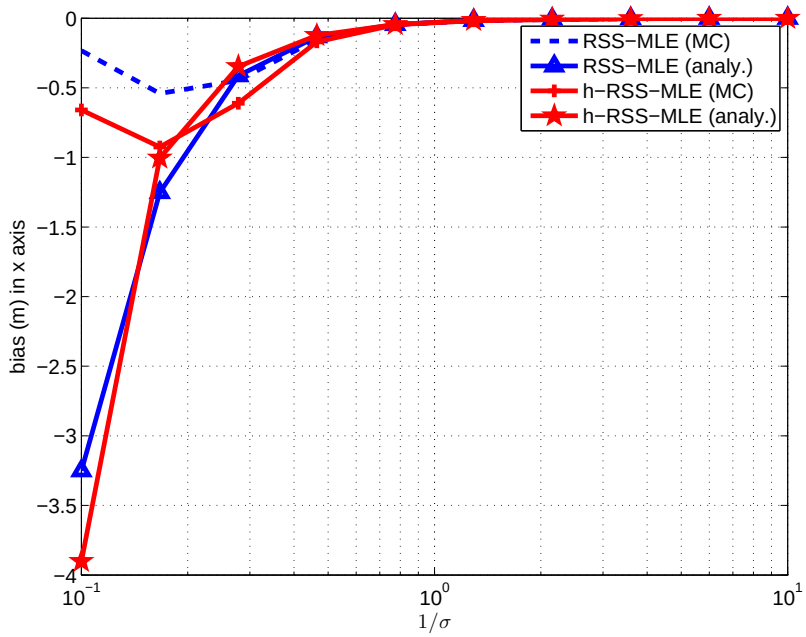

Figure 4.5: Comparison between 2-D analytical and simulation bias results of RSS-MLE and h-RSS-MLE in x-direction for blindfolded node at (3,1) and $P_{thr} = -65$ dBm

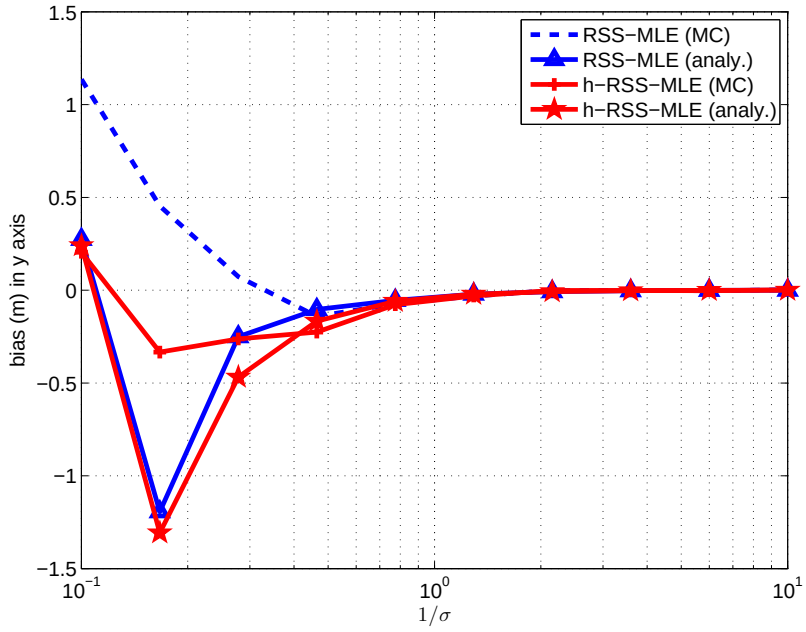

Figure 4.6: Comparison between 2-D analytical and simulation bias results of RSS-MLE and h-RSS-MLE in y-direction for blindfolded node at (3,1) and $P_{thr} = -65$ dBm

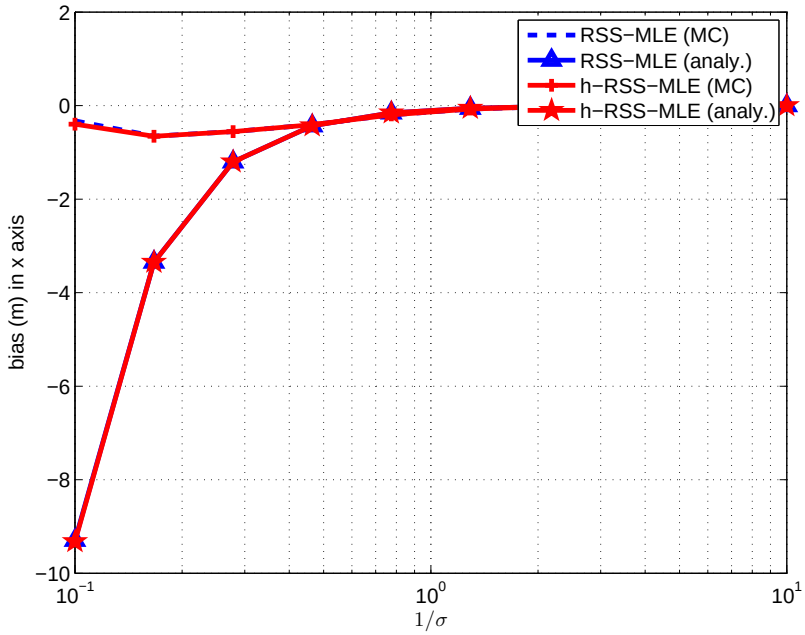

Figure 4.7: Comparison between 2-D analytical and simulation bias results of RSS-MLE and h-RSS-MLE in x-direction for blindfolded node at (1,1) and $P_{thr} = -80$ dBm

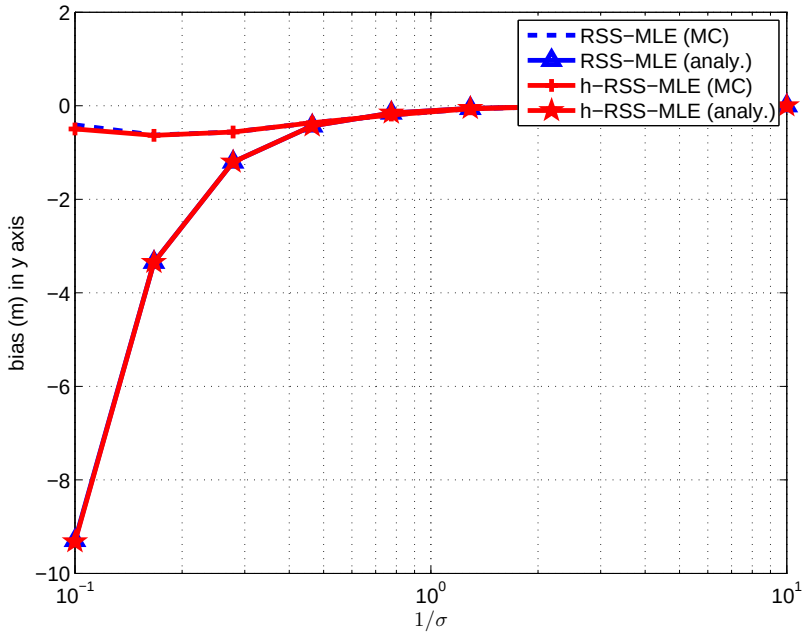

Figure 4.8: Comparison between 2-D analytical and simulation bias results of RSS-MLE and h-RSS-MLE in y-direction for blindfolded node at (1,1) and $P_{thr} = -80$ dBm

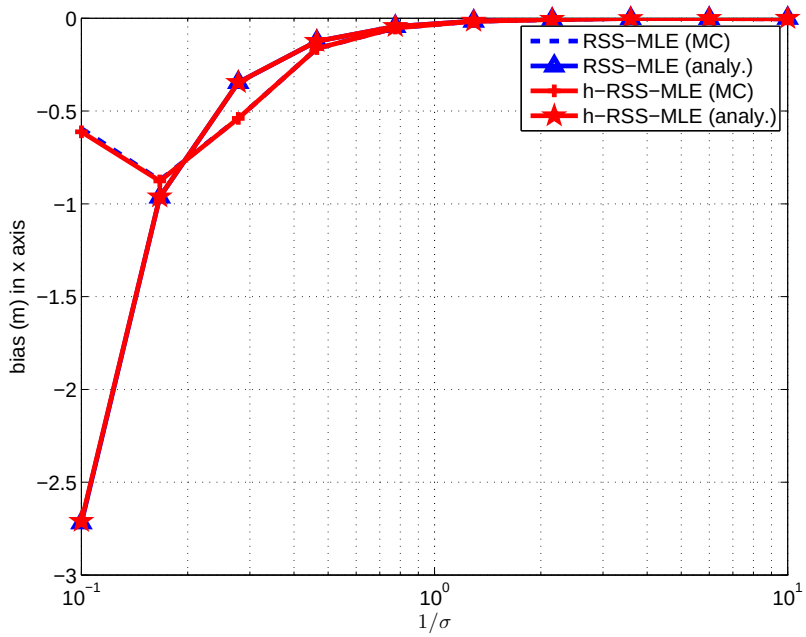

Figure 4.9: Comparison between 2-D analytical and simulation bias results of RSS-MLE and h-RSS-MLE in x-direction for blindfolded node at (3,1) and $P_{thr} = -80$ dBm

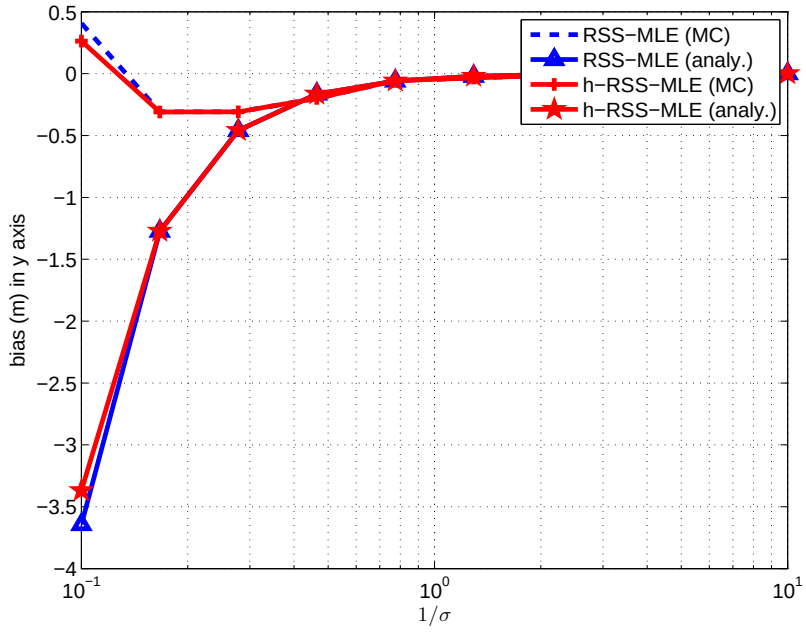

Figure 4.10: Comparison between 2-D analytical and simulation bias results of RSS-MLE and h-RSS-MLE in y-direction for blindfolded node at (3,1) and $P_{thr} = -80$ dBm

The figures which give information about 2-D bias characteristics of non-collaborative localization show that MC simulation results come closer to the analytical bias formula at high SNR [1]. However the bias values are too low in this situation, nearly unbiased. So we have to report that we cannot verify that the our bias formula given in Chapter 4 gives accurate prediction in 2-D localization for bias of MLEs compared to results obtained through simulation due to probably high nonlinearity of RSS-distance model. We conclude that an approach which is based on Taylor series expansion of MLE cost function as in [41] to find bias analytically is not a good choice in RSS-MLE localization of 2-D case.

[1] SNR cannot be actually defined in RSS localization problem due to multiplicative noise in linear domain. But we mean low distance values or low standard deviation of shadowing effect with high SNR

CHAPTER 5

AN ANALYTICAL BIAS ANALYSIS OF MLE BASED ON TAYLOR SERIES EXPANSION OF RSS MEASUREMENTS

We have derived an analytical bias formula by following similar methodology to [41], which is based on Taylor series expansion of the MLE cost function in previous chapter. We said that this formula is not applicable to 2-D RSS localization problem, since it has high nonlinearities and CRLB might not be a good approximation for MSE of the estimator in the related analytical expression. Therefore we propose a new method to derive an analytical bias formula based on Taylor series expansion of RSS measurements themselves instead of the cost function. It can be said that the newly-proposed bias formula is valid for FSS-MLE at some cases. Furthermore it can be also extended to the case that search space goes to infinity, i.e., FSS-MLE becomes identical to RSS-MLE. However it is observed that our proposed bias formula becomes the same as the previous one surprisingly, although two analytical expressions has different approaches, when search space is so large. Moreover it should be stated that we could not put connectivity constraints in this case. An effort to remedy this problem may be a future study.

In this chapter, newly proposed analytical bias for FSS-MLE is introduced and verified via simulation studies on a 2-D example.

5.1 Derivation of the Analytical Bias Formula for FSS-MLE based on RSS Range Measurements

MLE cost function gives a nonlinear least squares type cost. We therefore linearize the measurement to obtain the performance of least squares. Consider measurement below

$$y = P_0 - 10\alpha \log_{10} d + v \tag{5.1}$$

where $v \sim \mathcal{N}(v; 0, \sigma^2)$. For given a measurement y, we can calculate the ML estimate $\hat{d}_{ML}$ of d as follows.

$$\hat{d}_{ML} \triangleq 10^{\frac{P_0 - y}{10\alpha}} \tag{5.2}$$

It is easy to see that

$$\hat{d}_{ML} = d\, 10^{-v/10\alpha} \tag{5.3}$$

$$\approx \sqrt{(\hat{x} - x)^2 + (\hat{y} - y)^2} \tag{5.4}$$

Note that we will call $\hat{d}_{ML}$ as δ in the rest of this document. It is easy to see that $\log \delta \sim \mathcal{N}\left(\log d; 0, \sigma_{ML}^2\right)$ with $\sigma_{ML} = (\sigma \log 10)/(10\alpha)$.
To find the bias expression, the easiest method is to write Taylor series expansion of measurements around the true values. The second-order Taylor series approximation of N log-distance measurements will be that

$$\log \delta \approx \log \mathbf{d} + \mathbf{A}\tilde{\theta} + \frac{1}{2} \begin{bmatrix} \mathrm{tr}\left\{\mathbf{H}_1 \tilde{\theta}\tilde{\theta}^{\mathrm{T}}\right\} \\ \vdots \\ \mathrm{tr}\left\{\mathbf{H}_N \tilde{\theta}\tilde{\theta}^{\mathrm{T}}\right\} \end{bmatrix} \tag{5.5}$$

where

- $\theta = [x, y]^{\mathrm{T}}$: Position vector
- $\delta = [\delta_1, \delta_2, \cdots, \delta_N]^{\mathrm{T}}$: Distance measurement vector
- $\mathbf{d} = [d_1, d_2, \cdots, d_N]$: True inter-node distances
- $\tilde{\theta} = \hat{\theta} - \theta$: Difference between estimated and true position vector
- $\mathbf{H}_i = \Delta_{\hat{\theta}}^{\hat{\theta}} \log \delta_i$: Hessian matrix of related measurement

- $\mathbf{A} = \begin{bmatrix} \nabla_{\hat{\theta}} \log \delta_1 & \nabla_{\hat{\theta}} \log \delta_2 & \cdots & \nabla_{\hat{\theta}} \log \delta_N \end{bmatrix}^{\mathrm{T}}$: Jacobian matrix

Therefore the estimate $\hat{\theta}$ can be approximated as follows

$$\begin{aligned} \hat{\theta} &= \theta + \mathbf{A}^{+}(\log \delta - \log \mathbf{d}) - 0.5\mathbf{A}^{+} \begin{bmatrix} \mathrm{tr}\left\{\mathbf{H}_1 \tilde{\theta}\tilde{\theta}^{\mathrm{T}}\right\} & \cdots & \mathrm{tr}\left\{\mathbf{H}_N \tilde{\theta}\tilde{\theta}^{\mathrm{T}}\right\} \end{bmatrix}^{\mathrm{T}} \\ &= \theta + \bar{\mathbf{v}} - 0.5 \begin{bmatrix} \mathrm{tr}\left\{\mathbf{M}_{\mathbf{x}} \tilde{\theta}\tilde{\theta}^{\mathrm{T}}\right\} & \mathrm{tr}\left\{\mathbf{M}_{\mathbf{y}} \tilde{\theta}\tilde{\theta}^{\mathrm{T}}\right\} \end{bmatrix}^{\mathrm{T}} \end{aligned} \tag{5.6}$$

where $\mathbf{A}^{+}$ is pseudo inverse of $\mathbf{A}$, namely $\mathbf{A}^{+} = \left(\mathbf{A}^{\mathrm{T}}\mathbf{A}\right)^{-1}\mathbf{A}^{\mathrm{T}}$, $\mathbf{M}_{\mathbf{x}} = \sum_{i=1}^{N} \mathbf{A}_{1,i}\mathbf{H}_i$, $\mathbf{M}_{\mathbf{x}} = \sum_{i=1}^{N} \mathbf{A}_{2,i}\mathbf{H}_i$ and $\bar{\mathbf{v}} \sim \mathcal{N}(\bar{\mathbf{v}}; 0, \mathbf{\Sigma})$ with $\mathbf{\Sigma} = \mathbf{A}^{+}\sigma_{ML}^{2}\left(\mathbf{A}^{+}\right)^{\mathrm{T}}$.

Then $\tilde{\theta}\tilde{\theta}^{\mathrm{T}}$ terms can be approximated by first order expansion, namely $\tilde{\theta}\tilde{\theta}^{\mathrm{T}} \approx \bar{\mathbf{v}}\bar{\mathbf{v}}^{\mathrm{T}}$. Consequently

$$\hat{\theta} = \theta + \bar{\mathbf{v}} - 0.5 \begin{bmatrix} \mathrm{tr}\left\{\mathbf{M}_{\mathbf{x}} \bar{\mathbf{v}}\bar{\mathbf{v}}^{\mathrm{T}}\right\} & \mathrm{tr}\left\{\mathbf{M}_{\mathbf{y}} \bar{\mathbf{v}}\bar{\mathbf{v}}^{\mathrm{T}}\right\} \end{bmatrix}^{\mathrm{T}} \tag{5.7}$$

In this part, $\hat{\theta}$ is constrained by lower bound θ_{min} and upper bound θ_{max} depending on the search space in FSS-MLE. Bias can be found from (5.7) by calculating the mean and correlation matrix of $\bar{\mathbf{v}}$ as follows

$$\mathrm{E}\left\{\hat{\theta}\right\} - \theta = \mathrm{E}\left\{\bar{\mathbf{v}}\right\} - 0.5 \begin{bmatrix} \mathrm{tr}\left\{\mathbf{M}_{\mathbf{x}} \mathrm{E}\left(\bar{\mathbf{v}}\bar{\mathbf{v}}^{\mathrm{T}}\right)\right\} & \mathrm{tr}\left\{\mathbf{M}_{\mathbf{y}} \mathrm{E}\left(\bar{\mathbf{v}}\bar{\mathbf{v}}^{\mathrm{T}}\right)\right\} \end{bmatrix}^{\mathrm{T}} \tag{5.8}$$

The bounds should be considered at calculating first and second order statistics of $\bar{\mathbf{v}}$ in FSS-MLE. However considering (5.7), it is hard to find in which region integral should be taken in calculation of first and second moment of $\bar{\mathbf{v}}$. So we will propose two methods to calculate the bias in (5.8). These methods are presented in the following parts.

5.1.1 Method 1

In this method, we will determine the integral region from first-order approximation (i.e., $\hat{\theta} = \theta + \bar{\mathbf{v}}$). This mapping is given as follows

$$\hat{x} = \begin{cases} x_{\text{min}}, & \text{for } x + v_x \leqslant x_{\text{min}} \\ x + v_x, & \text{for } x_{\text{min}} < x + v_x < x_{\text{max}} \\ x_{\text{max}}, & \text{for } x + v_x \geqslant x_{\text{max}} \end{cases} \tag{5.9}$$

and

$$\hat{y} = \begin{cases} y_{\text{min}}, & \text{for } y + v_y \leqslant y_{\text{min}} \\ y + v_y, & \text{for } y_{\text{min}} < y + v_y < y_{\text{max}} \\ y_{\text{max}}, & \text{for } y + v_y \geqslant y_{\text{max}} \end{cases} \tag{5.10}$$

Because of the mapping above, random variable $\bar{\mathbf{v}}$ so called measurement error is also constrained as follows

$$v'_x = \begin{cases} x_{\text{min}} - x, & \text{for } v_x \leqslant x_{\text{min}} - x \\ v_x, & \text{for } x_{\text{min}} - x < v_x < x_{\text{max}} - x \\ x_{\text{max}} - x, & \text{for } v_x \geqslant x_{\text{max}} - x \end{cases} \tag{5.11}$$

and

$$v'_y = \begin{cases} y_{\text{min}} - y, & \text{for } v_y \leqslant y_{\text{min}} - y \\ v_y, & \text{for } y_{\text{min}} - y < v_y < y_{\text{max}} - y \\ y_{\text{max}} - y, & \text{for } v_y \geqslant y_{\text{max}} - y \end{cases} \tag{5.12}$$

By considering mapping above, 9 regions should be examined to calculate first and second order statistics of $\bar{\mathbf{v}}' \triangleq [v'_x, v'_y]^{\text{T}}$(truncated Gaussian random variable). The conditional first and second moments can be calculated as indicated in Appendix F. These regions are that

- $\mathcal{C}^{(1)} = \{v_x, v_y : x_{\text{min}} - x < v_x < x_{\text{max}} - x, y_{\text{min}} - y < v_y < y_{\text{max}} - y\}$
- $\mathcal{C}^{(2)} = \{v_x, v_y : v_x \leqslant x_{\text{min}} - x, y_{\text{min}} < v_y < y_{\text{max}} - y\}$
- $\mathcal{C}^{(3)} = \{v_x, v_y : v_x \geqslant x_{\text{max}} - x, y_{\text{min}} - y < v_y < y_{\text{max}} - y\}$
- $\mathcal{C}^{(4)} = \{v_x, v_y : x_{\text{min}} - x < v_x < x_{\text{max}} - x, v_y \geqslant y_{\text{max}} - y\}$
- $\mathcal{C}^{(5)} = \{v_x, v_y : x_{\text{min}} - x < v_x < x_{\text{max}} - x, v_y \leqslant y_{\text{min}} - y\}$
- $\mathcal{C}^{(6)} = \{v_x, v_y : v_x \geqslant x_{\text{max}} - x, v_y \geqslant y_{\text{max}} - y\}$
- $\mathcal{C}^{(7)} = \{v_x, v_y : v_x \leqslant x_{\text{min}} - x, v_y \geqslant y_{\text{max}} - y\}$

- $\mathcal{C}^{(8)} = \{v_x, v_y : v_x \geqslant x_{\text{max}} - x, v_y \leqslant y_{\text{min}} - y\}$
- $\mathcal{C}^{(9)} = \{v_x, v_y : v_x \leqslant x_{\text{min}} - x, v_y \leqslant y_{\text{min}} - y\}$

The first and second order statistics of $\bar{\mathbf{v}}'$:

$$\mathrm{E}\left\{\bar{\mathbf{v}}'\right\} = \sum_{i=1}^{9} \mathrm{E}\left\{\bar{\mathbf{v}}' | \mathcal{C}^{(i)}\right\} P(\mathcal{C}^{(i)}) \tag{5.13}$$

$$\mathrm{E}\left\{\bar{\mathbf{v}}'\bar{\mathbf{v}}'^{\mathrm{T}}\right\} = \sum_{i=1}^{9} \mathrm{E}\left\{\bar{\mathbf{v}}'\bar{\mathbf{v}}'^{\mathrm{T}} | \mathcal{C}^{(i)}\right\} P(\mathcal{C}^{(i)}) \tag{5.14}$$

Finally, we substitute (5.13) and (5.14) to the expression (5.8) directly to find the bias of the estimator. The resulting bias is as follows

$$\mathrm{E}\left\{\hat{\theta}\right\} - \theta = \mathrm{E}\left\{\bar{\mathbf{v}}'\right\} - 0.5 \left[\begin{array}{cc} \mathrm{tr}\left\{\mathbf{M_x}\,\mathrm{E}\left(\bar{\mathbf{v}}'\bar{\mathbf{v}}'^{\mathrm{T}}\right)\right\} & \mathrm{tr}\left\{\mathbf{M_y}\,\mathrm{E}\left(\bar{\mathbf{v}}'\bar{\mathbf{v}}'^{\mathrm{T}}\right)\right\} \end{array} \right]^{\mathrm{T}} \tag{5.15}$$

5.1.2 Method 2

In this method, we first calculate $\mathrm{E}\left\{\bar{\mathbf{v}}'\bar{\mathbf{v}}'^{\mathrm{T}}\right\}$ utilizing the equations given in Appendix F according to constraints (5.11) and (5.12). Then we form a new constraints on $\mathbf{v}$ such that

$$v_x'' = \begin{cases} x'_{\text{min}}, & \text{for } v_x \leqslant x'_{\text{min}} \\ v_x, & \text{for } x'_{\text{min}} < v_x < x'_{\text{max}} \\ x'_{\text{max}}, & \text{for } v_x \geqslant x'_{\text{max}} \end{cases} \tag{5.16}$$

and

$$v_y'' = \begin{cases} y'_{\text{min}}, & \text{for } v_y \leqslant y'_{\text{min}} \\ v_y, & \text{for } y'_{\text{min}} < v_y < y'_{\text{max}} \\ y'_{\text{max}}, & \text{for } v_y \geqslant y'_{\text{max}} \end{cases} \tag{5.17}$$

where $x'_{\text{min}} = x_{\text{min}} - x + 0.5\,\mathrm{tr}\left\{\mathbf{M_x}\,\mathrm{E}\left(\bar{\mathbf{v}}'\bar{\mathbf{v}}'^{\mathrm{T}}\right)\right\}$, $x'_{\text{max}} = x_{\text{max}} - x + 0.5\,\mathrm{tr}\left\{\mathbf{M_x}\,\mathrm{E}\left(\bar{\mathbf{v}}'\bar{\mathbf{v}}'^{\mathrm{T}}\right)\right\}$, $y'_{\text{min}} = y_{\text{min}} - y + 0.5\,\mathrm{tr}\left\{\mathbf{M_y}\,\mathrm{E}\left(\bar{\mathbf{v}}'\bar{\mathbf{v}}'^{\mathrm{T}}\right)\right\}$ and $y'_{\text{max}} = y_{\text{max}} - x + 0.5\,\mathrm{tr}\left\{\mathbf{M_y}\,\mathrm{E}\left(\bar{\mathbf{v}}'\bar{\mathbf{v}}'^{\mathrm{T}}\right)\right\}$

We calculate $\mathrm{E}\{\bar{\mathbf{v}}''\}$ due to constraints (5.16) and (5.17). Finally, we substitute resulting first and second moments, $\mathrm{E}\{\bar{\mathbf{v}}''\}$ and $\mathrm{E}\left\{\bar{\mathbf{v}}'\bar{\mathbf{v}}'^{\mathrm{T}}\right\}$ respectively to (5.8) to find the bias of the estimator. The bias will be that

$$\mathrm{E}\left\{\hat{\theta}\right\} - \theta = \mathrm{E}\{\bar{\mathbf{v}}''\} - 0.5\left[\begin{array}{cc} \mathrm{tr}\left\{\mathbf{M_x}\,\mathrm{E}\left(\bar{\mathbf{v}}'\bar{\mathbf{v}}'^{\mathrm{T}}\right)\right\} & \mathrm{tr}\left\{\mathbf{M_y}\,\mathrm{E}\left(\bar{\mathbf{v}}'\bar{\mathbf{v}}'^{\mathrm{T}}\right)\right\} \end{array}\right]^{\mathrm{T}} \quad (5.18)$$

5.2 Simulation Results

In this section, Method 1 and 2, which are proposed to calculate the bias of FSS-MLE in Section 5.1, are analyzed via a simulation study. They are also compared to bias formula based on Taylor series expansion of RSS-MLE cost function itself in Chapter 4, the previous one, with infinite finite search space. For simulation, we deployed the anchors in coordinates (0,0), (10,0), (0,10) and (10,10). Moreover, one blindfolded node is placed in various locations of observation area of 10 m $\times$ 10 m. Because of the fact that a connectivity constraint with respect to a threshold power cannot be put into the second formula, we did not attach connectivity events to our simulations here. Hence we assume fully connected nodes. Additionally, we implemented FSS-MLE localization with two different search space area. The first is 10 m $\times$ 10 m (grid1 in the simulations), while the other is 40 m $\times$ 40 m (grid2 in simulations). To see the validity of the analytical formula, we compare the simulation results with the analytical one (Method 1 and 2) for some values of standard deviation of shadowing effect in the channel, since there is no one metric combining all uncertainty metrics together to our best knowledge. These uncertainty metrics can be path loss exponent, standard deviation of shadowing effect, distance to observer, reference power in RSS based localization problem. We made a MC simulation with 10000 runs to obtain a comparison between analytical bias formulas and simulation results for $\alpha = 3$, $\mathrm{P}_0 = -30$ dBm and some values of standard deviation of shadowing effect. The bias pictures for FSS-MLE (grid1) showing the performance of Method 1 are presented for standard deviation 6.15, 3.79 and 2.97 dB in Figures 5.1, 5.3 and 5.5. The bias pictures showing the performance of Method 2 for standard deviation 6.15, 3.79 and 2.97 dB can also be found in Figures 5.2, 5.4 and 5.6 respectively. It should be also noted that the results related to only the first quarter of observation area are provided in these related figures.

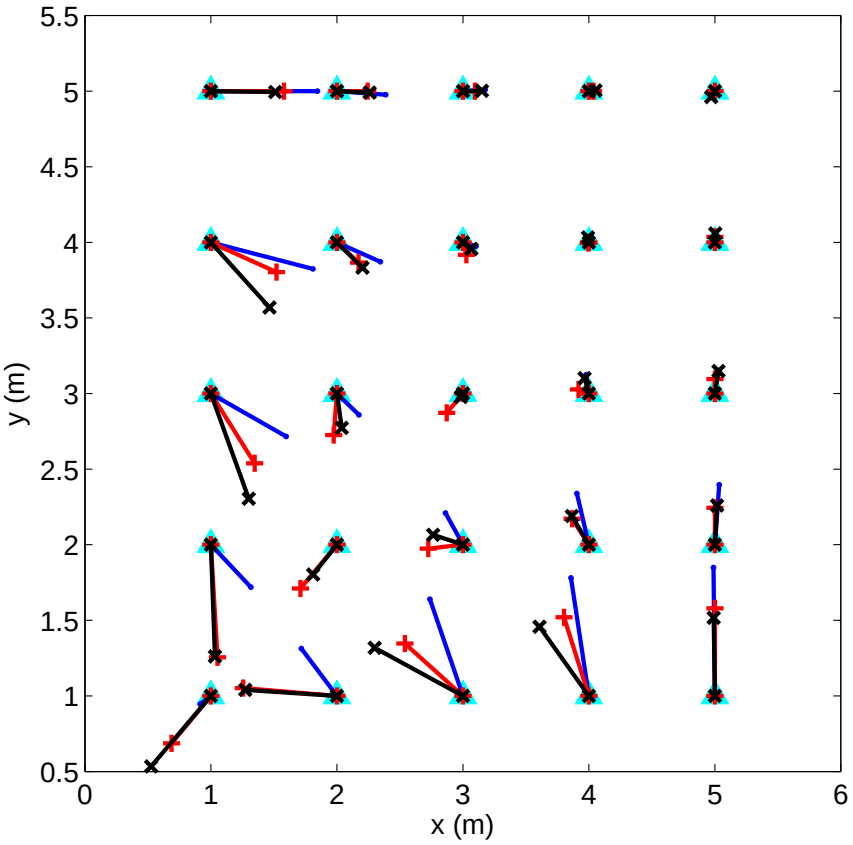

Figure 5.1: Comparison between mean of 2-D non-collaborative FSS-MLE localization by simulation and Method 1 at $\sigma = 6.15$ dB for different location of blindfolded nodes: True position of blindfolded node (▲), mean of FSS-MLE (grid1) localization (MC)(**.-**), Method 1 (analy.) (**+-**), MC expectation of eqn (6.8) (×**-**)

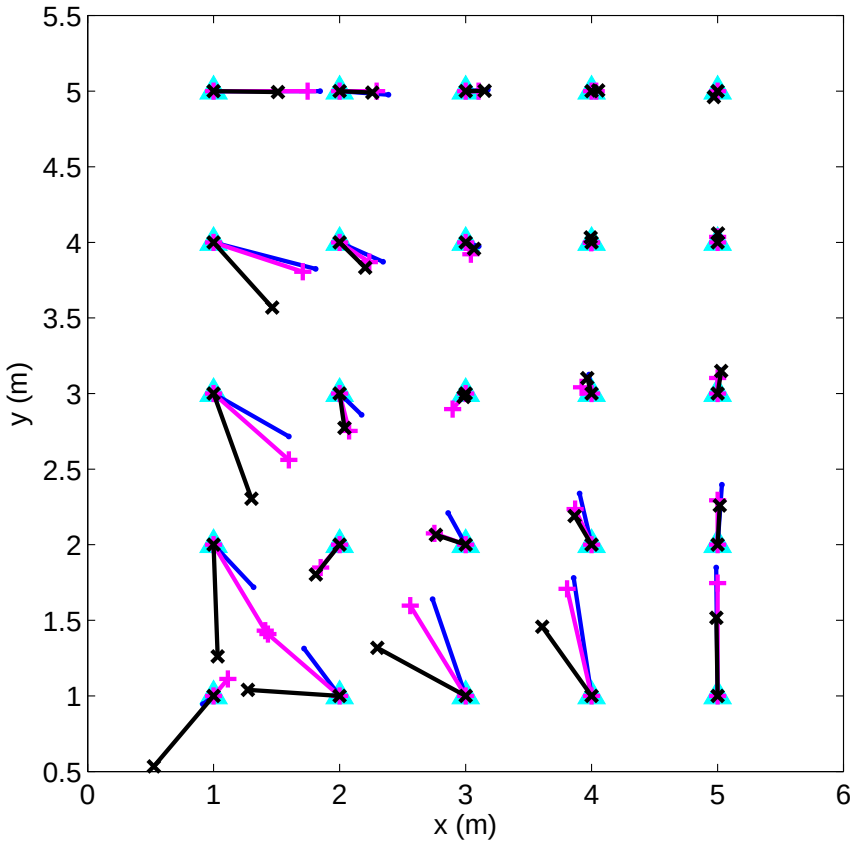

Figure 5.2: Comparison between mean of 2-D non-collaborative FSS-MLE localization by simulation and Method 2 at $\sigma = 6.15$ dB for different location of blindfolded nodes: True position of blindfolded node (▲), mean of FSS-MLE (grid1) localization (MC)(.-), Method 2 (analy.) (+-), MC expectation of eqn (6.8) (×-)

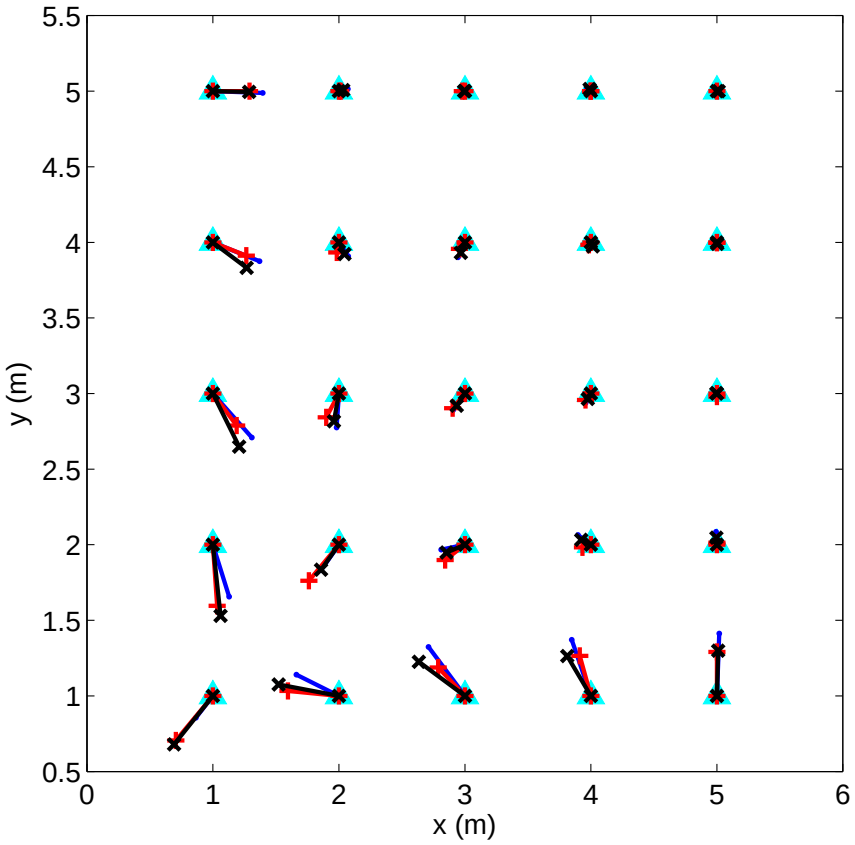

Figure 5.3: Comparison between mean of 2-D non-collaborative FSS-MLE localization by simulation and Method 1 at $\sigma = 3.79$ dB for different location of blindfolded nodes: True position of blindfolded node (▲), Mean of FSS-MLE (grid1) localization (MC)(.-), Method 1 (analy.) (+-), MC expectation of eqn (6.8) (×-)

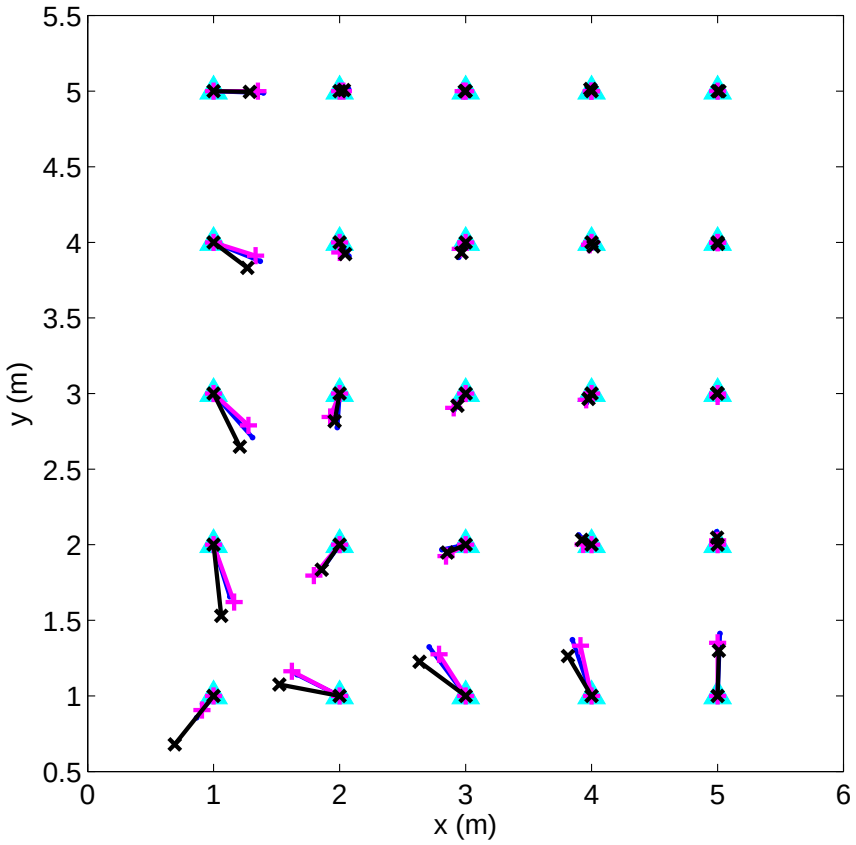

Figure 5.4: Comparison between mean of 2-D non-collaborative FSS-MLE localization by simulation and Method 2 at $\sigma = 3.79$ dB for different location of blindfolded nodes: True position of blindfolded node (▲), mean of FSS-MLE (grid1) localization (MC)(.-), Method 2 (analy.) (+-), MC expectation of eqn (6.8) (×-)

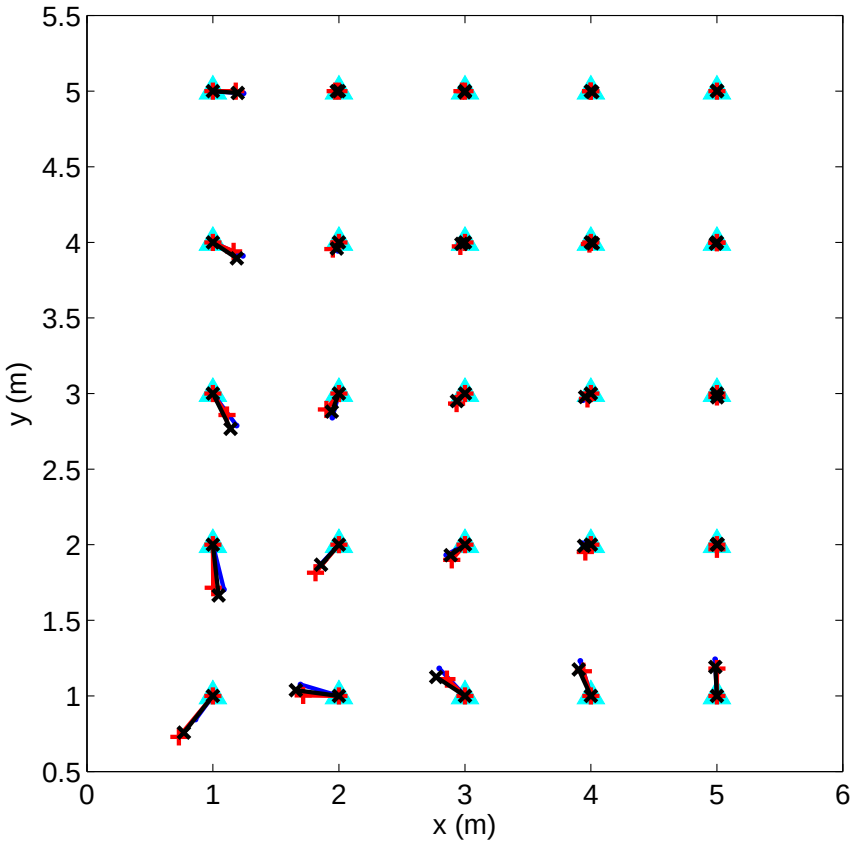

Figure 5.5: Comparison between mean of 2-D non-collaborative FSS-MLE localization by simulation and Method 1 at $\sigma = 2.97$ dB for different location of blindfolded nodes: True position of blindfolded node (▲), mean of FSS-MLE (grid1) localization (MC)(**.-**), Method 1 (analy.) (**+-**), MC expectation of eqn (6.8) (×**-**)

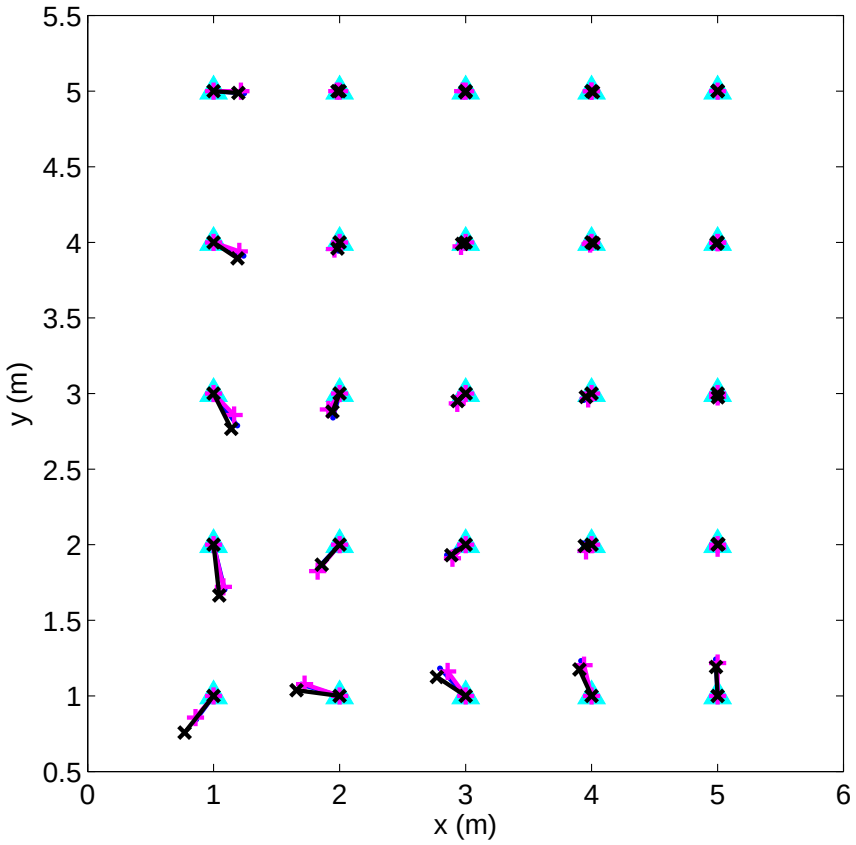

Figure 5.6: Comparison between mean of 2-D non-collaborative FSS-MLE localization by simulation and Method 2 at $\sigma = 2.97$ dB for different location of blindfolded nodes: True position of blindfolded node (▲), mean of FSS-MLE (grid1) localization (MC)(.-), Method 2 (analy.) (+-), MC expectation of eqn (6.8) (×-)

When Figures 5.1-5.6 are examined, it can be observed that Method 2 has better match to simulation results than Method 1 especially at lower values of standard deviation. The predicted bias values, in FSS-MLE (grid1) for maximum 10 meter distance to anchor, are acceptable when the standard deviation $\sigma = 3.79$ dB is considered, a relatively high uncertainty. Additionally it is also beneficial to see the characteristics of our bias formula along with simulation results. Therefore the bias figures with respect to varying σ's at some position coordinates of the blindfolded node are provided in Figures 5.7-5.10.

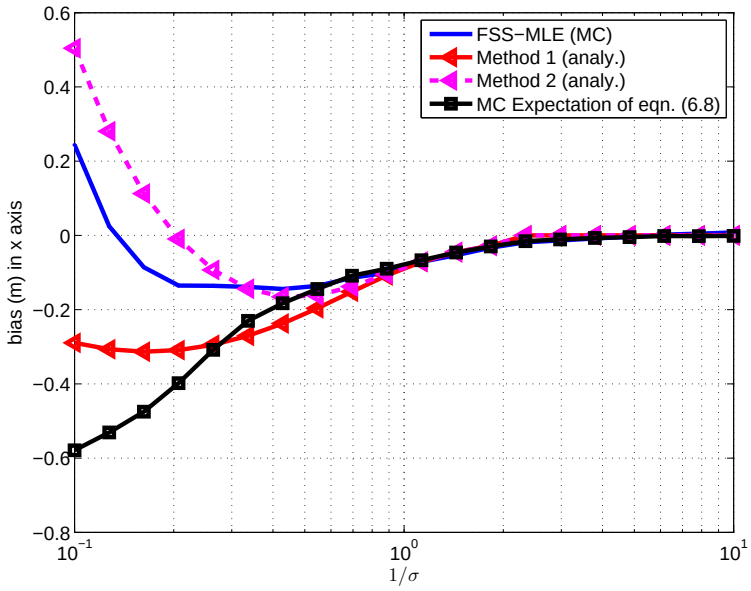

Figure 5.7: Comparison between simulation and analytical bias in x-direction at point (1,1) wrt $1/\sigma$'s: FSS-MLE (grid1), Method 1 (analy.), Method 2 (analy.), MC expectation of eqn. (6.8)

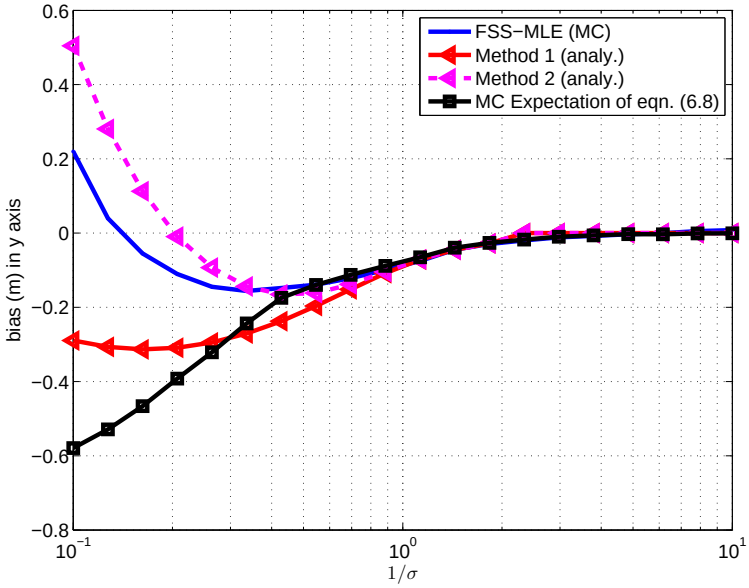

Figure 5.8: Comparison between simulation and analytical bias in y-direction at point (1,1) wrt $1/\sigma$'s: FSS-MLE (grid1), Method 1 (analy.), Method 2 (analy.), MC expectation of eqn. (6.8)

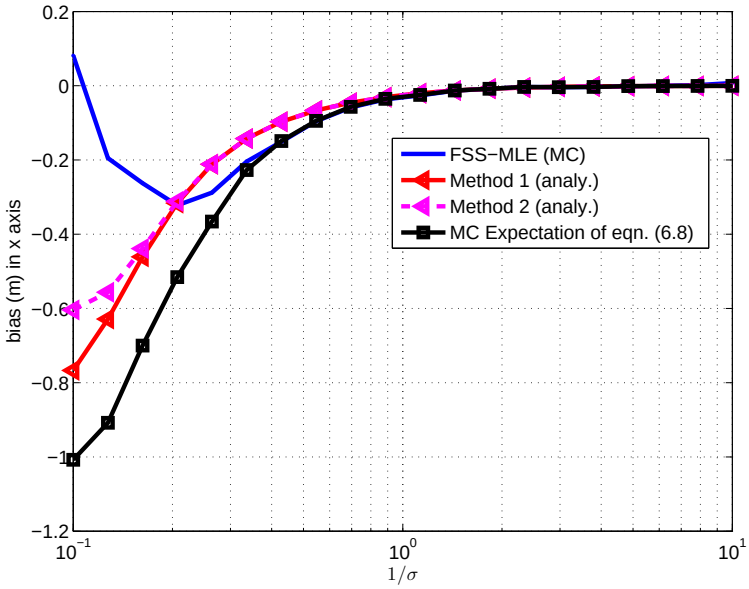

Figure 5.9: Comparison between simulation and analytical bias in x-direction at point (3,1) wrt $1/\sigma$'s: FSS-MLE (grid1), Method 1 (analy.), Method 2 (analy.), MC expectation of eqn. (6.8)

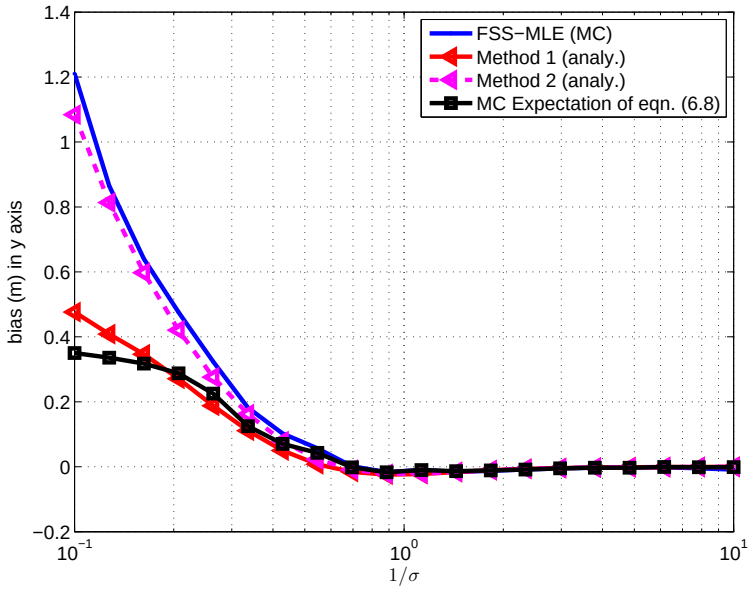

Figure 5.10: Comparison between simulation and analytical bias in y-direction at point (3,1) wrt $1/\sigma$'s: FSS-MLE (grid1), Method 1 (analy.), Method 2 (analy.), MC expectation of eqn. (6.8)

As mentioned before, it is known that FSS-MLE converges to RSS-MLE when the area of search space is large enough. The question here is: Does Method 1 or 2 still have good prediction of bias at considerably high standard deviation values? Can this formula be applicable for RSS-MLE like FSS-MLE at some search space too? The answer of these questions is surprisingly "no". It was intuitively expectable for us that the analytical bias formula could validate at larger search spaces for FSS-MLE localization, but the following figures tell the other way. The bias figures for FSS-MLE (grid2) showing the performance of Method 1 and 2 for different standard deviation values are presented in Figures 5.11-5.16. Additionally the bias figures with respect to varying σ's at some position coordinates of the blindfolded node are provided in Figures 5.17-5.20.

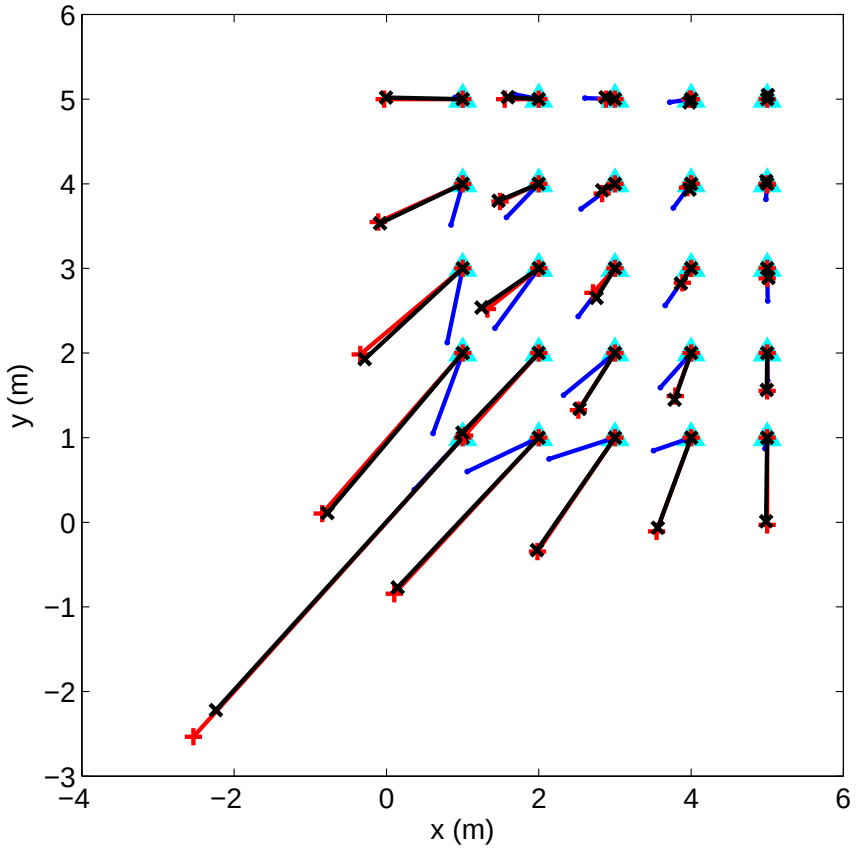

Figure 5.11: Comparison between mean of 2-D non-collaborative FSS-MLE localization by simulation and Method 1 at $\sigma = 6.15$ dB for different location of blindfolded nodes: True position of blindfolded node (▲), mean of FSS-MLE (grid2) localization (MC)(.-), Method 1 (analy.) (+-), MC expectation of eqn (6.8) (×-)

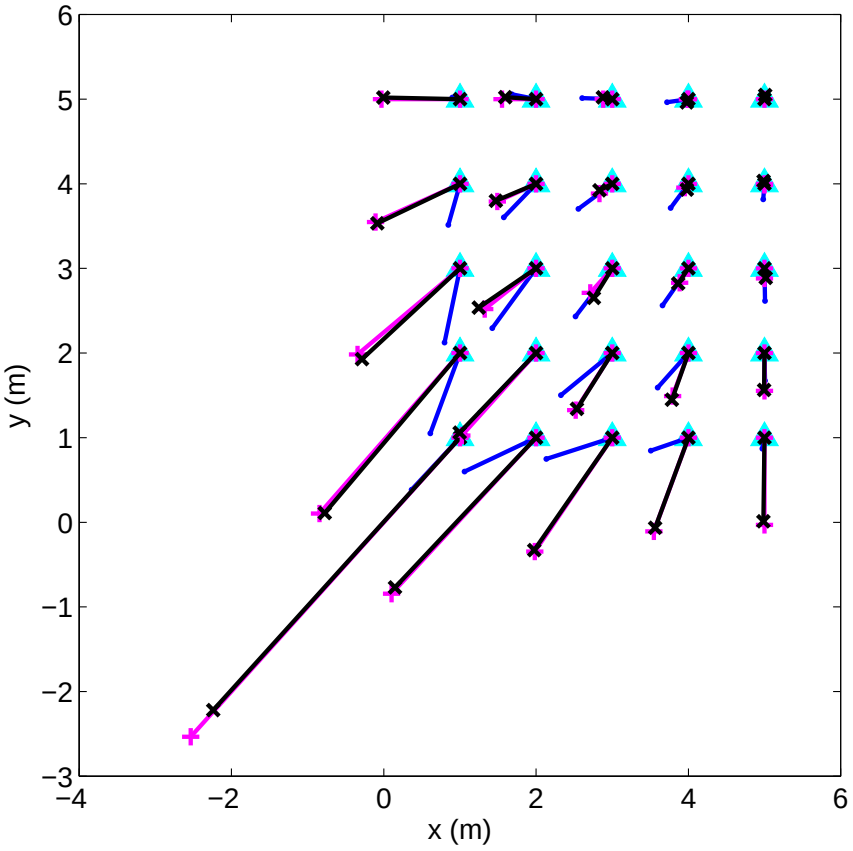

Figure 5.12: Comparison between mean of 2-D non-collaborative FSS-MLE localization by simulation and Method 2 at $\sigma = 6.15$ dB for different location of blindfolded nodes: True position of blindfolded node (▲), mean of FSS-MLE (grid2) localization (MC)(.-), Method 2 (analy.) (+-), MC expectation of eqn (6.8) (×-)

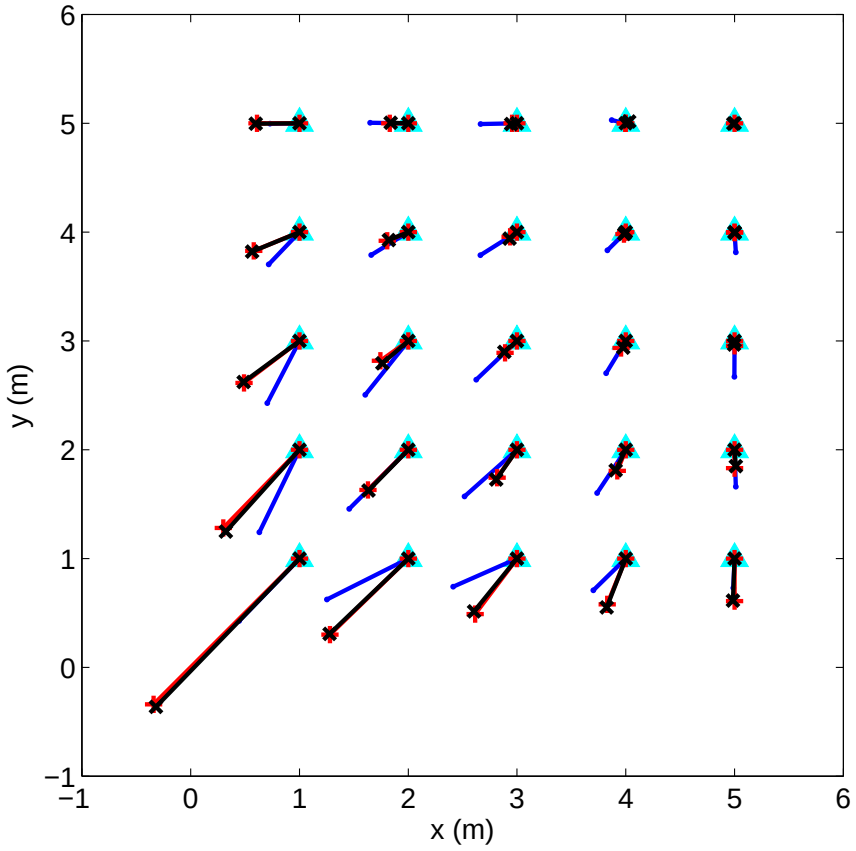

Figure 5.13: Comparison between mean of 2-D non-collaborative FSS-MLE localization by simulation and Method 1 at $\sigma = 3.79$ dB for different location of blindfolded nodes: True position of blindfolded node (▲), mean of FSS-MLE (grid2) localization (MC)(**.-**), Method 1 (analy.) (**+-**), MC expectation of eqn (6.8) (×**-**)

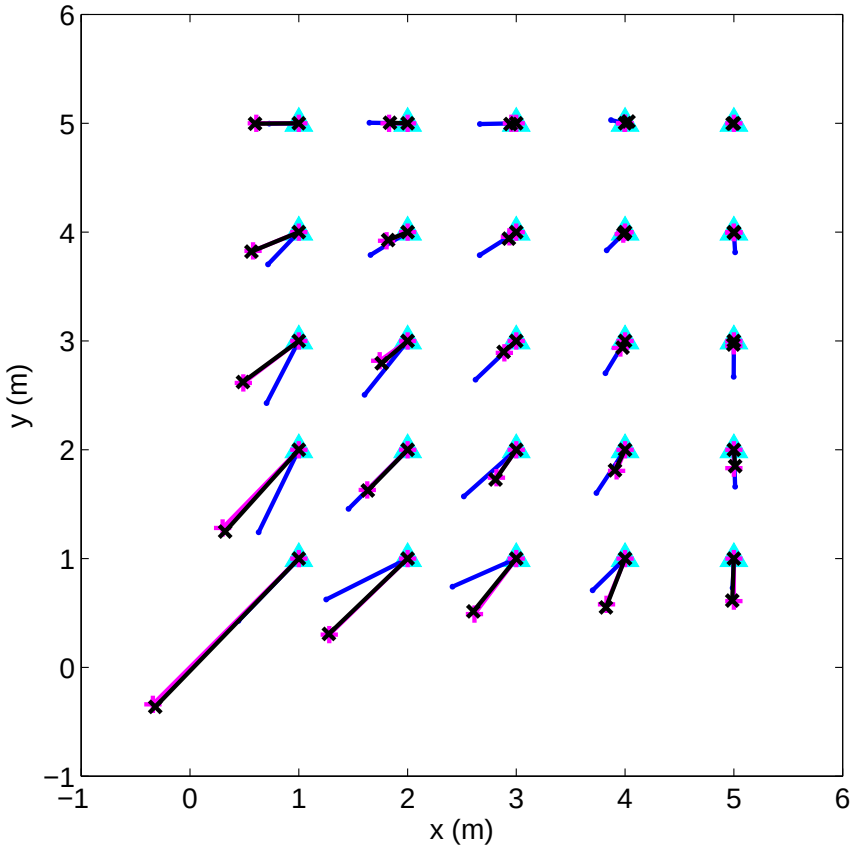

Figure 5.14: Comparison between mean of 2-D non-collaborative FSS-MLE localization by simulation and Method 2 at $\sigma = 3.79$ dB for different location of blindfolded nodes: True position of blindfolded node (▲), mean of FSS-MLE (grid2) localization (MC)(.-), Method 2 (analy.) (+-), MC expectation of eqn (6.8) (×-)

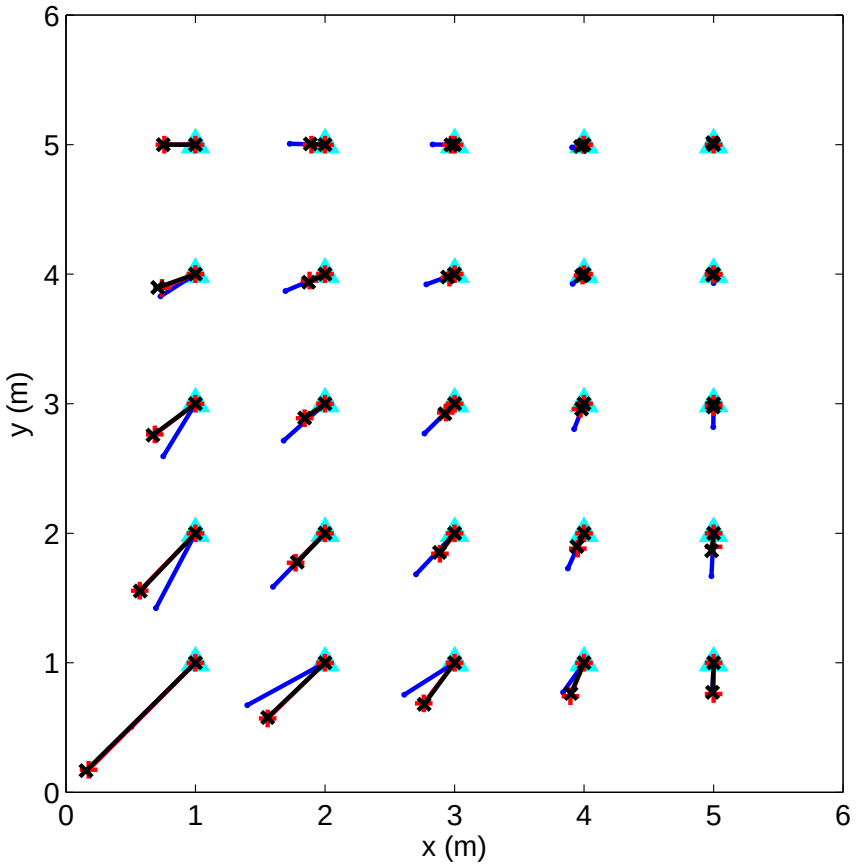

Figure 5.15: Comparison between mean of 2-D non-collaborative FSS-MLE localization by simulation and Method 1 at $\sigma = 2.97$ dB for different location of blindfolded nodes: True position of blindfolded node (▲), mean of FSS-MLE (grid2) localization (MC)(**.-**), Method 1 (analy.) (**+-**), MC expectation of eqn (6.8) (×**-**)

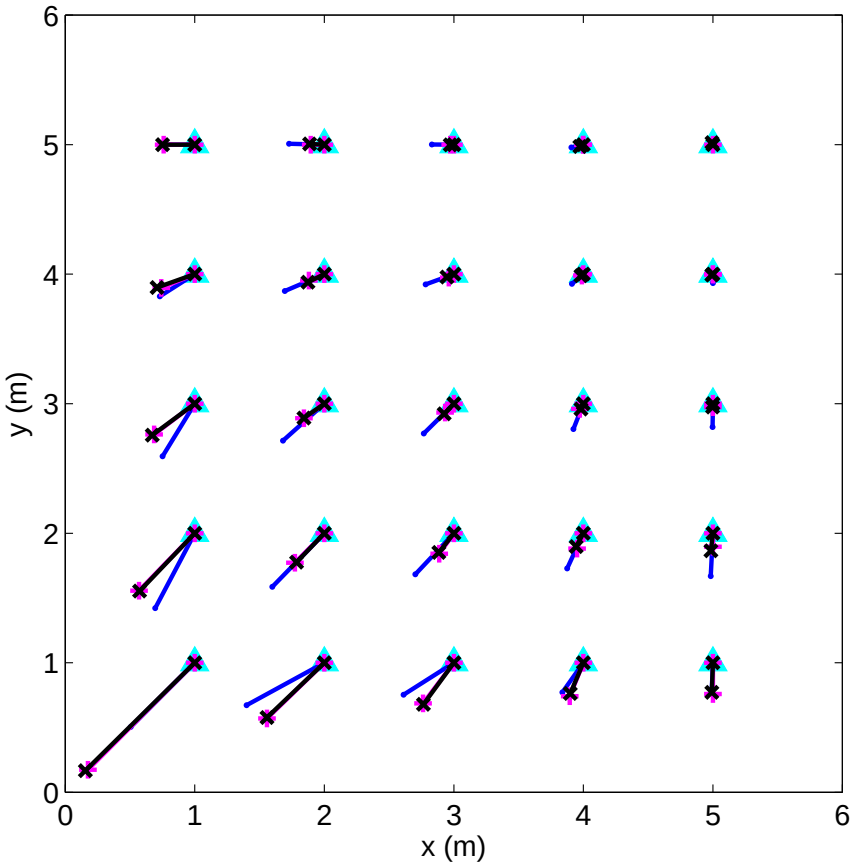

Figure 5.16: Comparison between mean of 2-D non-collaborative FSS-MLE localization by simulation and Method 2 at $\sigma = 2.97$ dB for different location of blindfolded nodes: True position of blindfolded node (▲), mean of FSS-MLE (grid2) localization (MC)(.-), Method 2 (analy.) (+-), MC expectation of eqn (6.8) (×-)

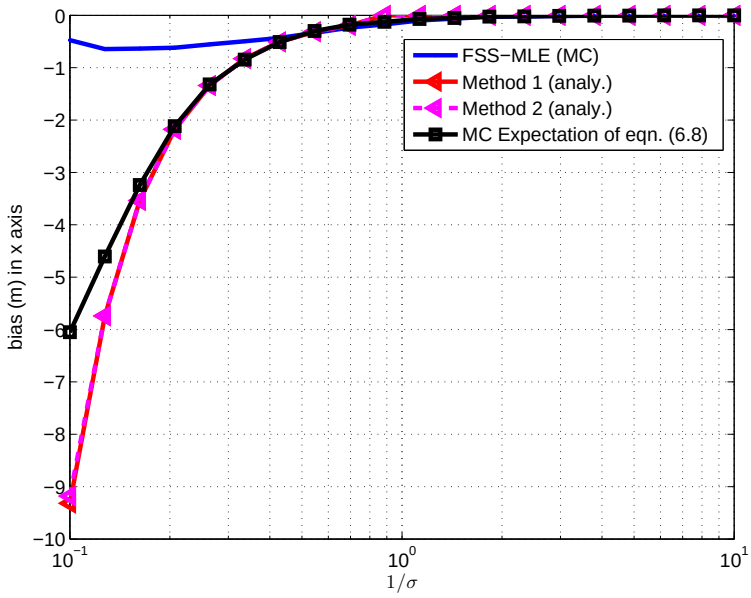

Figure 5.17: Comparison between simulation and analytical bias in x-direction at point (1,1) wrt $1/\sigma$'s: FSS-MLE (grid2), Method 1 (analy.), Method 2 (analy.), MC expectation of eqn (6.8)

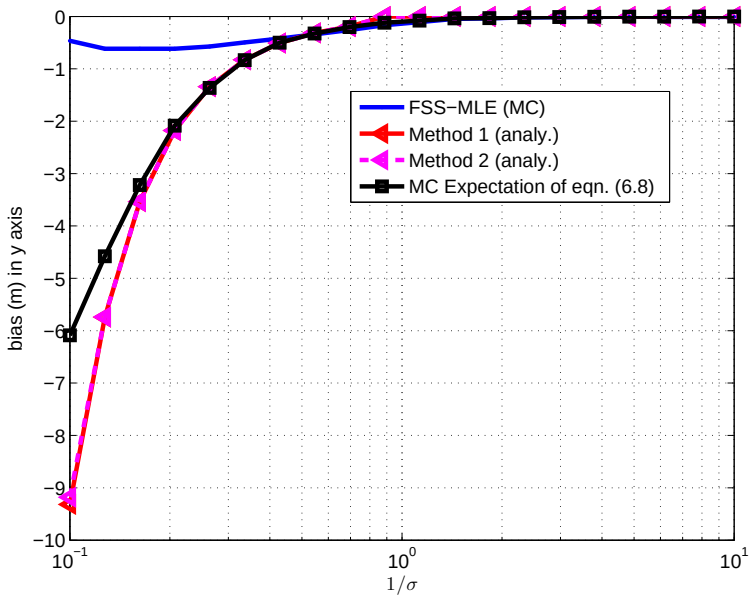

Figure 5.18: Comparison between simulation and analytical bias in y-direction at point (1,1) wrt $1/\sigma$'s: FSS-MLE (grid2), Method 1 (analy.), Method 2 (analy.), MC expectation of eqn (6.8)

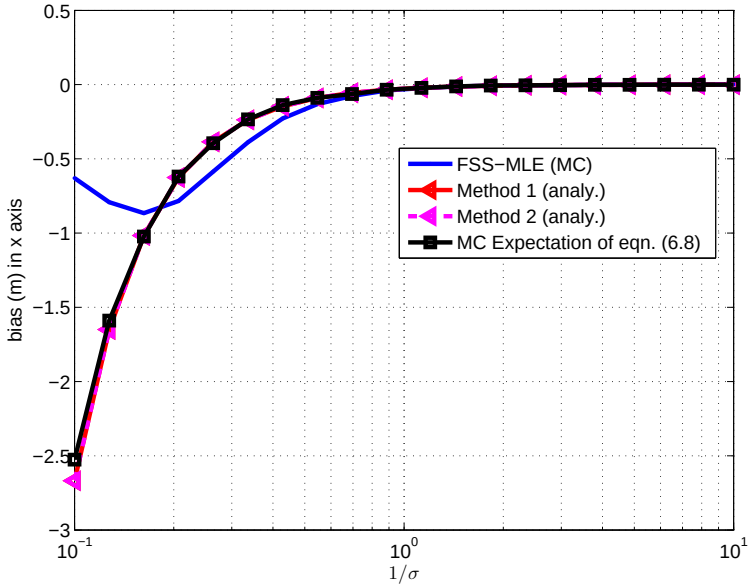

Figure 5.19: Comparison between simulation and analytical bias in x-direction at point (3,1) wrt $1/\sigma$'s: FSS-MLE (grid2), Method 1 (analy.), Method 2 (analy.), MC expectation of eqn (6.8)

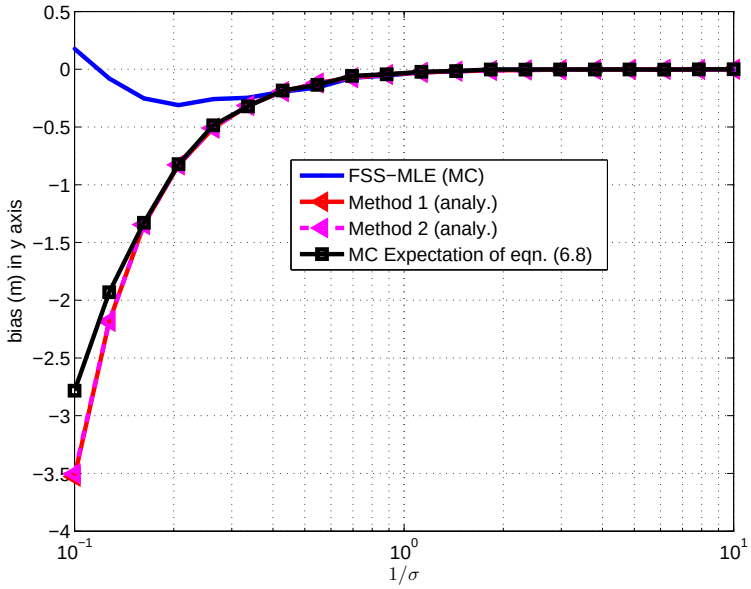

Figure 5.20: Comparison between simulation and analytical bias in y-direction at point (3,1) wrt $1/\sigma$'s: FSS-MLE (grid2), Method 1 (analy.), Method 2 (analy.), MC expectation of eqn (6.8)

From bias related figures for FSS-MLE (grid2), it is not possible to give an accurate prediction for bias with second formula, namely Method 1 and 2, in the situation that the area of search space is so large. However comparing the first bias formula in Chapter 4 with second formula in this chapter may give information about unexplained conditions. For that, we would like to compare these analytical bias formulas derived from different approaches. The figures related to this are shown in Figures 5.21-5.24.

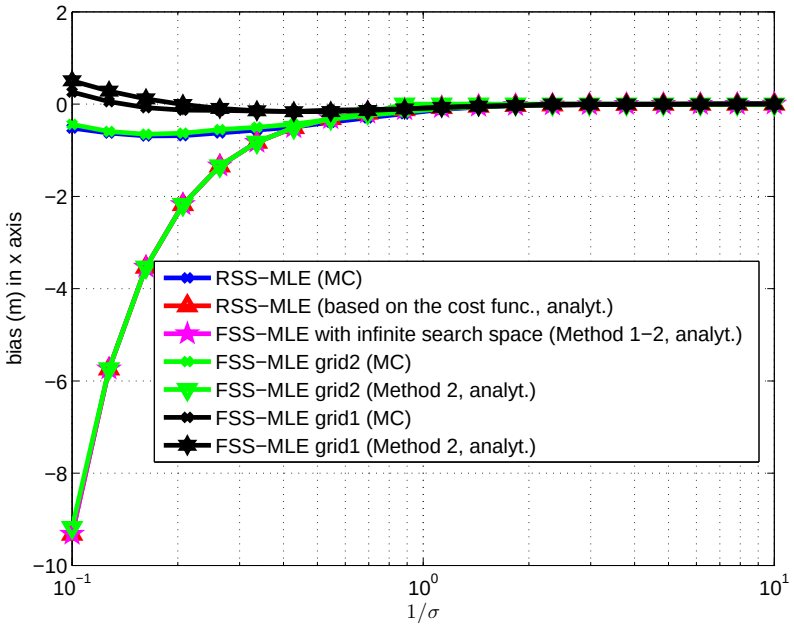

Figure 5.21: Comparison between simulation and analytical bias in x-direction at point (1,1) wrt $1/\sigma$'s: RSS-MLE (gradient based, MC), RSS-MLE (based on the cost func., analy.), FSS-MLE with infinite search space (Method 1-2, analy.), FSS-MLE grid1 (MC), FSS-MLE grid1 (Method 2, analy.), FSS-MLE grid2 (MC), FSS-MLE grid2 (Method 2, analy.)

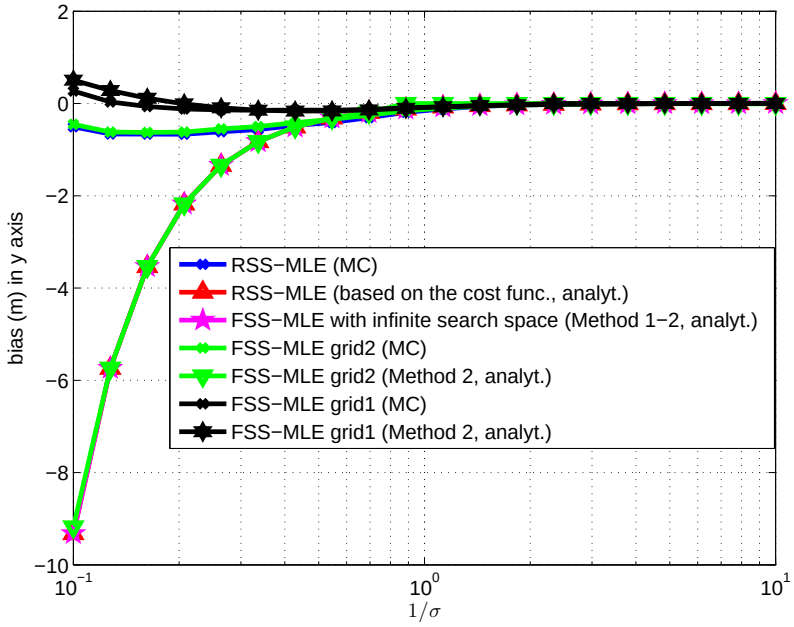

Figure 5.22: Comparison between simulation and analytical bias in y-direction at point (1,1) wrt $1/\sigma$'s: RSS-MLE (gradient based, MC), RSS-MLE (based on the cost func., analy.), FSS-MLE with infinite search space (Method 1-2, analy.), FSS-MLE grid1 (MC), FSS-MLE grid1 (Method 2, analy.), FSS-MLE grid2 (MC), FSS-MLE grid2 (Method 2, analy.)

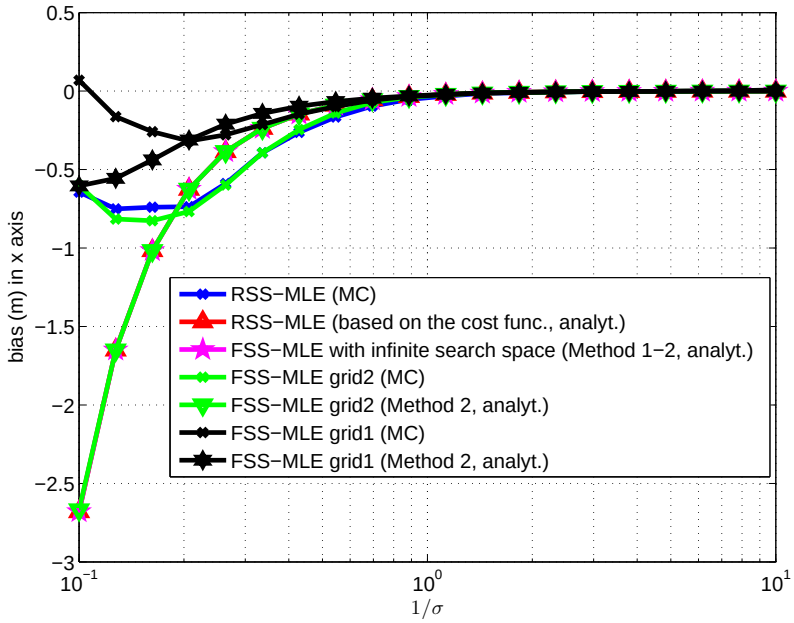

Figure 5.23: Comparison between simulation and analytical bias in x-direction at point (3,1) wrt $1/\sigma$'s: RSS-MLE (gradient based, MC), RSS-MLE (based on the cost func., analy.), FSS-MLE with infinite search space (Method 1-2, analy.), FSS-MLE grid1 (MC), FSS-MLE grid1 (Method 2, analy.), FSS-MLE grid2 (MC), FSS-MLE grid2 (Method 2, analy.)

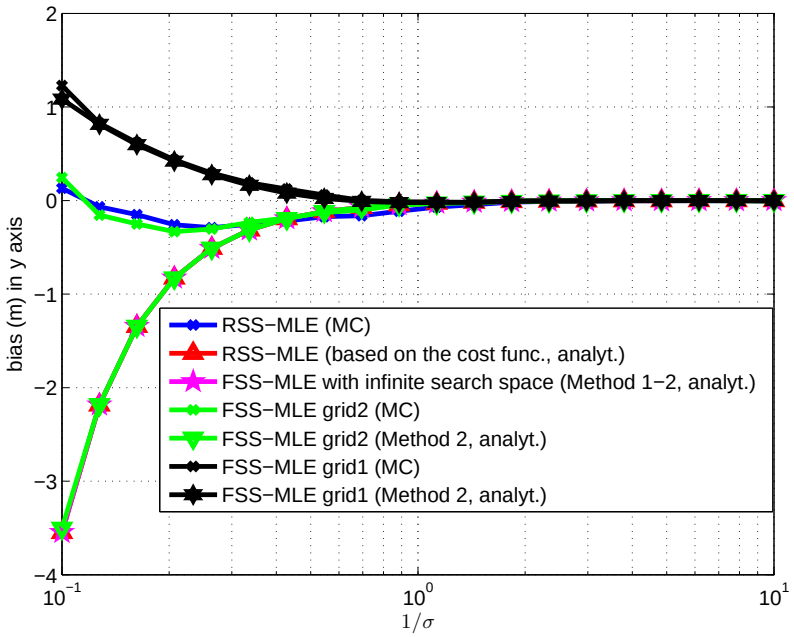

Figure 5.24: Comparison between simulation and analytical bias in y-direction at point (3,1) wrt $1/\sigma$'s: RSS-MLE (gradient based, MC), RSS-MLE (based on the cost func., analy.), FSS-MLE with infinite search space (Method 1-2, analy.), FSS-MLE grid1 (MC), FSS-MLE grid1 (Method 2, analy.), FSS-MLE grid2 (MC), FSS-MLE grid2 (Method 2, analy.)

It is seen from figures above that there is no significant difference between FSS-MLE (grid-2) and RSS-MLE at points (1,1) and (3,1). In addition to this, two analytical bias expressions introduced in this thesis are the same unexpectedly despite different approaches. This is because the approximation of estimate covariance in (5.14) becomes equal to CRLB which is used for approximation for related covariance as the search space goes to infinity. As a result, the bias calculation we propose is not applicable for RSS-MLE, but applicable for some scenarios of FSS-MLE. The connectivity constraint can be added into this bias formula, but this requires a future study to be conducted.

CHAPTER 6

CONCLUSION AND FUTURE WORK

In this thesis, RSS based localization methods are discussed in wireless sensor networks. It is observed that gradient based algorithms which are utilized in MLE cost function is prone to local optima of MLE cost function when the random initialization is used. Therefore it is necessary to supply initial values to the algorithm near local minimum points of the cost function to obtain better results than the solution with random initialization. Therefore MDS and WLS solution with different weights are used as initialization to MLE method. We solve MDS cost function with Quasi-Newton and SMACOF algorithm in which anchors are taken as unknown in the cost function. Then Procrustes transformation is applied to estimate configuration being output of the algorithm in which anchors are taken as unknown parameters. Additionally, we solve WLS cost function on distance measurements in which anchors are known in the function, it gives the best results to compare with three methods (MLE, MDS with Quasi-Newton and MDS with SMACOF).

We also apply adaptive neighborhood selection method given in [9] for reducing the bias of neighbor nodes. When we apply the adaptive neighborhood selection method to the algorithms and use the WLS cost function optimized through Quasi-Newton algorithm, the MLE solution with the WLS method which is given to the MLE method as initial value has estimate variance which is very close to CRLB and approximately zero bias for specific collaborative scenarios in Section 2.5.1.

h-RSS-MLE and RSS-MLE localization methods are also compared to each other in some scenarios including collaborative and non-collaborative cases. It is observed that h-RSS-MLE mitigates the bias significantly in uniform deployment of blind-

folded nodes in collaborative localization because of the information that h-RSS-MLE has additional probability of non-connectivities of the nodes in its cost function. However, this effect cannot be totally observed in a non-collaborative localization scenario.

Secondly, we implemented conventional tracking algorithms and static localization which is RSS-MLE and h-RSS-MLE optimized through grid-search method for non-collaborative scenario in simulations. It can be observed that particle filter has the best performance among them, but its disadvantage is that it is computationally to expensive. Additionally we performed an experiment for the non-collaborative case. It was observed that tracking algorithms are better than static localization methods, since they have the property of time-averaging or improving estimates iteratively by using both a dynamic motion model and a measurement model.

Finally we obtained analytical bias expressions for h-RSS-MLE to understand its bias reducing property. We derived an analytical bias formula for both RSS-MLE and h-RSS-MLE by following a similar methodology with [41] and putting connectivity constraints into the problem. It can be said that the analytical formula which is derived by using Taylor series expansion of the cost function is suitable for 1-D non-collaborative case. However we could not confirm the derived formula with simulation results for the 2-D case. The reason of non-validation of the analytical formula may be higher non-linearities of the 2-D case. Consequently, we can say that the approach to derive bias formula introduced in [41] may not be convenient for MLE or its hybrid version based on RSS measurements.

In addition to this, we derived another analytical expression for the bias of FSS-MLE by utilizing Taylor series expansion of RSS distance measurements themselves instead of Taylor series expansion of the cost function with assumption of fully connected nodes. The bias formula holds at some standard deviations of channel measurements in FSS-MLE localization. However if we expand the area of search space in grid-search for FSS-MLE cost function, FSS-MLE becomes equivalent to RSS-MLE, and the bias formula for FSS-MLE in Chapter 5 converges surprisingly to the formula for RSS-MLE in Chapter 4, although the derivation of these analytical expressions makes use of different approaches. We think, the reason of this is that

approximate covariance used in bias formula for FSS-MLE in Chapter 5 becomes identical to CRLB which is used in Chapter 4. We have eventually an analytical bias formula of FSS-MLE which can be used as benchmark in some situations.

As a future work, collaborative tracking and localization methods can be compared via simulation studies and experimental work. We anticipate that collaborative tracking can have higher accuracy than collaborative localization, non-collaborative localization and tracking. Moreover, incorporating intra-node measurements (e.g., accelerometer, gyroscope) and hybrid measurement techniques (e.g., TOA-RSS) into the localization and tracking problem can be another future work, since these measurements can improve the results considerably. Finally, range based positioning techniques can be compared with fingerprinting based one via an experimental study in future.

REFERENCES

[1] http://arduino.cc. [Last accessed on March 2014].

[2] http://www.digi.com. [Last accessed on March 2014].

[3] I. F. Akyildiz, W. Su, Y. Sankarasubramaniam, and E. Cayirci. Wireless sensor networks: A survey. *Computer Networks*, 38:393–422, 2002.

[4] B. Anderson and J. Moore. *Optimal Filtering*. Prentice-Hall, Englewood Cliffs, NJ, 1979.

[5] S. S. Blackman and R. Popoli. *Design and analysis of modern tracking systems*. Artech House radar library. Artech House, Boston, London, 1999.

[6] I. Borg and P. J. F. Groenen. *Modern multidimensional scaling: Theory and applications*. Springer Verlag, 2005.

[7] W. Cheng, K. Tan, V. Omwando, J. Zhu, and P. Mohapatra. RSS-ratio for enhancing performance of RSS-based applications. In *INFOCOM, 2013 Proceedings IEEE*, pages 3075–3083, April 2013.

[8] A. Coluccia and F. Ricciato. On ML estimation for automatic RSS-based indoor localization. In *Wireless Pervasive Computing (ISWPC), 2010 5th IEEE International Symposium on*, pages 495–502, May 2010.

[9] J. A. Costa, N. Patwari, and A. O. Hero, III. Distributed weighted-multidimensional scaling for node localization in sensor networks. *ACM Trans. Sen. Netw.*, 2(1):39–64, Feb. 2006.

[10] B. Dil and P. Havinga. On the calibration and performance of RSS-based localization methods. In *Internet of Things (IOT), 2010*, pages 1–8, Nov 2010.

[11] B. Dil and P. Havinga. RSS-based localization with different antenna orientations. In *Telecommunication Networks and Applications Conference (ATNAC), 2010 Australasian*, pages 13–18, Oct 2010.

[12] M. B. G and S. Wilhelm. Moments Calculation For the Doubly Truncated Multivariate Normal Density. *ArXiv e-prints*, June 2012.

[13] G. Giorgetti, S. K. Gupta, and G. Manes. Optimal RSS threshold selection in connectivity-based localization schemes. In *Proceedings of the 11th International Symposium on Modeling, Analysis and Simulation of Wireless and Mobile Systems*, MSWiM '08, pages 220–228, New York, NY, USA, 2008. ACM.

[14] G. Giorgetti, S. K. S. Gupta, and G. Manes. Understanding the limits of RF-based collaborative localization. *Networking, IEEE/ACM Transactions on*, 19(6):1638–1651, Dec 2011.

[15] A. Goldsmith. *Wireless Communications*. Cambridge University Press, New York, NY, USA, 2005.

[16] Y. Gu, A. Lo, and I. Niemegeers. A survey of indoor positioning systems for wireless personal networks. *Communications Surveys Tutorials, IEEE*, 11(1):13–32, First 2009.

[17] F. Gustafsson. Particle filter theory and practice with positioning applications. *Aerospace and Electronic Systems Magazine, IEEE*, 25(7):53–82, July 2010.

[18] F. Gustafsson. *Statistical sensor fusion*. Studentlitteratur, Lund, 2010.

[19] F. Gustafsson and F. Gunnarsson. Mobile positioning using wireless networks: Possibilities and fundamental limitations based on available wireless network measurements. *Signal Processing Magazine, IEEE*, 22(4):41–53, July 2005.

[20] F. Gustafsson, F. Gunnarsson, N. Bergman, U. Forssell, J. Jansson, R. Karlsson, and P.-J. Nordlund. Particle filters for positioning, navigation, and tracking. *Signal Processing, IEEE Transactions on*, 50(2):425–437, Feb 2002.

[21] H. Hashemi. The indoor radio propagation channel. *Proceedings of the IEEE*, 81(7):943–968, Jul 1993.

[22] A. Host-Madsen. On the existence of efficient estimators. *Signal Processing, IEEE Transactions on*, 48(11):3028–3031, Nov 2000.

[23] S. Julier and J. Uhlmann. Unscented filtering and nonlinear estimation. *Proceedings of the IEEE*, 92(3):401–422, Mar 2004.

[24] R. E. Kalman. A new approach to linear filtering and prediction problems. *Transactions of the ASME–Journal of Basic Engineering*, 82(Series D):35–45, 1960.

[25] S. Kay and Y. Eldar. Rethinking biased estimation [lecture notes]. *Signal Processing Magazine, IEEE*, 25(3):133–136, May 2008.

[26] S. M. Kay. *Fundamentals of Statistical Signal Processing: Estimation Theory*. Prentice-Hall, Inc., Upper Saddle River, NJ, USA, 1993.

[27] A. Koneru, X. Li, and M. Varanasi. Comparative study of RSS-based collaborative localization methods in sensor networks. In *Region 5 Conference, 2006 IEEE*, pages 243–248, April 2006.

[28] J. Lategahn, M. Muller, and C. Rohrig. TDOA and RSS based extended Kalman filter for indoor person localization. In *Vehicular Technology Conference (VTC Fall), 2013 IEEE 78th*, pages 1–5, Sept 2013.

[29] X. Li. Collaborative localization with received-signal strength in wireless sensor networks. *Vehicular Technology, IEEE Transactions on*, 56(6):3807–3817, Nov 2007.

[30] G. Mao and B. Fidan. *Localization Algorithms and Strategies for Wireless Sensor Networks*. Information Science Reference - Imprint of: IGI Publishing, Hershey, PA, 2009.

[31] G. Mao, B. Fidan, and B. D. Anderson. Wireless sensor network localization techniques. *Computer Networks*, 51(10):2529 – 2553, 2007.

[32] U. Orguner. EE 793 Target Tracking, Lecture 1: Introduction to state estimation. Available at http://www.eee.metu.edu.tr/ umut/ee793/files/METULecture1.pdf, 2013. [Last accessed on December 2014].

[33] N. Patwari, J. Ash, S. Kyperountas, A. Hero, R. Moses, and N. Correal. Locating the nodes: Cooperative localization in wireless sensor networks. *Signal Processing Magazine, IEEE*, 22(4):54–69, July 2005.

[34] N. Patwari, A. Hero, M. Perkins, N. Correal, and R. O'Dea. Relative location estimation in wireless sensor networks. *Signal Processing, IEEE Transactions on*, 51(8):2137–2148, Aug 2003.

[35] N. Patwari and A. O. Hero, III. Using proximity and quantized RSS for sensor localization in wireless networks. In *Proceedings of the 2Nd ACM International Conference on Wireless Sensor Networks and Applications*, WSNA '03, pages 20–29, New York, NY, USA, 2003. ACM.

[36] N. Patwari, R. O'Dea, and Y. Wang. Relative location in wireless networks. In *Vehicular Technology Conference, 2001. VTC 2001 Spring. IEEE VTS 53rd*, volume 2, pages 1149–1153 vol.2, 2001.

[37] K. B. Petersen and M. S. Pedersen. The matrix cookbook, nov 2012. Version 20121115.

[38] J. Picard and A. Weiss. Theoretical facts on RSSI-based geolocation. In *Electrical Electronics Engineers in Israel (IEEEI), 2012 IEEE 27th Convention of*, pages 1–5, Nov 2012.

[39] T. Rappaport. *Wireless Communications: Principles and Practice*. Prentice Hall PTR, Upper Saddle River, NJ, USA, 2nd edition, 2001.

[40] L. Rui and K. Ho. Bias compensation for target tracking from range based maximum likelihood position estimates. In *Sensor Array and Multichannel Signal Processing Workshop (SAM), 2012 IEEE 7th*, pages 193–196, June 2012.

[41] L. Rui and K. C. Ho. Bias analysis of source localization using the maximum likelihood estimator. In *Acoustics, Speech and Signal Processing (ICASSP), 2012 IEEE International Conference on*, pages 2605–2608, March 2012.

[42] A. Savvides, H. Park, and M. B. Srivastava. The bits and flops of the n-hop multilateration primitive for node localization problems. In *Proceedings of the 1st ACM International Workshop on Wireless Sensor Networks and Applications*, WSNA '02, pages 112–121, New York, NY, USA, 2002. ACM.

[43] Y. Shen, S. Mazuelas, and M. Win. Network navigation: Theory and interpretation. *Selected Areas in Communications, IEEE Journal on*, 30(9):1823–1834, October 2012.

[44] H. So, Y. Chan, K. Ho, and Y. Chen. Simple formulae for bias and mean square error computation [dsp tips and tricks]. *Signal Processing Magazine, IEEE*, 30(4):162–165, July 2013.

[45] D. Tse and P. Viswanath. *Fundamentals of Wireless Communication*. Cambridge University Press, 2005.

[46] L. Van Trees, H. *Detection, Estimation, and Modulation Theory, Part I*. New York: Wiley, 1968.

[47] H. Wymeersch, J. Lien, and M. Win. Cooperative localization in wireless networks. *Proceedings of the IEEE*, 97(2):427–450, Feb 2009.

[48] S. Xi and M. Zoltowski. A practical complete MLE cooperative localization solution. In *Acoustics Speech and Signal Processing (ICASSP), 2010 IEEE International Conference on*, pages 3554–3557, March 2010.

[49] A. Zanella and A. Bardella. RSS-based ranging by multichannel RSS averaging. *Wireless Communications Letters, IEEE*, 3(1):10–13, February 2014.

[50] R. Zekavat and R. M. Buehrer. *Handbook of Position Location: Theory, Practice and Advances*. Wiley-IEEE Press, 1st edition, 2011.

[51] J. Zhou, Y. Shen, S. Shao, and Y. Tang. Cooperative spectrum sensing scheme with hard decision based on location information in cognitive radio networks. *Wireless Personal Communications*, 71(4):2637–2656, 2013.

APPENDIX A

DERIVATION OF MLE COST FUNCTION

Consider the measurement model below.

$$y_{ij} = f(d_{ij}) + v_{ij} \tag{A.1}$$

for $i = 1, \ldots, n$, $j = i+1, \ldots, N$ and $i \neq j$ where

- $d_{ij} \triangleq \|\mathbf{x_i} - \mathbf{x_j}\|$ is Euclidean distance between ith and jth node, and $\mathbf{x_i}, \mathbf{x_j} \in \mathbb{R}^m$ is the m-dimensional position vector of ith and jth nodes respectively.
- $y_{ij} \in \mathbb{R}$ is the measurement vector;
- $f(\cdot)$ is a twice differentiable, in general nonlinear function;
- $v_{ij} \sim \mathcal{N}(v_{ij}; 0, \sigma^2)$ is the Gaussian measurement noise. We assume that v_{ij}'s are independent.

In general, the measurements might not be obtained if there are connectivity constraints. We model the connectivity event related to y_{ij} as a Bernoulli random variable w_{ij}, with $w_{ij} = 1$ meaning that y_{ij} is collected and $w_{ij} = 0$ otherwise.

The likelihood function of one measurement event:

$$p(y_{ij}; \mathbf{x_i}, \mathbf{x_j}) = \begin{cases} \mathcal{N}(y_{ij}; f(d_{ij}), \sigma^2), & \text{if } y_{ij} \geq y_{thr} \\ Pr(w_{ij} = 0), & \text{otherwise} \end{cases} \tag{A.2}$$

where $Pr(w_{ij} = 0) = Pr(y_{ij} < y_{thr}) = \Phi(\frac{t(d_{ij})}{\sigma})$, $t(d_{ij}) = y_{thr} - f(d_{ij})$ and $\Phi(\cdot)$ is the standard normal CDF. One can write the following estimation problem for d_{ij}

when RSS measurement is observed, namely when $w_{ij} = 1$

$$\begin{aligned}\delta_{ij} \triangleq \hat{d}_{ij} &= \arg\max_{d_{ij}} p(y_{ij}; \mathbf{x_i}, \mathbf{x_j}) \\ &= \arg\max_{d_{ij}} \mathcal{N}(y_{ij}; f(d_{ij}), \sigma^2) \\ &= \arg\max_{d_{ij}} \log \mathcal{N}(y_{ij}; f(d_{ij}), \sigma^2) \end{aligned} \tag{A.3}$$

where δ_{ij} is also used as a distance measurement in ML based localization. It is known that $y_{ij} = P_{ij}$, $f(d_{ij}) = P_0 - 10\alpha \log_{10}(d_{ij}/d_0)$ and $y_{yhr} = P_{thr}$ in the RSS measurement model. Assume that $d_0 = 1$ in this problem. Then the distance measurement δ_{ij} can be found as

$$\begin{aligned}\delta_{ij} &= \arg\max_{d_{ij}} \left\{ \log \frac{1}{\sqrt{2\pi\sigma_v^2}} - \frac{\left(P_{ij} - \bar{P}_{ij}\right)^2}{2\sigma_v^2} \right\} \\ &= \arg\min_{d_{ij}} \left(P_{ij} - \bar{P}_{ij}\right)^2 \end{aligned} \tag{A.4}$$

where $\bar{P}_{ij} = P_0 - 10\alpha \log_{10} d_{ij}$. So derivative of term in (A.4) with respect to distance d_{ij} at the estimate must be zero

$$\begin{aligned} \frac{\partial \left(P_{ij} - P_0 + 10\alpha \log_{10} d_{ij}\right)^2}{\partial d_{ij}}|_{d_{ij}=\delta_{ij}} &= 0 \\ 2\left(P_{ij} - P_0 + 10\alpha \log_{10} \hat{d}_{ij}\right)\left(\frac{10\alpha}{\delta_{ij} \log 10}\right) &= 0 \\ P_{ij} - P_0 + 10\alpha \log_{10} \delta_{ij} &= 0 \end{aligned} \tag{A.5}$$

From equation in (A.5), the distance measurement can be found as

$$\delta_{ij} = 10^{\frac{P_0 - P_{ij}}{10\alpha}} \tag{A.6}$$

Considering independent measurements, the likelihood function of the set of measurements is written as follows

$$p(\mathbf{y}; \mathbf{X}) = \prod_{i,j \in \mathcal{S}(i,j)} \mathcal{N}(y_{ij}; f(d_{ij}), \sigma^2) \prod_{i,j \in \bar{\mathcal{S}}(i,j)} \Phi\left(\frac{t(d_{ij})}{\sigma}\right) \tag{A.7}$$

where $\mathcal{S}(i,j) = \{i, j : w_{ij} = 1\}$ and $\mathbf{X} = [\mathbf{x_1}, \mathbf{x_2}, \ldots, \mathbf{x_n}]$ is the configuration matrix including the position of the blindfolded nodes to be estimated. The logarithm of

the function in (A.7):

$$\begin{aligned}\log p(\mathbf{y};\mathbf{X}) &= \sum_{i,j} w_{ij} \log \mathcal{N}(y_{ij}; f(d_{ij}), \sigma^2) \\ &\quad + (1-w_{ij}) \log \Phi\left(\frac{t(d_{ij})}{\sigma}\right) + C \\ &= \sum_{i,j} -\frac{w_{ij}}{2\sigma^2}\left(y_{ij} - f(d_{ij})\right)^2 + (1-w_{ij}) \log \Phi\left(\frac{t(d_{ij})}{\sigma}\right) + C \end{aligned} \tag{A.8}$$

where C is a constant and independent of $\mathbf{X}$. ML estimation rule is given as follows

$$\begin{aligned}\hat{\mathbf{X}} &= \arg\max_{\mathbf{X}} \log p(\mathbf{y};\mathbf{X}) \\ &= \arg\max_{\mathbf{X}} \sum_{i,j} -\frac{w_{ij}}{2\sigma^2}\left(y_{ij} - f(d_{ij})\right)^2 + (1-w_{ij}) \log \Phi\left(\frac{t(d_{ij})}{\sigma}\right) + C \\ &= \arg\min_{\mathbf{X}} \sum_{i,j} \frac{w_{ij}}{2\sigma^2}\left(y_{ij} - f(d_{ij})\right)^2 - (1-w_{ij}) \log \Phi\left(\frac{t(d_{ij})}{\sigma}\right) \end{aligned} \tag{A.9}$$

ML cost function using the distance measurements δ_{ij} can be deduced from (A.9) as

$$\begin{aligned}C_{\text{h-RSS-MLE}} &= \sum_{i,j} \frac{1}{2}\left(\frac{10\alpha}{\sigma \log 10}\right)^2 w_{ij}\left(\log \delta_{ij} - \log d_{ij}\right)^2 \\ &\quad - (1-w_{ij}) \log \Phi\left(\frac{t(d_{ij})}{\sigma}\right) \end{aligned} \tag{A.10}$$

Additionally one can utilize some portion of the log-likelihood function, i.e., only observed distance measurements such that δ_{ij} is observed when $w_{ij} = 1$, in (A.8) as was done in [29, 34]. The resulting ML cost function will be called as RSS-MLE and is given as

$$C_{\text{RSS-MLE}} = \sum_{i,j} w_{ij}\left(\log \delta_{ij} - \log d_{ij}\right)^2 \tag{A.11}$$

Obviously, it can be seen that there is no un(connectivity) related information in (A.11).

APPENDIX B

SMACOF ALGORITHM AND ADAPTIVE NEIGHBORHOOD SELECTION METHOD

B.1 SMACOF Algorithm

MDS cost function in (2.4) can be optimized by SMACOF algorithm. SMACOF algorithm can be found in [6]. Solving the cost function with gradient based methods can be harder than with SMACOF, especially when the number of unknown parameters in the cost function is too many. SMACOF algorithm uses a majorized function instead of the original one for the solution. Iterative majorization in SMACOF algorithm generates a monotically nonincreasing sequence of function values if the original function is bounded from below. The main idea of majorization is to replace iteratively the original function $f(x)$ by auxiliary function $g(x, z)$ where z is some fixed supporting point. Iterative majorization has some requirements:

- $g(x, z)$ must be simpler to minimize than $f(x)$
- $f(x) \leqslant g(x, z)$
- $f(z) = g(z, z)$

MDS cost function can be divided into some parts as follows

$$\begin{aligned} C_{\text{MDS}}(\mathbf{X}) &= \sum_{i=1}^{N-1} \sum_{j=i+1}^{N} w_{ij}(d_{ij} - \delta_{ij})^2 \\ &= \sum_{i<y} w_{ij}\delta_{ij}^2 + \sum_{i<j} w_{ij}d_{ij}^2 - 2\sum_{i<j} w_{ij}\delta_{ij}d_{ij} \\ &= \Sigma^2 + L^2(\mathbf{X}) - 2\rho(\mathbf{X}) \end{aligned} \tag{B.1}$$

The first term is constant, the second and the third are to be majorized. Principles of majorization can be found in [6]. The second term can be written in explicit form as follows

$$\begin{aligned} L^2(\mathbf{X}) &= w_{ij} \operatorname{Tr}\left\{\left(\mathbf{X}^{\mathrm{T}}\mathbf{A}_{i,j}\mathbf{X}\right)\right\} \\ &= \operatorname{Tr}\left\{\mathbf{X}^{\mathrm{T}}\left(\sum_{i<j} w_{ij}\mathbf{A}_{ij}\right)\mathbf{X}\right\} \\ &= \operatorname{Tr}\left\{\mathbf{X}^{\mathrm{T}}\mathbf{V}\mathbf{X}\right\} \end{aligned} \tag{B.2}$$

where $\mathbf{A}_{ij}$ has $a_{ii} = a_{jj} = 1$, $a_{ij} = a_{ji} = -1$ and the other elements are zero. $\mathbf{X}$ is the configuration or coordinate matrix of all nodes (i.e., blindfolded nodes and anchors). $\mathbf{V}$ has $v_{ij} = -w_{ij}$ if $i \neq j$ and $v_{ii} = \sum_{j=1, j\neq i}^{N} w_{ij}$ otherwise. The third term of MDS cost function can be majorized by Cauchy-Schwarz inequality as follows

$$\begin{aligned} -\rho(\mathbf{X}) &= -\sum_{i<j}(w_{ij}\delta_{ij})d_{ij}(\mathbf{X}) \\ &\leqslant -\operatorname{Tr}\left\{\mathbf{X}^{\mathrm{T}}\left(\sum_{i<j} b_{ij}\mathbf{A}_{ij}\right)\mathbf{Z}\right\} \\ &= -\operatorname{Tr}\left\{\mathbf{X}^{\mathrm{T}}B(\mathbf{Z})\mathbf{Z}\right\} \end{aligned} \tag{B.3}$$

Equality occurs if $\mathbf{X} = \mathbf{Z}$ and elements of $B(\mathbf{Z})$ are given as

$$\begin{aligned} b_{ij} &= \begin{cases} \frac{-w_{ij}\delta_{ij}}{d_{ij}(\mathbf{Z})}, & \text{if } i \neq j,\, d_{ij}(\mathbf{Z}) \neq 0 \end{cases} \\ b_{ii} &= -\sum_{j=1, i\neq j}^{N} b_{ij} \end{aligned} \tag{B.4}$$

To find the local minimum of $\mathbf{X}$, derivative of the cost function must be equated to zero at the local minimum.

$$\begin{aligned} C_{\text{MDS}}(\mathbf{X}) &= \Sigma^2 + L^2(\mathbf{X}) - 2\rho(\mathbf{X}) \\ &\leqslant \Sigma^2 + \operatorname{Tr}\left\{\mathbf{X}^{\mathrm{T}}\mathbf{V}\mathbf{X}\right\} - 2\operatorname{Tr}\left\{\mathbf{X}^{\mathrm{T}}B(\mathbf{Z})\mathbf{Z}\right\} \\ &= H(\mathbf{X}, \mathbf{Z}) \end{aligned} \tag{B.5}$$

$$\begin{aligned} \nabla H(\mathbf{X}, \mathbf{Z}) &= 2\mathbf{V}\mathbf{X} - 2B(\mathbf{Z})\mathbf{Z} \\ &= 0 \end{aligned} \tag{B.6}$$

From (B.6), it can be seen that

$$\mathbf{V}\mathbf{X} = B(\mathbf{Z})\mathbf{Z} \tag{B.7}$$

Algorithm 1 Pseudo Code for SMACOF Algorithm

$\mathbf{Z} \leftarrow \mathbf{X}^{[0]}$ where $\mathbf{X}^{[0]}$ is random or non-random initial value for algorithm

$k \leftarrow 0$, $\epsilon \leftarrow$ a very small positive value

Compute $C_{\mathbf{MDS}}(\mathbf{X}^{[0]})$

$C_{\mathbf{MDS}}(\mathbf{X}^{[-1]}) \leftarrow C_{\mathbf{MDS}}(\mathbf{X}^{[0]})$

while $k = 0$ **or** $C_{\mathbf{MDS}}(\mathbf{X}^{[k-1]}) - C_{\mathbf{MDS}}(\mathbf{X}^{[k]}) > \epsilon$ **do**

$k \leftarrow k + 1$

$\mathbf{X}[k] \leftarrow \mathbf{V}^{+} B(\mathbf{Z})\mathbf{Z}$

Compute $C_{\mathbf{MDS}}(\mathbf{X}^{[k]})$

$\mathbf{Z} \leftarrow \mathbf{X}^{[k]}$

end while

$\mathbf{V}^{-1}$ doesn't exist, since $\mathbf{V}$ is not full rank matrix. Therefore pseudo inverse of $\mathbf{V}$ is given by

$$\mathbf{V}^{+} = \left(\mathbf{V} + \mathbf{1}\mathbf{1}^{\mathrm{T}}\right)^{-1} - N^{-2}\mathbf{1}\mathbf{1}^{\mathrm{T}} \tag{B.8}$$

where $\mathbf{1}$ is a vector of ones and N is the number of all nodes.

Then the solution at the local minimum is given as

$$\mathbf{X}^{u} = \mathbf{V}^{+} B(\mathbf{Z})\mathbf{Z} \tag{B.9}$$

Note that the derivation of SMACOF algorithm has been totally taken from [6].

B.2 Adaptive Neighborhood Selection Method

- In the first step, run the algorithm with a connectivity matrix based on the available range measurements (i.e., $w_{ij} = 0$ if $\delta_{ij} > \delta_{thr}$)
- In the second step, compute a new connectivity matrix from the estimate configuration which is the output of the first run. Then run the algorithm again with the same measurements δ_{ij} as in the first run, new connectivity matrix formed at the beginning of the second run and the estimated configuration from the first run as initialization to the second run.

This method is proposed by [9].

APPENDIX C

DERIVATION OF CRAMÉR-RAO LOWER BOUND FOR H-RSS-MLE AND RSS-MLE UNDER CONNECTIVITY CONSTRAINTS

Consider the measurement model below

$$P_{ij} = f(d_{ij}) + v_{ij} \tag{C.1}$$

for $i = 1, ..., n$, and $j = i + 1, ..., N$ where

- P_{ij}: Received power (dBm) in ith sensor when jth transmits
- $f(d_{ij}) = P_0 - 10\alpha \log_{10} d_{ij}$
- $v_{ij} \sim \mathcal{N}(v_{ij}, 0, \sigma^2)$ represents the Gaussian noise
- P_0: First-meter reference power (dBm)
- d_{ij}: Euclidean distance between ith and jth sensor
- α: Path loss exponent
- n: Number of the blindfolded sensors
- N: Total number of sensors including reference ones also

The log-likelihood function can be written due to total observation for maximum likelihood estimator based on RSS measurements in (C.1).

$$\log p(\mathbf{P}; \theta) = \sum_{i,j} (1 - w_{ij}) \log \Phi \left(\frac{t_{ij}}{\sigma} \right) - \frac{w_{ij}}{2} \left(\frac{10\alpha}{\sigma \log 10} \right)^2 \left(\log \frac{d_{ij}}{\delta_{ij}} \right)^2 \tag{C.2}$$

where

- $\mathbf{P} = [P_{12},\ P_{13},\ \cdots,\ P_{1N},\ \cdots, P_{n1},\ \cdots, P_{nn-1},\ P_{nn+1},\ \cdots,\ P_{nN}]$
- $w_{ij} \sim Bern\left(1 - \Phi\left(\frac{t_{ij}}{\sigma}\right)\right)$: Connectivity which can be 1 or 0
- $t_{ij} = (P_{thr} - f(d_{ij}))$
- P_{thr}: Threshold power (dBm)
- $\theta = [x_1,\ x_2,\ \cdots,\ x_n,\ y_1,\ y_2,\ \cdots,\ y_n]$ is unknown position vector to be estimated in 2-D case
- $\Phi(.)$: Standard normal CDF

The right hand side of (C.2) can be divided into two parts which are given as

$$I^{(1)} = -\frac{1}{2}\left(\frac{10\alpha}{\sigma \log 10}\right)^2 \sum_{i,j} w_{ij}\ \left(\log \frac{d_{ij}}{\delta_{ij}}\right)^2 \tag{C.3}$$

$$I^{(2)} = \sum_{i,j}(1 - w_{ij}) \log \Phi\left(\frac{t_{ij}}{\sigma}\right) \tag{C.4}$$

Fisher Information Matrix (FIM) of First Term:

The elements of FIM can be written as follows:

$$f_{kl}^{(1)} = \begin{cases} -\sum_j\ E\left\{\frac{\partial^2 I_{kj}^{(1)}}{\partial \theta_k^2}\right\} & \text{if } k = l \\ -\ E\left\{\frac{\partial^2 I_{kl}^{(1)}}{\partial \theta_k \partial \theta_l}\right\} & \text{if } k \neq l \end{cases} \tag{C.5}$$

where $I_{kj}^{(1)} = -\frac{w_{ij}}{2}\left(\frac{10\alpha}{\sigma \log 10}\right)^2 (\log d_{ij} - \log \delta_{ij})^2$. The diagonal elements of FIM can be written as

$$\begin{aligned} f_{kk}^{(1)} =& \frac{1}{2}\left(\frac{10\alpha}{\sigma \log 10}\right)^2 \sum_j E\left[w_{kj} \frac{\partial^2}{\partial \theta_k^2} \log\left(\frac{d_{kj}}{\delta_{kj}}\right)^2\right] \\ =& \left(\frac{10\alpha}{\sigma \log 10}\right)^2 \sum_j E\left\{w_{kj}\left(\frac{1}{d_{kj}^2}\frac{\partial d_{kj}}{\partial \theta_k}\frac{\partial d_{kj}}{\partial \theta_k}\right)\right. \\ & \left. + w_{kj} \log \frac{d_{kj}}{\delta_{kj}}\left(\frac{1}{d_{kj}}\frac{\partial^2 d_{kj}}{\partial \theta_k^2} - \frac{1}{d_{kj}^2}\frac{\partial d_{kj}}{\partial \theta_k}\frac{\partial d_{kj}}{\partial \theta_k}\right)\right\} \\ =& \left(\frac{10\alpha}{\sigma \log 10}\right)^2 \sum_j \frac{E\left(w_{kj}\right)}{d_{kj}^2}\frac{\partial d_{kj}}{\partial \theta_k}\frac{\partial d_{kj}}{\partial \theta_k} \\ & + E\left(w_{kj} \log \frac{d_{kj}}{\delta_{kj}}\right)\left(\frac{1}{d_{kj}}\frac{\partial^2 d_{kj}}{\partial \theta_k^2} - \frac{1}{d_{kj}^2}\frac{\partial d_{kj}}{\partial \theta_k}\frac{\partial d_{kj}}{\partial \theta_k}\right) \end{aligned} \tag{C.6}$$

where $\log \delta_{kj} \sim \mathcal{N}(\log \delta_{kj}; \log d_{kj}, \sigma_v^2)$ and $\sigma_v = \sigma log10/10\alpha$. The expected values in (C.6) are given as

$$E(w_{kj}) = 1 - \Phi\left(\frac{t_{kj}}{\sigma}\right) \tag{C.7}$$

$$E\left[w_{kj}(\log d_{kj} - \log \delta_{kj})\right] = \frac{\log 10}{10\alpha}\sigma\mathcal{N}\left(\frac{t_{kj}}{\sigma}; 0, 1\right) \tag{C.8}$$

Substituting (C.7) and (C.8) into (C.6), the diagonal elements we get as

$$\begin{aligned} f_{kk}^{(1)} =& a^2 \sum_j \frac{1 - \Phi\left(t_{kj}/\sigma\right)}{d_{kj}^2} \frac{\partial d_{kj}}{\partial \theta_k} \frac{\partial d_{kj}}{\partial \theta_k} \\ &+ \frac{\mathcal{N}\left(t_{kj}/\sigma; 0, 1\right)}{a} \left(\frac{1}{d_{kj}} \frac{\partial^2 d_{kj}}{\partial \theta_k^2} - \frac{1}{d_{kj}^2} \frac{\partial d_{kj}}{\partial \theta_k} \frac{\partial d_{kj}}{\partial \theta_k}\right) \end{aligned} \tag{C.9}$$

and the elements except diagonals are given as follows

$$\begin{aligned} f_{kl}^{(1)} =& a^2 \left[\frac{1 - \Phi\left(t_{kl}/\sigma\right)}{d_{kl}^2} \frac{\partial d_{kl}}{\partial \theta_k} \frac{\partial d_{kl}}{\partial \theta_l} \right. \\ &\left. + \frac{\mathcal{N}\left(t_{kl}/\sigma; 0, 1\right)}{a} \left(\frac{1}{d_{kl}} \frac{\partial^2 d_{kl}}{\partial \theta_k \partial \theta_l} - \frac{1}{d_{kl}^2} \frac{\partial d_{kl}}{\partial \theta_k} \frac{\partial d_{kl}}{\partial \theta_l}\right)\right] \end{aligned} \tag{C.10}$$

where $a = 10\alpha/\left(\sigma \log 10\right)$. To obtain FIM along the x and y coordinates separately, one can write FIM in a block form which is given as follows

$$\mathbf{F} = \begin{bmatrix} \mathbf{F_{xx}} & \mathbf{F_{xy}} \\ \\ \mathbf{F_{xy}}^{\mathrm{T}} & \mathbf{F_{yy}} \end{bmatrix} \tag{C.11}$$

Each block of FIM should be found. The only parameters that can change according to the blocks are the derivatives wrt x and y which can be seen in the following. FIM elements (C.9) and (C.10), FIM from $I^{(1)}$ is calculated as follows

$$[\mathbf{F_{xx}}]_{kk}^{(1)} = \sum_j a^2 \frac{(x_k - x_j)^2}{d_{kj}^4} \left[1 - \Phi\left(\frac{t_{kj}}{\sigma}\right) - \frac{2\mathcal{N}(t_{kj}/\sigma; 0, 1)}{a}\right] + \frac{a\mathcal{N}(t_{kj}/\sigma; 0, 1)}{d_{kj}^2} \tag{C.12}$$

$$[\mathbf{F_{xx}}]_{kl}^{(1)} = a^2 \frac{(x_k - x_l)^2}{d_{kl}^4} \left[\Phi\left(\frac{t_{kl}}{\sigma}\right) - 1 + \frac{2\mathcal{N}(t_{kl}/\sigma; 0, 1)}{a}\right] - \frac{a\mathcal{N}(t_{kl}/\sigma; 0, 1)}{d_{kl}^2} \tag{C.13}$$

$$[\mathbf{F_{yy}}]_{kk}^{(1)} = \sum_j a^2 \frac{(y_k - y_j)^2}{d_{kj}^4} \left[1 - \Phi\left(\frac{t_{kj}}{\sigma}\right) - \frac{2\mathcal{N}(t_{kj}/\sigma; 0, 1)}{a}\right] + \frac{a\mathcal{N}(t_{kj}/\sigma; 0, 1)}{d_{kj}^2} \tag{C.14}$$

$$[\mathbf{F_{yy}}]_{kl}^{(1)} = a^2 \frac{(y_k - y_l)^2}{d_{kl}^4} \left[\Phi\left(\frac{t_{kl}}{\sigma}\right) - 1 + \frac{2\mathcal{N}(t_{kl}/\sigma; 0, 1)}{a}\right] - \frac{a\mathcal{N}(t_{kl}/\sigma; 0, 1)}{d_{kl}^2} \tag{C.15}$$

$$[\mathbf{F_{xy}}]_{kk}^{(1)} = a^2 \sum_j \frac{(x_k - x_j)(y_k - y_j)}{d_{kj}^4} \left[1 - \Phi\left(\frac{t_{kj}}{\sigma}\right) - \frac{2\mathcal{N}(t_{kl}/\sigma; 0, 1)}{a}\right] \tag{C.16}$$

$$[\mathbf{F_{xy}}]_{kl}^{(1)} = a^2 \frac{(x_k - x_l)(y_k - y_l)}{d_{kl}^4} \left[\Phi\left(\frac{t_{kl}}{\sigma}\right) - 1 + \frac{2\mathcal{N}(t_{kl}/\sigma; 0, 1)}{a}\right] \tag{C.17}$$

The elements of FIM coming from the first part of likelihood function, i.e., $I^{(1)}$, are given in (C.17) and FIM in block form in (C.11). CRLB cannot be defined for RSS-MLE when the connectivity w_{ij} is random, since the regularity condition given in [26] does not hold in this case.

The regularity condition is written for the first part of likelihood function which is actually $I^{(1)}$, i.e., cost function of RSS-MLE given in (2.8) as follows

$$\mathrm{E}\left[\frac{\partial I^{(1)}}{\partial \theta_k}\right] = 0 \tag{C.18}$$

To check this statement above, take the derivative of RSS-MLE related part of likelihood function shown in (C.2) as

$$\begin{aligned}\mathrm{E}\left[\frac{\partial I^{(1)}}{\partial \theta_k}\right] =& \frac{1}{2}a^2 \sum_j E\left\{2w_{kj}\log\frac{d_{kj}}{\delta_{kj}}\frac{\partial d_{kj}}{\partial \theta_k}\right\} \\ \neq& 0\end{aligned} \tag{C.19}$$

So CRLB of RSS-MLE cannot be defined for random connectivity event. But we can still approximate the CRLB or MSE for RSS-MLE as

$$\mathbf{CRLB} \simeq (\mathbf{F^{(1)}})^{-1} \tag{C.20}$$

Note that we use this approximate CRLB given in (C.20) for RSS-MLE in its analytical bias expression presented in Chapter 4 and tracking simulations in Chapter 3.

Additionally CRLB can be written for RSS-MLE when the connectivity is modelled as deterministic parameter such that

$$w_{kj} = \begin{cases} 1, & \text{if } d_{kj} \leqslant d_{thr} \\ 0, & \text{otherwise} \end{cases} \tag{C.21}$$

With deterministic connectivity, take the expectation of (C.6) for both x and y coordinates, namely find the expression in (C.5). Then the elements of FIM for RSS-MLE

which were firstly derived by Patwari et. al. in [34] is that

$$[\mathbf{F}_{\mathbf{xx}}]_{kk}^{(\text{RSS})} = a^2 \sum_j w_{kj} \frac{(x_k - x_j)^2}{d_{kj}^4} \tag{C.22}$$

$$[\mathbf{F}_{\mathbf{xx}}]_{kl}^{(\text{RSS})} = -a^2 w_{kl} \frac{(x_k - x_l)^2}{d_{kl}^4} \tag{C.23}$$

$$[\mathbf{F}_{\mathbf{yy}}]_{kk}^{(\text{RSS})} = a^2 \sum_j w_{kj} \frac{(y_k - y_j)^2}{d_{kj}^4} \tag{C.24}$$

$$[\mathbf{F}_{\mathbf{yy}}]_{kl}^{(\text{RSS})} = -a^2 w_{kl} \frac{(y_k - y_l)^2}{d_{kl}^4} \tag{C.25}$$

$$[\mathbf{F}_{\mathbf{xy}}]_{kk}^{(\text{RSS})} = a^2 \sum_j w_{kj} \frac{(x_k - x_j)(y_k - y_j)}{d_{kj}^4} \tag{C.26}$$

$$[\mathbf{F}_{\mathbf{xy}}]_{kl}^{(\text{RSS})} = -a^2 w_{kl} \frac{(x_k - x_l)(y_k - y_l)}{d_{kl}^4} \tag{C.27}$$

Then CRLB for RSS-MLE is given as follows

$$\mathbf{CRLB}_{(\text{RSS})} = \left(\mathbf{F}^{(\text{RSS})}\right)^{-1} \tag{C.28}$$

Fisher Information Matrix of the Second Term:

The second term $I^{(2)}$ corresponds to (un)connectivity information part of the total likelihood function, i.e., h-RSS-MLE.

The second term of total likelihood function (C.2) is given as

$$I^{(2)} = \sum_{i,j} (1 - w_{ij}) \log \Phi \left(\frac{t_{kl}}{\sigma} \right) \tag{C.29}$$

Fisher information matrix of the second term can be written as follows

$$\begin{aligned} f_{kk}^{(2)} &= -\sum_j E(1 - w_{kj}) \left[\frac{\partial^2 \log \Phi \left(\frac{t_{kj}}{\sigma} \right)}{\partial \theta_k} \right] \\ &= -\sum_j E\left(1 - w_{kj}\right) \left[\frac{\partial^2 \Phi_{kj}}{\partial \theta_k^2} \frac{1}{\Phi_{kj}^2} - \frac{1}{\Phi_{kj}^2} \frac{\partial \Phi_{kj}}{\partial \theta_k} \frac{\partial \Phi_{kj}}{\partial \theta_k} \right] \end{aligned} \tag{C.30}$$

where $E\left(1 - w_{kj}\right) = \Phi_{kj}$, $\Phi_{kj} \triangleq \Phi\left(t_{kj}/\sigma\right)$, $\mathcal{N}_{kj} \triangleq \mathcal{N}\left(t_{kj}/\sigma; 0, 1\right)$, $\frac{\partial \Phi_{kj}}{\partial \theta_k} = \mathcal{N}_{kj} a \frac{\partial d_{kj}}{\partial \theta_k}$, $\frac{\partial^2 \Phi_{kj}}{\partial \theta_k^2} = \mathcal{N}_{kj} \frac{\partial^2 d_{kj}}{\partial \theta_k^2} - \left[\mathcal{N}_{kj} t_{kj} a^2/\sigma + \mathcal{N}_{kj} a\right] \frac{\partial d_{kj}}{\partial \theta_k} \frac{\partial d_{kj}}{\partial \theta_k}$. The diagonal elements are given as

$$f_{kk}^{(2)} = -\sum_j \mathcal{N}_{kj} a \frac{\partial^2 \Phi_{kj}}{\partial \theta_k^2} - \frac{\partial \Phi_{kj}}{\partial \theta_k} \frac{\partial \Phi_{kj}}{\partial \theta_k} \left(\frac{\mathcal{N}_{kj} t_{kj} a^2}{\sigma} + \mathcal{N}_{kj} a + \Phi_{kj}^{-1} \mathcal{N}_{kj}^2 a^2 \right) \tag{C.31}$$

Other elements except the diagonal elements are given as

$$f_{kl}^{(2)} = -\mathcal{N}_{kl} a \frac{\partial^2 \Phi_{kl}}{\partial \theta_k \partial \theta_l} + \frac{\partial \Phi_{kl}}{\partial \theta_k} \frac{\partial \Phi_{kl}}{\partial \theta_l} \left(\frac{\mathcal{N}_{kl} t_{kl} a^2}{\sigma} + \mathcal{N}_{kl} a + \Phi_{kl}^{-1} \mathcal{N}_{kl}^2 a^2 \right) \tag{C.32}$$

The elements of FIM of 2nd term along the x-y positions are given as

$$[\mathbf{F}_{\mathbf{xx}}]_{kk}^{(2)} = \sum_j \frac{(x_k - x_j)^2}{d_{kj}^4} \left(\frac{\mathcal{N}_{kj} t_{kj} a^2}{\sigma} + 2\mathcal{N}_{kj} a + \Phi_{kj}^{-1} \mathcal{N}_{kj}^2 a^2 \right) - \frac{\mathcal{N}_{kj} a}{d_{kj}^2} \tag{C.33}$$

$$[\mathbf{F}_{\mathbf{xx}}]_{kl}^{(2)} = \frac{\mathcal{N}_{kl} a}{d_{kl}^2} - \frac{(x_k - x_l)^2}{d_{kl}^4} \left(\frac{\mathcal{N}_{kl} t_{kl} a^2}{\sigma} + 2\mathcal{N}_{kl} a + \Phi_{kl}^{-1} \mathcal{N}_{kl}^2 a^2 \right) \tag{C.34}$$

$$[\mathbf{F}_{\mathbf{yy}}]_{kk}^{(2)} = \sum_j \frac{(y_k - y_j)^2}{d_{kj}^4} \left(\frac{\mathcal{N}_{kj} t_{kj} a^2}{\sigma} + 2\mathcal{N}_{kj} a + \Phi_{kj}^{-1} \mathcal{N}_{kj}^2 a^2 \right) - \frac{\mathcal{N}_{kj} a}{d_{kj}^2} \tag{C.35}$$

$$[\mathbf{F}_{\mathbf{yy}}]_{kl}^{(2)} = \frac{\mathcal{N}_{kl} a}{d_{kl}^2} - \frac{(y_k - y_l)^2}{d_{kl}^4} \left(\frac{\mathcal{N}_{kl} t_{kl} a^2}{\sigma} + 2\mathcal{N}_{kl} a + \Phi_{kl}^{-1} \mathcal{N}_{kl}^2 a^2 \right) \tag{C.36}$$

$$[\mathbf{F}_{\mathbf{xy}}]_{kk}^{(2)} = \sum_j \frac{(x_k - x_j)(y_k - y_j)}{d_{kj}^4} \left(\frac{\mathcal{N}_{kj} t_{kj} a^2}{\sigma} + 2\mathcal{N}_{kj} a + \Phi_{kj}^{-1} \mathcal{N}_{kj}^2 a^2 \right) \tag{C.37}$$

$$[\mathbf{F}_{\mathbf{xy}}]_{kl}^{(2)} = - \frac{(x_k - x_l)(x_k - x_l)}{d_{kl}^4} \left(\frac{\mathcal{N}_{kl} t_{kl} a^2}{\sigma} + 2\mathcal{N}_{kl} a + \Phi_{kl}^{-1} \mathcal{N}_{kl}^2 a^2 \right) \tag{C.38}$$

FIM of h-RSS-MLE can then be given as follows

$$\mathbf{F}_{\text{h-RSS-MLE}} = \mathbf{F}^{(1)} + \mathbf{F}^{(2)} \tag{C.39}$$

Hence FIM of h-RSS-MLE is given as

$$[\mathbf{F}_{\mathbf{xx}}]_{kk} = \sum_j a^2 \frac{(x_k - x_j)^2}{d_{kj}^4} \left(1 - \Phi_{kj} + \frac{\mathcal{N}_{kj} t_{kj}}{\sigma} + \Phi_{kj}^{-1} \mathcal{N}_{kj}^2 \right) \tag{C.40}$$

$$[\mathbf{F}_{\mathbf{xx}}]_{kl} = - a^2 \frac{(x_k - x_l)^2}{d_{kl}^4} \left(1 - \Phi_{kl} + \frac{\mathcal{N}_{kl} t_{kl}}{\sigma} + \Phi_{kl}^{-1} \mathcal{N}_{kl}^2 \right) \tag{C.41}$$

$$[\mathbf{F}_{\mathbf{yy}}]_{kk} = \sum_j a^2 \frac{(y_k - y_j)^2}{d_{kj}^4} \left(1 - \Phi_{kj} + \frac{\mathcal{N}_{kj} t_{kj}}{\sigma} + \Phi_{kj}^{-1} \mathcal{N}_{kj}^2 \right) \tag{C.42}$$

$$[\mathbf{F}_{\mathbf{yy}}]_{kl} = - a^2 \frac{(y_k - y_l)^2}{d_{kl}^4} \left(1 - \Phi_{kl} + \frac{\mathcal{N}_{kl} t_{kl}}{\sigma} + \Phi_{kl}^{-1} \mathcal{N}_{kl}^2 \right) \tag{C.43}$$

$$[\mathbf{F}_{\mathbf{xy}}]_{kk} = \sum_j a^2 \frac{(x_k - x_j)(y_k - y_j)}{d_{kj}^4} \left(1 - \Phi_{kj} + \frac{\mathcal{N}_{kj} t_{kj}}{\sigma} + \Phi_{kj}^{-1} \mathcal{N}_{kj}^2 \right) \tag{C.44}$$

$$[\mathbf{F}_{\mathbf{xy}}]_{kl} = - a^2 \frac{(x_k - x_l)(y_k - y_l)}{d_{kl}^4} \left(1 - \Phi_{kl} + \frac{\mathcal{N}_{kl} t_{kl}}{\sigma} + \Phi_{kl}^{-1} \mathcal{N}_{kl}^2 \right) \tag{C.45}$$

and CRLB of h-RSS-MLE is given as follows

$$\mathbf{CRLB}_{\text{h-RSS-MLE}} = {\mathbf{F}_{\text{h-RSS-MLE}}}^{-1} \tag{C.46}$$

APPENDIX D

ON PERFORMANCE CRITERIA OF LOCALIZATION SYSTEMS

The true position and position estimate configuration can be shown as $\hat{\mathbf{X}}_i = [\hat{x}_i,\ \hat{y}_i]^{\mathrm{T}}$ $\hat{\mathbf{X}}_{\mathrm{BN}} = \left[\hat{\mathbf{X}}_1,\ \hat{\mathbf{X}}_2,\ \cdots,\ \hat{\mathbf{X}}_n\right]$, $\mathbf{X}_i = [x_i,\ y_i]^{\mathrm{T}}$, $\mathbf{X}_{\mathrm{BN}} = [\mathbf{X}_1,\ \mathbf{X}_2,\ \cdots,\ \mathbf{X}_n]$ where $\hat{\mathbf{X}}_i$ and $\mathbf{X}_i$ are the estimated and true 2-D configuration matrix of the ith blindfolded node respectively, $\hat{\mathbf{X}}_{\mathrm{BN}}$ and $\mathbf{X}_{\mathrm{BN}}$ are the estimated and true configuration matrix of all blindfolded nodes in the network respectively and n is the number of blindfolded nodes. Estimation error, bias, variance and MSE value of 2-D position estimator are defined in [29] as follows

Estimation error:

$$e\left(\hat{\mathbf{X}}_i\right) = \|\hat{\mathbf{X}}_i - \mathbf{X}_i\| \tag{D.1}$$

$$e\left(\hat{\mathbf{X}}_{\mathrm{BN}}\right) = \sqrt{\frac{1}{n}\sum_{i=1}^{n} e^2(\hat{\mathbf{X}}_i)} \tag{D.2}$$

Bias of 2-D localization:

$$b\left(\hat{\mathbf{X}}_i\right) = \|E[\hat{\mathbf{X}}_i] - \mathbf{X}_i\| \tag{D.3}$$

$$b\left(\hat{\mathbf{X}}_{\mathrm{BN}}\right) = \sqrt{\frac{1}{n}\sum_{i=1}^{n} b^2(\hat{\mathbf{X}}_i)} \tag{D.4}$$

Variance of 2-D localization:

$$\mathrm{var}\left(\hat{\mathbf{X}}_i\right) = \mathrm{var}(\hat{x}_i) + \mathrm{var}(\hat{y}_i) \tag{D.5}$$

$$\mathrm{var}\left(\hat{\mathbf{X}}_{\mathrm{BN}}\right) = \frac{1}{n}\sum_{i=1}^{n} \mathrm{var}(\hat{\mathbf{X}}_i) \tag{D.6}$$

Mean squared error (MSE) of 2-D localization:

$$\text{MSE}\left(\hat{\mathbf{X}}_i\right) = \text{var}(\hat{\mathbf{X}}_i) + b^2(\hat{\mathbf{X}}_i) \tag{D.7}$$

$$\text{MSE}\left(\hat{\mathbf{X}}_{\text{BN}}\right) = \text{var}(\hat{\mathbf{X}}_{\text{BN}}) + b^2(\hat{\mathbf{X}}_{\text{BN}}) \tag{D.8}$$

APPENDIX E

SOME ELEMENTARY EXPECTED VALUES

We here take some elementary expected values used in some chapters. Let $x \sim \mathcal{N}(x; \mu, \sigma^2)$ be scalar Gaussian random variable. We are going to calculate the following expected values: $E(I(x \geq t))$, $E(I(x \geq t)x)$, $E(I(x \geq t)x^2)$ where $I(A)$ denotes the indicator function for the argument event A and $t \in \mathbb{R}$ is a threshold.

E.1 Calculation of $E(I(x \geq t))$

$$\begin{aligned} E(I(x \geq t)) &= \int_t^\infty \mathcal{N}(x; \mu, \sigma^2)\mathrm{d}x = Q\left(\frac{t-\mu}{\sigma}\right) \\ &= 1 - \Phi\left(\frac{t-\mu}{\sigma}\right) \end{aligned} \tag{E.1}$$

E.2 Calculation of $E(I(x \geq t)x)$

$$\begin{aligned}
E(I(x \geq t)x) =& \int_t^\infty x\mathcal{N}(x;\mu,\sigma^2)\mathrm{d}x \\
=& \frac{1}{\sqrt{2\pi}\sigma}\int_t^\infty x\exp\left(-\frac{1}{2\sigma^2}(x-\mu)^2\right)\mathrm{d}x \\
=& \frac{1}{\sqrt{2\pi}\sigma}\int_t^\infty (x-\mu)\exp\left(-\frac{1}{2\sigma^2}(x-\mu)^2\right)\mathrm{d}x \\
&+ \mu\int_t^\infty \mathcal{N}(x;\mu,\sigma^2)\mathrm{d}x \\
=& -\frac{1}{\sqrt{2\pi}\sigma}\sigma^2\exp\left(-\frac{1}{2\sigma^2}(x-\mu)^2\right)\Big|_t^\infty \\
&+ \mu Q\left(\frac{t-\mu}{\sigma}\right) \\
=& \sigma\mathcal{N}\left(\frac{t-\mu}{\sigma};0,1\right) + \mu\left[1-\Phi\left(\frac{t-\mu}{\sigma}\right)\right]
\end{aligned} \tag{E.2}$$

E.3 Calculation of $E(I(x \geq t)x^2)$

$$\begin{aligned}
E(I(x \geq t)x^2) =& \int_t^\infty x^2\mathcal{N}(x;\mu,\sigma^2)\mathrm{d}x \\
=& \frac{1}{\sqrt{2\pi}\sigma}\int_t^\infty x^2\exp\left(-\frac{1}{2\sigma^2}(x-\mu)^2\right)\mathrm{d}x \\
=& \frac{1}{\sqrt{2\pi}\sigma}\int_t^\infty (x-\mu)^2\exp\left(-\frac{1}{2\sigma^2}(x-\mu)^2\right)\mathrm{d}x \\
&+ \frac{2\mu}{\sqrt{2\pi}\sigma}\int_t^\infty x\exp\left(-\frac{1}{2\sigma^2}(x-\mu)^2\right)\mathrm{d}x \\
&- \frac{\mu^2}{\sqrt{2\pi}\sigma}\int_t^\infty \exp\left(-\frac{1}{2\sigma^2}(x-\mu)^2\right)\mathrm{d}x
\end{aligned} \tag{E.3}$$

We now use integration by parts on the first integral by defining

$$u \triangleq x-\mu \qquad \mathrm{d}v \triangleq (x-\mu)\exp\left(-\frac{1}{2\sigma^2}(x-\mu)^2\right) \tag{E.4}$$

which gives

$$\mathrm{d}u = \mathrm{d}x \qquad v = -\sigma^2\exp\left(-\frac{1}{2\sigma^2}(x-\mu)^2\right). \tag{E.5}$$

We can now the calculate the result of the first integral as

$$\begin{aligned}\int_t^\infty (x-\mu)^2 \exp\left(-\frac{1}{2\sigma^2}(x-\mu)^2\right) \mathrm{d}x &= uv|_t^\infty - \int_t^\infty v\mathrm{d}u \\ &= -\sigma^2(x-\mu)\exp\left(-\frac{1}{2\sigma^2}(x-\mu)^2\right)\Big|_t^\infty \\ &\quad + \sigma^2 \int_t^\infty \exp\left(-\frac{1}{2\sigma^2}(x-\mu)^2\right)\mathrm{d}x \\ &= \sigma^2(t-\mu)\exp\left(-\frac{1}{2\sigma^2}(t-\mu)^2\right) \\ &\quad + \sigma^2 \int_t^\infty \exp\left(-\frac{1}{2\sigma^2}(x-\mu)^2\right)\mathrm{d}x \end{aligned} \tag{E.6}$$

Substituting this result back, we get

$$\begin{aligned} E(I(x\geq t)x^2) =& \sigma(t-\mu)\mathcal{N}\left(\frac{t-\mu}{\sigma};0,1\right) + \sigma^2\int_t^\infty \mathcal{N}\left(x;\mu,\sigma^2\right)\mathrm{d}x \\ &+ 2\mu\int_t^\infty x\mathcal{N}(x;\mu,\sigma^2)\mathrm{d}x - \mu^2\int_t^\infty \mathcal{N}(x;\mu,\sigma^2)\mathrm{d}x \\ =& \sigma(t-\mu)\mathcal{N}\left(\frac{t-\mu}{\sigma};0,1\right) + \sigma^2 Q\left(\frac{t-\mu}{\sigma}\right) \\ &+ 2\mu\sigma\mathcal{N}\left(\frac{t-\mu}{\sigma};0,1\right) + 2\mu^2 Q\left(\frac{t-\mu}{\sigma}\right) \\ &- \mu^2 Q\left(\frac{t-\mu}{\sigma}\right) \\ =& \sigma(t+\mu)\mathcal{N}\left(\frac{t-\mu}{\sigma};0,1\right) + (\sigma^2+\mu^2)\left[1-\Phi\left(\frac{t-\mu}{\sigma}\right)\right] \end{aligned} \tag{E.7}$$

APPENDIX F

FIRST AND SECOND MOMENTS OF TRUNCATED MULTIVARIATE GAUSSIAN RANDOM VARIABLES

Suppose that $\mathbf{X} = (X_1, X_2, \cdots X_N)^T$ is a multivariate Gaussian random vector having a mean μ and covariance $\mathbf{\Sigma}$ (i.e., $\mathbf{X} \sim \mathcal{N}(\mu, \mathbf{\Sigma})$) in a region $(\mathbf{a} < \mathbf{x} < \mathbf{b})$ where $\mathbf{a} = (a_1, a_2, \cdots, a_N)$ and $\mathbf{b} = (b_1, b_2, \cdots, b_N)$. To find the first and second moment of $\mathbf{X}$, we utilize the moment generating function of N-dimensional Gaussian random variable. The probability density function (PDF) of the N-dimensional Gaussian random variable is given as follows

$$f_{\mathbf{X}}(\mathbf{x}) = \frac{1}{(2\pi)^{N/2}|\mathbf{\Sigma}|^{1/2}} \exp\left(-\frac{1}{2}(\mathbf{x}-\mu)^T\mathbf{\Sigma}^{-1}(\mathbf{x}-\mu)\right) \tag{F.1}$$

Then PDF of the truncated multivariate Gaussian random variable which we call $f_{\mathbf{X}'}(\mathbf{x})$ in $(\mathbf{a} < \mathbf{x} < \mathbf{b})$ can be written as follows

$$f_{\mathbf{X}'}(\mathbf{x}) = \begin{cases} \frac{f_{\mathbf{X}}(\mathbf{x})}{\alpha}, & \text{for } \mathbf{a} < \mathbf{x} < \mathbf{b} \\ 0, & \text{otherwise} \end{cases} \tag{F.2}$$

where $\alpha = P(\mathbf{a} < \mathbf{x} < \mathbf{b})$ The moment generating function of an N-dimensional truncated random variable $\mathbf{X}$ is defined as

$$M(\mathbf{t}) = \mathrm{E}\left\{e^{\mathbf{t}^T\mathbf{x}}\right\} = \int_{\mathbf{a}}^{\mathbf{b}} e^{\mathbf{t}^T\mathbf{x}} f_{\mathbf{X}'}(\mathbf{x})\mathrm{d}\mathbf{x} \tag{F.3}$$

For simplicity $\mu \triangleq 0$. The moment generating function of truncated multivariate Gaussian random variable is given as

$$M(\mathbf{t}) = \frac{1}{\alpha(2\pi)^{N/2}|\mathbf{\Sigma}|^{1/2}} \int_{\mathbf{a}}^{\mathbf{b}} \exp\left\{-\frac{1}{2}\left[\mathbf{X}^T\mathbf{\Sigma}^{-1}\mathbf{X} - 2\mathbf{t}^T\mathbf{X}\right]\right\} \tag{F.4}$$

Substituting $-\frac{1}{2}\left[\mathbf{X}^T\mathbf{\Sigma}^{-1}\mathbf{X} - 2\mathbf{t}^T\mathbf{X}\right]$ with $\frac{1}{2}\mathbf{t}^T\mathbf{\Sigma}\mathbf{t} - \frac{1}{2}(\mathbf{X}-\gamma)^T\mathbf{\Sigma}^{-1}(\mathbf{X}-\gamma)$ where $\gamma = \mathbf{\Sigma}\mathbf{t}$.

The moment generating function can be written as

$$M(\mathbf{t}) = \frac{e^{\mathbf{L}}}{\alpha(2\pi)^{N/2}|\mathbf{\Sigma}|^{1/2}} \int_{\mathbf{a}}^{\mathbf{b}} \exp\left\{-\frac{1}{2}\left[(\mathbf{X}-\gamma)^T\mathbf{\Sigma}^{-1}(\mathbf{X}-\gamma)\right]\right\} \mathrm{d}\mathbf{x} \tag{F.5}$$

where $\mathbf{L} = \frac{1}{2}\mathbf{t}^T\mathbf{\Sigma}\mathbf{t}$.

(F.5) can also be reduced as follows

$$\begin{aligned} M(\mathbf{t}) &= \frac{e^{\mathbf{L}}}{\alpha(2\pi)^{N/2}|\mathbf{\Sigma}|^{1/2}} \int_{\mathbf{a}-\gamma}^{\mathbf{b}-\gamma} \exp\left\{-\frac{1}{2}\mathbf{X}^T\mathbf{\Sigma}^{-1}\mathbf{X}\right\} \mathrm{d}\mathbf{x} \\ &= e^{\mathbf{L}} F_\alpha \end{aligned} \tag{F.6}$$

where

$$F_\alpha = \frac{1}{\alpha(2\pi)^{N/2}|\mathbf{\Sigma}|^{1/2}} \int_{\mathbf{a}-\gamma}^{\mathbf{b}-\gamma} \exp\left\{-\frac{1}{2}\mathbf{X}^T\mathbf{\Sigma}^{-1}\mathbf{X}\right\} \mathrm{d}\mathbf{x} \tag{F.7}$$

First and second moments can be found by taking derivative of the moment generating function in (F.6) with respect to t_i as

$$\frac{\partial M(\mathbf{t})}{\partial t_i} = e^{\mathbf{L}}\frac{\partial F_\alpha}{\partial t_i} + F_\alpha \frac{\partial e^{\mathbf{L}}}{\partial t_i} \tag{F.8}$$

In the equation above, we have

$$\frac{\partial e^{\mathbf{L}}}{\partial t_i} = e^{\mathbf{L}} \sum_{i=1}^{N} \sigma_{i,k}^2 t_k \tag{F.9}$$

and

$$\frac{\partial F_\alpha}{\partial t_i} = \frac{\partial}{\partial t_i} \int_{a_1^*}^{b_1^*} \int_{a_2^*}^{b_2^*} \cdots \int_{a_N^*}^{b_N^*} F_\alpha \mathrm{d}\mathbf{x} \tag{F.10}$$

where $a_i^* = a_i - \sum_{i=1}^N \sigma_{i,k}^2 t_k$, $b_i^* = b_i - \sum_{i=1}^N \sigma_{i,k}^2 t_k$ and $\sigma_{i,k}^2 = [\mathbf{\Sigma}]_{i,k}$

By Leibniz's Rule, (F.10) will be

$$\frac{\partial F_\alpha}{\partial t_i} = \sum_{i=1}^{N} \sigma_{i,k}^2 \left[f_k(a_k^*) - f_k(b_k^*)\right] \tag{F.11}$$

where

$$f_k(x_k) = \int_{a_1^*}^{b_1^*} \cdots \int_{a_{k-1}^*}^{b_{k-1}^*} \int_{a_{k+1}^*}^{b_{k+1}^*} \cdots \int_{a_N^*}^{b_N^*} f_{\mathbf{X}'}(\mathbf{x}) \mathrm{d}\mathbf{x}_{-k} \tag{F.12}$$

and $\mathbf{x}_{-k} = (x_1, x_2, \cdots, x_{k-1}, x_{k+1}, \cdots, x_N)$

At $t_k = 0$, for all $k = 1, 2, \cdots, t_N$, $a_i^* = a_i$ and $b_i^* = b_i$. Therefore $f_i(x_i) = f_{x_i}(x_i)$ (ith marginal density) at $t_i = 0$. As a result the first moment is given as

$$\begin{aligned} \mathrm{E}\, X_i &= \frac{\partial M(\mathbf{t})}{\partial t_i}\Big|_{\mathbf{t}=0} \\ &= \sum_{i=1}^{N} \sigma_{i,k}^2 \left[f_{x_k}(a_k) - f_{x_k}(b_k)\right] \end{aligned} \tag{F.13}$$

To find the second moment, we take the derivative of (F.8) as follows

$$\frac{\partial^2 M(\mathbf{t})}{\partial t_j \partial t_i} = e^{\mathbf{L}} \frac{\partial^2 F_\alpha}{\partial t_j \partial t_i} + \frac{\partial F_\alpha}{\partial t_i}\frac{\partial e^{\mathbf{L}}}{\partial t_j} + F_\alpha \frac{\partial^2 e^{\mathbf{L}}}{\partial t_j \partial t_i} + \frac{\partial e^{\mathbf{L}}}{\partial t_i}\frac{\partial F_\alpha}{\partial t_j} \tag{F.14}$$

and

$$\frac{\partial^2 e^{\mathbf{L}}}{\partial t_j \partial t_i} = e^{\mathbf{L}} \sigma_{i,j}^2 + C(\mathbf{t}) \tag{F.15}$$

where $C(\mathbf{0}) = 0$.

The partial derivative of (F.11) with respect to t_j is given as

$$\frac{\partial^2 F_\alpha}{\partial t_j \partial t_i} = \sum_{i=1}^{N} \left(\sigma_{i,k}^2 \frac{\partial f_k(a_k^*)}{\partial t_j} \right) - \sum_{i=1}^{N} \left(\sigma_{i,k}^2 \frac{\partial f_k(b_k^*)}{\partial t_j} \right) \tag{F.16}$$

and the partial derivative of $f_k(a_k^*)$ can be written as follows

$$\begin{aligned} \frac{\partial f_k(a_k^*)}{\partial t_j} &= \frac{\partial}{\partial t_j} \int_{a_1^*}^{b_1^*} \cdots \int_{a_{k-1}^*}^{b_{k-1}^*} \int_{a_{k+1}^*}^{b_{k+1}^*} \cdots \int_{a_N^*}^{b_N^*} f_{\mathbf{X'}_{-k}}(\mathbf{x}_{-k}, a_k^*) \mathrm{d}\mathbf{x} \\ &= \frac{\sigma_{j,k}^2 a_k^* f_k(a_k^*)}{\sigma_{k,k}^2} + \sum_{q \neq k} \left(\sigma_{j,q}^2 - \frac{\sigma_{k,q}^2 \sigma_{j,k}^2}{\sigma_{k,k}^2} \right) \left[f_{k,q}(a_k^*, a_q^*) - f_{k,q}(b_k^*, b_q^*) \right] \end{aligned} \tag{F.17}$$

where

$$f_{k,q}(x_k, x_q) = \int_{a_1^*}^{b_1^*} \cdots \int_{a_{k-1}^*}^{b_{k-1}^*} \int_{a_{k+1}^*}^{b_{k+1}^*} \cdots \int_{a_{q-1}^*}^{b_{q-1}^*} \int_{a_{q+1}^*}^{b_{q+1}^*} \cdots \int_{a_N^*}^{b_N^*} f_{\mathbf{X'}}(\mathbf{x}) \mathrm{d}\mathbf{x}_{-k,-q} \tag{F.18}$$

Note that for all $t_k = 0$, the term (F.18) converts to bivariate marginal PDF of $\mathbf{X}$, i.e., $f_{X_k,X_q}(x_k, x_q)$. Substituting (F.15),(F.16) and (F.17) to (F.14), evaluating at $\mathbf{t} = 0$, we get

$$\begin{aligned} \mathrm{E}\left\{X_i X_j\right\} &= \frac{\partial^2 M(\mathbf{t})}{\partial t_j t_i}\Big|_{\mathbf{t}=0} \\ &= \sigma_{i,j}^2 + \sum_{i=1}^{N} \sigma_{i,k}^2 \frac{\sigma_{j,k}^2 \left[a_k f_k(a_k) - b_k f_k(b_k) \right]}{\sigma_{k,k}^2} \\ &+ \sum_{i=1}^{N} \sigma_{i,k}^2 \sum_{q \neq k} \left(\sigma_{j,q}^2 - \frac{\sigma_{k,q}^2 \sigma_{j,k}^2}{\sigma_{k,k}^2} \right) \left[f_{X_k,X_q}(a_k, a_q) - f_{X_k,X_q}(a_k, b_q) \right. \\ &\left. - f_{X_k,X_q}(b_k, a_q) + f_{X_k,X_q}(b_k, b_q) \right] \end{aligned} \tag{F.19}$$

The first and second moments of X_i have been calculated for $\mu = 0$ so far. The formulation can be generalized for an arbitrary μ in a simple way. The first moment of an arbitrary Y_i is given as

$$E\left\{Y_i\right\} = E\left\{X_i\right\} + \mu_i \tag{F.20}$$

and the covariance will be the same as $\mathbf{X}$'s, i.e.,

$$\mathrm{Cov}(\mathbf{Y}) = \mathrm{Cov}(\mathbf{X}) \tag{F.21}$$

We should emphasize that the derivation related to finding first and second moments of truncated Gaussian random vector has been taken from [12].

2-D Example

Assume that $\mathbf{V} = [V_x, V_y]^T$ has Gaussian distribution (i.e., $\mathbf{V} \sim \mathcal{N}(\mathbf{v}; 0, \mathbf{\Sigma})$) in a region $\mathcal{C}$ such that $\mathcal{C} = \{v_x, v_y : a_x < v_x < b_x, a_y < v_y < b_y\}$. For this random variable. The mean and covariance values are given according to previous section as follows

$$\mathrm{E}\{V_x\} = \Sigma_{v_x v_x}\left[f_{V_x}(a_x) - f_{V_x}(b_x)\right] + \Sigma_{v_x v_y}\left[f_{V_y}(a_y) - f_{V_y}(b_y)\right] \tag{F.22}$$

$$\mathrm{E}\{V_y\} = \Sigma_{v_y v_y}\left[f_{V_y}(a_y) - f_{V_y}(b_y)\right] + \Sigma_{v_x v_y}\left[f_{V_x}(a_x) - f_{V_x}(b_x)\right] \tag{F.23}$$

and the covariance:

$$\begin{aligned}\mathrm{E}\left\{V_x^2\right\} = {} & \Sigma_{v_x v_x} + \Sigma_{v_x v_x}\left[a_x f_{V_x}(a_x) - b_x f_{V_x}(b_x)\right] + \frac{\left(\Sigma_{v_x v_y}\right)^2}{\Sigma_{v_y v_y}}\left[a_y f_{V_y}(a_y) - b_y f_{V_y}(b_y)\right] \\ & + \frac{\Sigma_{v_x v_y}}{\Sigma_{v_y v_y}}|\mathbf{\Sigma}|\left[f_{V_x V_y}(a_x, a_y) - f_{V_x V_y}(b_x, a_y) - f_{V_x V_y}(a_x, b_y) + f_{V_x V_y}(b_x, b_y)\right]\end{aligned} \tag{F.24}$$

$$\begin{aligned}\mathrm{E}\left\{V_y^2\right\} = {} & \Sigma_{v_y v_y} + \Sigma_{v_y v_y}\left[a_y f_{V_y}(a_y) - b_y f_{V_y}(b_y)\right] + \frac{\left(\Sigma_{v_x v_y}\right)^2}{\Sigma_{v_x v_x}}\left[a_x f_{V_x}(a_x) - b_x f_{V_x}(b_x)\right] \\ & + \frac{\Sigma_{v_x v_y}}{\Sigma_{v_x v_x}}|\mathbf{\Sigma}|\left[f_{V_x V_y}(a_x, a_y) - f_{V_x V_y}(b_x, a_y) - f_{V_x V_y}(a_x, b_y) + f_{V_x V_y}(b_x, b_y)\right]\end{aligned} \tag{F.25}$$

$$\begin{aligned}\mathrm{E}\{V_x V_y\} = {} & \Sigma_{v_x v_y} + \Sigma_{v_x v_y}\left[a_y f_{V_y}(a_y) - b_y f_{V_y}(b_y)\right] + \Sigma_{v_x v_y}\left[a_x f_{V_x}(a_x) - b_x f_{V_x}(b_x)\right] \\ & + |\mathbf{\Sigma}|\left[f_{V_x V_y}(a_x, a_y) - f_{V_x V_y}(a_x, b_y) - f_{V_x V_y}(b_x, a_y) + f_{V_x V_y}(b_x, b_y)\right]\end{aligned} \tag{F.26}$$

where

$$f_{V_x}(v_x) = \int_{a_y}^{b_y} \frac{\mathcal{N}(\mathbf{v}; 0, \mathbf{\Sigma})}{P(\mathcal{C})} \mathrm{d}v_y$$
$$= \frac{\mathcal{N}(v_x; 0, \Sigma_{v_x v_x})}{P(\mathcal{C})} \left[\Phi\left(\frac{\Sigma_{v_x v_x} b_y - \Sigma_{v_x v_y} v_x}{\sqrt{\Sigma_{v_x v_x} |\mathbf{\Sigma}|}} \right) - \Phi\left(\frac{\Sigma_{v_x v_x} a_y - \Sigma_{v_x v_y} v_x}{\sqrt{\Sigma_{v_x v_x} |\mathbf{\Sigma}|}} \right) \right] \tag{F.27}$$

$$f_{V_y}(v_y) = \int_{a_x}^{b_x} \frac{\mathcal{N}(\mathbf{v}; 0, \mathbf{\Sigma})}{P(\mathcal{C})} \mathrm{d}v_x$$
$$= \frac{\mathcal{N}(v_y; 0, \Sigma_{v_y v_y})}{P(\mathcal{C})} \left[\Phi\left(\frac{\Sigma_{v_y v_y} b_x - \Sigma_{v_x v_y} v_y}{\sqrt{\Sigma_{v_y v_y} |\mathbf{\Sigma}|}} \right) - \Phi\left(\frac{\Sigma_{v_y v_y} a_x - \Sigma_{v_x v_y} v_y}{\sqrt{\Sigma_{v_y v_y} |\mathbf{\Sigma}|}} \right) \right] \tag{F.28}$$

$f_{V_x}(v_x)$ and $f_{V_y}(v_y)$ are marginal PDFs, $f_{V_x,V_y}(v_x, v_y) = \mathcal{N}(\mathbf{v}; 0, \mathbf{\Sigma})/P(\mathcal{C})$ is the joint PDF of the truncated Gaussian random vector.